

Joint Institute for Wood Products Innovation



**Cellulose Nanocrystals as a Value-Based Additive for Low Carbon
Footprint Concrete with Limestone**

Final Report

Authors:

Krishna Siva Teja Chopperla, Postdoctoral Scholar, Oregon State University, Corvallis, OR
Sivakumar Ramanathan, Postdoctoral Scholar, Oregon State University, Corvallis, OR
Keshav Bharadwaj Ravi, Postdoctoral Scholar, Oregon State University, Corvallis, OR
Angel Mateos, Research Engineer, University of California Pavement Research Center, Berkeley, CA
John Harvey, Professor, University of California, Davis, CA
Somayeh Nassiri, Associate Professor, University of California, Davis, CA
Jeffrey Alan Buscheck, Lab Manager, University of California Pavement Research Center, Berkeley, CA
Sabbie Miller, Assistant Professor, University of California, Davis, CA
O. Burkan Isgor, PI, Oregon State University, Corvallis, OR
W. Jason Weiss, PI, Oregon State University, Corvallis, OR

March 8, 2023

Table of Contents

1. Executive Summary	1
2. CHAPTER 1: Background	3
2.1. Computational Modeling Framework.....	4
2.2. Organization and Contents of the Report.....	5
2.3. Research Objectives.....	6
3. CHAPTER 2: Reducing GHG Emissions using CNCs, OPC, and Limestone	7
3.1. Constituent Materials and Characterization Procedures	7
3.2. Mixing Procedures.....	8
3.2.1. Paste mixing.....	8
3.2.2. Mortar mixing.....	8
3.3. Tests on Cementitious Pastes.....	9
3.3.1. Isothermal calorimetry	9
3.3.2. Ball-on-three-ball (B3B) flexural strength.....	9
3.3.3. Thermogravimetric analysis (TGA).....	9
3.3.4. Porosity and bulk resistivity of cementitious pastes	10
3.3.5. Dynamic vapor sorption (DVS).....	12
3.4. Tests on Cementitious Mortars	13
3.4.1. Drying shrinkage.....	13
3.5. Experimental Results and Discussion.....	13
3.5.1. Heat release.....	13
3.5.2. Thermogravimetric analysis – calcium hydroxide and non-evaporable water content	19
3.5.3. B3B flexural strength.....	21
3.5.4. Bulk resistivity and pore structure characteristics	23
3.5.5. Drying shrinkage.....	27
3.5.6. Dynamic vapor sorption.....	28
3.5.7. Thoughts on developing “greener” mixtures with CNCs	30
3.6. Conclusions.....	33
4. CHAPTER 3: Performance of Mixtures with SCMs and CNCs	34

4.1. Constituent Materials and Characterization Procedures	34
4.1.1. Materials	34
4.1.2. Paste mixing and sample preparation	35
4.1.3. Tests on cementitious pastes	36
4.2. Experimental Results and Discussion	36
4.2.1. Heat flow	36
4.2.2. B3B flexural strength	41
4.2.3. Bulk resistivity and pore structure characteristics	43
4.3. Conclusions	47
5. CHAPTER 4: Full Scale Field Trials of Slabs Placement using Mixtures with Limestone and CNCs at UC Davis Pavement Research Center	49
5.1. Test Sections Preparation	49
5.1.1. Test sections configuration	50
5.1.2. Test section instrumentation	52
5.2. Materials and Mixtures	53
5.2.1. OPC mixture	53
5.2.2. PLC mixture	54
5.2.3. CNC mixture	55
5.3. Test Sections Construction	55
5.3.1. Control of water content	58
5.3.2. CNC addition	58
5.4. Experimental Methods	59
5.5. Experimental Results	60
5.5.1. Fresh properties	60
5.5.2. Setting time	61
5.5.3. Hardened properties	62
5.5.4. Hygrothermal deformation of the slabs	66
5.6. Discussion of Test Sections Experimental Results	74
5.6.1. Effects of the CNC addition	74
5.6.2. Comparison of OPC and PLC	75
6. CHAPTER 5: Conclusions	77

7. References	79
8. Appendix	85
8.1. CNC Amounts.....	85
8.2. Mill Certificates	86

List of Tables

Table 1. Chemical composition (in wt%) and physical properties of the OPC and LS.....	8
Table 2. Slope (m_i) and intercept (b_i) values for best fit lines	32
Table 3. Comparison of properties between LS20-CNC0.2 and LS0-CNC0.0 mixtures	32
Table 4. Chemical composition and particle size parameters of the OPC, PLC, and SCMs (NA: not applicable).....	35
Table 5. Chemical composition and fineness of OPC, PLC, and Slag used (NA: not available). 53	
Table 6. OPC mixture design (1 cy)	54
Table 7. List of hardened properties tested	60
Table 8. Fresh concrete testing results	61
Table 9. Setting time results (ASTM C403)	62
Table 10. Acres of forest management biomass that can be used in one lane mile construction of a freeway for different CNC dosages in concrete and different pavement thicknesses	85

List of Figures

Figure 1. Change in heat flow with varying CNC dosage – (a) LS0 (b) LS10 (c) LS20 (d) LS30	15
Figure 2. Representative 7-day heat release of mixtures at different CNC dosages for LS30 mixtures.....	18
Figure 3. Effect of CNC dosage on 7-day heat release.....	19
Figure 4. 28-day calcium hydroxide content of different mixtures	20
Figure 5. 28-day non-evaporable water content of the mixtures	21
Figure 6. Effect of CNC dosage on B3B flexural strength – (a) 7 days (b) 28 days. A data point on the 1:1 line indicates similar performance, and a data point above the 1:1 line indicates better performance for mixtures with added CNCs (i.e., the measurement on the Y-axis). 1 MPa = 145.04 psi.....	22
Figure 7. Effect of CNC dosage on saturated bulk resistivity (a) 7-days (b) 28-days.....	24
Figure 8. Effect of CNC dosage on saturated formation factor (a) 7-days (b) 28-days.....	25
Figure 9. 28-day porosity of mixtures with and without CNCs. The ends of the error bars shown here represent the measured values and the markers show the average value of the two samples. The limestone replacement percentages also account for the limestone present in the cement clinker (4.1% for this cement).	26
Figure 10. Pore connectivity in mixtures with and without CNCs at 28 days. The ends of the error bars shown here represent the measured values and the markers show the average value of the two samples.....	27
Figure 11. Drying shrinkage results of the mortar specimens	28
Figure 12. Cumulative pore volume of LS20 paste samples with and without CNC.....	29
Figure 13. Pore size distribution of LS20 paste samples with and without CNC.....	29
Figure 14. 28-day saturated bulk resistivity versus GHG emissions for OPC-LS mixtures with and without CNCs. The ends of the error bars shown here represent the measured values and the markers show the average value of the two samples.	31
Figure 15. Change in heat flow with varying CNC dosage – (a) OPC-50SL (b) PLC-50SL (c) OPC- 20FA5SF (d) PLC-20FA5SF (e) OPC-25FA25SL (f) PLC-25FA25SL	39
Figure 16. Effect of CNC dosage on 7-day heat release (a) OPC mixtures (b) PLC mixtures	41
Figure 17. Effect of CNC dosage on B3B flexural strength – (a) 28 days (b) 56 days. A data point on the 1:1 line indicates similar performance, and a data point above the 1:1 line indicates better performance for mixtures with added CNCs (i.e., the measurement on the Y-axis).....	42
Figure 18. Effect of CNC addition on saturated bulk resistivity of the mixtures with SCMs (a) 28 days (b) 56 days.	44
Figure 19. Porosity of the paste samples at (a) 28 days (b) 56 days.....	45
Figure 20. Effect of CNC dosage on pore connectivity (β) in the pastes (a) 28 days (b) 56 days	47
Figure 21. Location of test sections (white path at the bottom of the picture; picture taken after the application of the curing compound on the lean concrete base).	49
Figure 22. Test sections (from picture bottom to top: PLC, CNC, and OPC).....	50

Figure 23. Test sections layout	51
Figure 24. Test section configuration	51
Figure 25. Test section instrumentation (Not to scale)	52
Figure 26. Unrestrained shrinkage prisms	53
Figure 27. Test section instrumentation; left: thermocouple rod and pair of VWSFs; right: thermocouple rod and two RH sensors	56
Figure 28. Slabs construction pictures; (a) before concrete pouring; (b) placing PLC concrete; (c) consolidating CNC concrete; (d) finishing OPC concrete section.....	57
Figure 29. Trowel finishing of PLC section (bottom of photograph); CNC section already sprayed with curing compound (middle of photograph; note that white covering is from the curing compound and not the CNC effect); rolling screed consolidation of OPC concrete (middle-top of photograph).....	57
Figure 30. Measured water content (evaporable water / dry weight of mixture, AASHTO T 318) (Note: The theoretical water content includes the design batch water plus the water absorbed by the aggregates in the saturated surface-dry (SSD) condition.)	58
Figure 31. Addition of the CNC suspension to the ready-mix truck at the construction site	59
Figure 32. Specimen preparation and wooden boxes	60
Figure 33. Penetration resistance (ASTM C403); temperature in the plot is measured in a dummy penetration resistance specimen.....	62
Figure 34. Flexural strength of the different mixtures	63
Figure 35. Compressive strength of the different mixtures.	64
Figure 36. Modulus of elasticity of the different mixtures.	64
Figure 37. Bulk electrical resistivity of the different mixtures.	65
Figure 38. CTE of the different mixtures.....	65
Figure 39. Drying shrinkage of the different mixtures.	66
Figure 40. Mean strain measured in the slabs (average of top and bottom VWSGs; for each section, the average of two pairs of VWSGs is shown).....	67
Figure 41. Differential strain measured in the slabs (difference between top and bottom VWSGs multiplied by H/D, where H is slab thickness [4 in.] and D is distance between VWSGs [2.4 in.]; for each section, the average of two pairs of VWSGs is shown).....	68
Figure 42. Strain measured in the unrestrained shrinkage prisms (for each mixture, the average of three unrestrained shrinkage prisms shown; one of the PLC prisms was regarded an outlier and discarded).....	68
Figure 43. Example of diurnal variation of mean strain measured in the slabs (average of top and bottom VWSGs; Corner1 and Corner2 correspond to each of the two instrumented corners in each section; Mean Temp is the mean temperature of the slabs).....	69
Figure 44. Mean drying shrinkage estimated in the slabs (Corner1 and Corner2 are each of the two instrumented corners in each section).....	70
Figure 45. Differential drying shrinkage estimated in the slabs (Corner1 and Corner2 are each of the two instrumented corners in each section).....	71

Figure 46. Drying shrinkage estimated in the unrestrained shrinkage prisms (USP1, USP2, and USP3 are the three prisms for each of the mixtures; PLC USP3 was regarded an outlier and discarded)..... 71

Figure 47. Apparent CTE of the slabs in terms of expansion-contraction (Corner1 and Corner2 are each of the two instrumented corners in each section); for a given day, the apparent CTE can be defined as the ratio between changes in slab's horizontal strain and slab's mean temperature..... 72

Figure 48. RH measured in the concrete, at 0.8 in. depth (RH1 and RH2 are each of the two RH sensors embedded in each of the sections) 73

Figure 49. Diurnal variation of RH versus temperature (for a given day, the ratio $\Delta RH/\Delta T$ indicates how much concrete internal RH changes versus temperature while the moisture of the concrete remains essentially constant) 74

1 **1. Executive Summary**

2 This project evaluated cellulose nanocrystals (CNCs) as an additive that can aid in concrete
3 mixture modifications in an effort to reduce concrete’s carbon footprint. This project explored the
4 use of CNCs in cementitious materials containing various amounts of limestone (LS). The heat of
5 hydration, porosity, flexural strength, and drying shrinkage were measured. The binders were also
6 evaluated for their resistance to ion transport by measuring their electrical resistivity. The scope
7 was extended to also study binders that include supplementary cementitious materials (SCMs) and
8 CNCs. The SCM mixtures studied were (i) 50% slag, (ii) 25% fly ash and 25% slag, and (iii) 20%
9 fly ash and 5% silica fume. In addition, full-scale field trials were done at the University of
10 California at Davis to demonstrate CNCs use with Ordinary Portland Cement (OPC) and Portland-
11 Limestone Cement (PLC) in the field. An embodied carbon calculator was used to evaluate the
12 benefits of utilizing CNCs.

13 In general, the following observations were made from the evaluation of the performance of the
14 mixtures with CNCs and limestone:

- 15 • Lower dosages of CNC (up to 0.5% CNCs) to OPC-LS mixtures resulted in an increased
16 degree of hydration of binder at all ages. At early ages, the increase in the degree of
17 hydration of cement clinker was attributed to the combined effect of LS and CNCs. At a
18 later age, the increased degree of hydration of cement clinker was primarily attributed to
19 the CNCs.
- 20 • CNCs addition did not have a significant impact on the overall porosity and flexural
21 strength of the paste samples.
- 22 • CNCs addition did not have a statistically significant impact on the drying shrinkage of
23 mortar samples with limestone.
- 24 • The addition of CNCs to OPC-LS mixtures resulted in up to 38% increase in the 28-day
25 bulk resistivity mainly due to increase clinker hydration and reduction in pore connectivity.
26 It was observed that a mixture for which 22% of the OPC was replaced with LS and
27 containing 0.2% CNC had an equivalent performance in terms of transport properties
28 compared to the 100% OPC system.
- 29 • The addition of 20% LS and 0.2% CNCs together resulted in mixtures with ~19% reduced
30 GHG emissions with comparable mechanical and transport properties to the conventional
31 100% OPC mixture.

32 From the evaluation of the performance of the OPC-SCM and PLC-SCM mixtures with CNCs,
33 the following observations were made:

- 34 • CNCs addition did not have a significant impact on the 7-day heat release values for most
35 SCM mixtures. Future research includes understanding the mechanism of CNCs effect on
36 the hydration of SCM mixtures.

- 37 • CNCs addition did not have a significant impact on the overall porosity, and the B3B
38 flexural strengths of majority of the SCM mixtures with CNCs were within $\pm 15\%$ of the
39 flexural strength of mixtures without CNCs.
- 40 • CNCs addition to the SCM mixtures resulted in an increase in the overall pore connectivity
41 and a reduction in the bulk resistivity when measured at 28 and 56 days, however the bulk
42 resistivity of the SCM mixtures are significantly higher than the reference OPC mixture.
43 The observed trend may be due to the agglomeration of CNCs, changes in the pore structure
44 due to delayed early age hydration when CNCs are used, and adsorption of CNCs on SCMs
45 resulting in slightly altering the reaction kinetics of SCMs. Further research is needed to
46 understand the mechanisms behind the effect of CNCs on the pore structure characteristics
47 and transport properties of the SCM mixtures.

48 The use of CNC with PLC was successfully used in field trials in California. The PLC mixtures
49 with and without CNCs had similar fresh concrete properties including slump, air content, set time
50 and unit weight. Hardened properties such as strength, modulus of elasticity, resistivity, and
51 shrinkage were also similar for both mixtures.

52 2. CHAPTER 1: Background

53 Cellulose nanomaterials (CNMs) are non-toxic, non-petroleum-based materials that may be used
54 as concrete additives [1-3]. CNMs are derived from bio-degradable carbon-neutral sources [1-5]
55 and include cellulose nanofibers (CNFs) and cellulose nanocrystals (CNCs). CNFs are fibrillated
56 and are typically ~500-2000 nm long and 4-20 nm wide. CNCs are rod shaped crystals that are
57 typically made using acid hydrolysis (though different processing approaches may be used) and
58 are 50-500 nm in length and 3-20 nm in width [1, 6]. CNCs have been used in cementitious
59 mixtures and have shown potential to improve mechanical properties of concrete [2, 3, 7-13]
60 Similarly, it was shown that the addition of CNFs could improve concrete performance by
61 promoting crack bridging and improving the post peak behavior of concrete [3, 9, 14-16].

62 Past work showed that the addition of CNCs improve the hydration of cementitious mixtures
63 containing ordinary portland cement (OPC) [17]. This was attributed to two mechanisms – steric
64 stabilization and short circuit diffusion (SCD) [17, 18]. Steric stabilization¹ contribute to property
65 improvement at lower CNC dosages (up to 0.3% by binder volume), presumably due to a
66 dispersing effect on the particles [17, 19]. It was also hypothesized that the adsorption of CNCs
67 on cement grains resulted in the formation of preferential pathways for water to ingress through
68 the C-S-H layer around the cement grains (i.e., short circuit diffusion), which increased the
69 hydration of cement. This observation of improved hydration was confirmed by other researchers
70 for mixtures containing up to 0.5% CNCs [3, 17, 18, 20-22].

71 Moon et al. [2] showed that modifying the CNC production process and cellulose source produces
72 CNCs with different surface charges and attached functional groups. To study the effect of CNC
73 type, Fu et al. [23] evaluated Type I/II and Type V OPC mixtures with CNCs derived from
74 different sources and produced using different processing methods. It was reported that in addition
75 to the CNC type, the chemistry of the cement also plays a role in material performance. Fu et al.
76 [23] observed that the aluminate phases might influence early age hydration due to their surface
77 charge, which results in preferential adsorption of CNCs on C₃A rather than the C₃S clinker phases.
78 The preferential adsorption of CNCs on C₃A implied that the degree of reaction of the clinker of
79 Type V OPC was higher when compared to Type I/II OPC. The literature also reported that while
80 early-age cement hydration may be retarded due to CNC addition (probably due to the CNC
81 blocking the surface of the cement), this retardation generally occurs before 20 hours after mixing.
82 After approximately 30-40 hours, the rate of hydration increases with CNC. This accelerated
83 hydration also results in an increase in the ultimate degree of hydration (up to 8%) compared to a
84 mixture with no added CNCs [17, 23]. (This 8% increase refers to the mixture with 1% CNCs
85 which had a degree of hydration of ~63 % at 7 days compared to a mixture without CNCs which
86 had a degree of hydration of ~55% at the same age).

¹ Dispersion of cement grains due to adsorption on CNCs on their surfaces

87 The addition of CNCs was shown to improve the mechanical properties of the cementitious
88 mixtures. Some of the previous studies on the addition of CNCs showed a 20-30% increase in
89 compressive strengths and 11-20% increase in flexural strengths [19-21]. On the other hand, there
90 are studies that also show that CNC addition did not have any statistically significant effect on
91 strength [16]. The increase in strength when it occurred was attributed to both the increase in the
92 degree of cement hydration and an increase in pore filling and refinement [14, 20-22, 24, 25]. In
93 addition, improvement in the elastic modulus of C-S-H due to CNC addition was reported [17, 19,
94 21, 23, 26].

95 CNCs were also reported to refine pores in cementitious mixtures by reducing the pore size
96 distribution, improving the transport properties of the hardened mixtures [22, 27, 28]. Various
97 researchers have reported a decrease in the porosity of cementitious mixtures containing CNCs.
98 The tortuosity of the cementitious matrix was also reported to increase with the addition of CNCs
99 [26]. It was shown in literature that the addition of CNCs resulted in the improvement of electrical
100 resistivity of the cementitious mixtures [3, 24, 26, 29]. The increase in bulk resistivity indicates
101 that the transport properties of mixtures could be improved by CNC addition [24, 30].

102 In addition to the research work done in the laboratory, CNCs have been used in the field for
103 construction of a parking lot pavement in Greenville, South Carolina in 2018. Also, CNCs have
104 recently been produced and placed commercially in a bridge in Yreka, California in 2020 [31, 32]
105 to demonstrate the feasibility of using CNCs in large-scale concrete structures in the field. It was
106 reported that the concrete with CNCs had similar or slightly better 28-day compressive strength
107 compared to concrete with no added CNCs.

108 While CNCs may improve the mechanical and transport properties of cementitious materials, steps
109 have not been taken to demonstrate potential reductions in clinker and greenhouse gas (GHG) or
110 CO₂ emissions. This project discusses the potential of using CNCs to reduce the clinker content in
111 the concrete and thus reducing GHG emissions [33-35]. In this work, CNCs were used in
112 conjunction with the use of limestone to replace OPC.

113 Portland limestone cements (PLCs) are a viable alternative to OPCs [36-41]. Mixtures made using
114 PLC (ASTM C595 cement) have similar performance to mixtures made using OPC [41, 42].
115 Similar studies were performed using added limestone [36, 38, 43-45]. It was shown that the size
116 of the limestone can play a critical role due nucleation, particle packing, and dilution [38, 42, 44-
117 46]. PLCs could reduce up to 15% of the emissions associated with the production phase of cement
118 [47]. Therefore, this research was conducted to determine whether LS and CNCs can be used
119 synergistically to lower GHG emissions while not compromising on performance.

120 2.1. Computational Modeling Framework

121 A thermodynamic and pore partitioning model for concrete (PPMC) modeling framework is used
122 in this study to predict the performance of concrete [48-51]. The details of this modeling

123 framework will not be repeated here for brevity and interested readers are pointed to reading the
124 cited documents. Briefly, the chemical composition of the OPC and SCM, and the maximum
125 degree of reactivity (DOR*; measured using the Pozzolanic Reactivity Test [52-54]) of the SCM
126 are used as inputs to a kinetic [55] model and thermodynamic modeling [56] framework. The
127 GEMS3K software [57, 58] in conjunction with the CemData v18.01 thermodynamic database
128 [59] is used to perform thermodynamic calculations to predict the reaction products that form when
129 OPC and OPC+SCM binders react [56, 59-66]. The volumes of gel pores (<5nm in size) and
130 capillary pores (>5nm) in the hydrated cementitious paste is calculated from the reaction products
131 using a Pore Partitioning Model [67, 68]. The pore volumes are scaled to concrete using the PPMC,
132 which is then used to predict the performance of concrete [49, 50]. This modeling framework has
133 been shown to accurately predict the porosity, formation factor, and compressive strength of
134 concrete made with OPCs, PLCs, and SCMs [48-50, 69-71].

135 2.2. Organization and Contents of the Report

136 This report is composed of five chapters. The first chapter (section 2) consists of background on
137 CNCs research, introduction of the work performed, and the list of main research objectives. It
138 also briefs the computational modeling framework used in the study to predict the performance of
139 the mixtures such as porosity. The background section of this chapter gives a brief description of
140 CNCs and literature review of CNCs use in cementitious materials. The authors of this chapter are
141 S. Ramanathan, K.S.T. Chopperla, K. Bharadwaj, O.B. Isgor, and W.J. Weiss.

142 The second chapter (section 3) presents the research findings observed from evaluating the OPC-
143 LS-CNC mixtures performance. Chapter 2 briefs material characterization and the experimental
144 procedures used. Chapter 2 also includes the discussion on the results of the mixtures tested for
145 heat of hydration, non-evaporable water content, flexural strength, porosity, pore connectivity,
146 electrical resistivity, and drying shrinkage. The majority of the results and findings in the chapter
147 are published in ACI Materials Journal [72]. The authors of this chapter are S. Ramanathan, K.S.T.
148 Chopperla, O.B. Isgor, and W.J. Weiss.

149 The third chapter (section 4) presents the research findings from evaluating the performance of the
150 mixtures with SCMs and CNCs. The extended goal of this project is to evaluate the performance
151 of CNCs in mixtures with SCMs as using SCMs can enable further reducing the GHG emissions.
152 Chapter 3 includes the discussion of the results of the mixtures tested for heat of hydration, flexural
153 strength, porosity, pore connectivity, and electrical resistivity. Ongoing work is evaluating the
154 interactions between CNCs and SCMs, and the role of CNCs in improving the performance of the
155 mixtures with SCMs. The authors of this chapter are K.S.T. Chopperla, S. Ramanathan, O.B. Isgor,
156 and W.J. Weiss.

157 The fourth chapter (section 5) includes the details of the full-scale field trials done in California
158 using mixtures with OPC, PLC, and CNCs. The chapter includes details of the test sections

159 preparation and construction, fresh and hardened concrete properties, and hydrothermal
160 deformation of the slabs. Chapter 4 is authored by A. Mateos, J. Harvey, S. Nassiri, J.A. Buscheck,
161 and S. Miller. The final chapter (section 6) summarizes the studies and their findings and includes
162 the overall conclusions. The report also includes an appendix (section 8) that contains the estimate
163 of the amount of CNCs required in construction of a lane mile of concrete pavement and the mill
164 certificates of the materials used in the field trials.

165 2.3. Research Objectives

166 The main objectives of the project are:

- 167 • To evaluate whether an OPC-LS-CNC can be designed to have a similar performance to
168 the conventional OPC mixture to lower GHG emissions
- 169 • To calculate the GHG emissions of the mixtures used and determine the optimum CNC
170 dosage needed to lower carbon footprint
- 171 • To demonstrate the use of LS and CNCs in full scale field trails in slabs and to monitor
172 their performance

173

174 **3. CHAPTER 2: Reducing GHG Emissions using CNCs, OPC, and Limestone**

175 This chapter focuses on the objective of examining whether OPC in a concrete mixture can be
176 replaced with LS and CNC to create a system with similar performance and a lower embodied
177 carbon content (greenhouse gas emissions).

178 **3.1. Constituent Materials and Characterization Procedures**

179 Commercially available Type II OPC and LS (96% purity) were used in this study. Four LS
180 replacement levels were used (0%, 10%, 20%, and 30% by mass of OPC). This is in addition to
181 the LS already present in OPC. CNCs that were obtained in the form of suspension with 11% w/w
182 CNC solids were used. The CNCs were manufactured by Forest Products Laboratory using sulfuric
183 acid hydrolysis process. Four CNC concentrations used were 0%, 0.2%, 0.5%, and 1.0% solid
184 volume by volume of binder (i.e., OPC+LS). CNC concentration was measured in terms of the
185 volume of binder to be consistent with the previous studies [3, 17].

186 The CNC suspension and ASTM type II deionized (DI) water were chilled to 5 °C before the
187 dispersion process. Chilled water (5°C) was used for dispersion to compensate the heat generated
188 from dispersion [73], The CNC suspension was batched in the bowl of a high shear blender
189 (Waring Commercial CB15VP blender) along with chilled DI water based on the procedure
190 adapted from specification 10A of the American Petroleum Institute (API). Shear mixing was
191 carried out for a total of 60 seconds at 4000 rpm in two sessions. After the first 30 seconds, the
192 sides and bottom of the mixing bowl were scraped using a silicone spatula to release any adhered
193 / agglomerated CNCs for about 15 seconds. The temperature of the solution was approximately 23
194 °C after the dispersion at the time of mixing. The water was adjusted to maintain a constant water-
195 to-binder ratio (w/b) was 0.40. Shear blending using a high shear mixer was chosen for CNC
196 dispersion as mechanical methods have been effective in dispersing agglomerates of nanomaterials
197 [73, 74].

198 The chemical composition and physical properties of the OPC and LS are shown in Table 1. The
199 chemical composition was determined using X-ray fluorescence (XRF) from which the oxide
200 composition was determined using the fused bead process according to ASTM C114-18 [41, 75,
201 76]. The loss on ignition (LOI) of the cementitious powders was determined by igniting
202 approximately 5 g of material in a ceramic crucible up to 1000 °C for three hours and measuring
203 the mass after ignition. The fused beads were prepared by combining 1 g of the ignited powder
204 with 5 g flux (for OPC) and 0.55 g powder with 5.5 g flux (for LS). The flux composed of 49.75%
205 lithium metaborate, 49.75% lithium tetraborate, and 0.50% lithium iodide was mixed gently in a
206 platinum crucible and fused in a furnace (Claisse LeNeo fluxer) for approximately 25 minutes at
207 1450 °C.

208

Table 1. Chemical composition (in wt%) and physical properties of the OPC and LS

Material	Na ₂ O	MgO	Al ₂ O ₃	SiO ₂	SO ₃	K ₂ O	CaO	Fe ₂ O ₃	LOI	d ₅₀ (µm)	G
OPC	0.21	1.43	3.95	19.95	2.55	0.48	63.32	2.28	2.71	13.9	3.15
Limestone	0.14	5.74	0.79	2.93	0.13	0.12	86.50	0.41	42.27	15.2	2.71

209

210 Particle size distribution was obtained using laser diffraction (Horiba LA-920) [41]. The powder
 211 was dispersed in isopropyl alcohol in front of a laser lamp assembly. Approximately 3-5 g of
 212 material was added slowly in 0.5 g increments, and the solution was sonicated and circulated to
 213 prevent the agglomeration of particles. Median particle size (d₅₀) and specific gravity (G) values
 214 of the SCMs are presented in Table 1 and are measured as an average of five runs. The specific
 215 gravity of OPC and LS powder are also presented in Table 1. No other chemical admixture was
 216 added to the mixture to avoid conflicting influences of CNCs and chemical admixtures.

217 A locally sources fine aggregate was used for making drying shrinkage samples. The oven dry
 218 specific gravity of the fine aggregate was 2.39 and absorption capacity was 2.59%.

219 3.2. Mixing Procedures

220 3.2.1. Paste mixing

221 The cementitious materials were dry mixed for 90 s using a vacuum mixer at 400 rpm and 70%
 222 vacuum. The CNC dispersed mix water was placed in a mixing bowl, and the dry mixed
 223 cementitious materials were added, and mixed using a vacuum mixer (Renfert Inc. model
 224 18281000) for 90 s at 400 rpm and a 70% vacuum level. The mixing cup was scraped using a
 225 silicone spatula for 15 s, and vacuum mixing was carried out for an additional 90 s. A similar
 226 mixing procedure was followed for cementitious paste mixing in literature [42].

227 3.2.2. Mortar mixing

228 Mortar samples having 0.40 water to binder ratio were prepared for drying shrinkage testing. The
 229 prepared mortar samples consisted of 50% by volume of fine aggregate. Mortar was mixed in a
 230 Hobart mixer as per ASTM C305-20. All the mixing water was placed in the bowl. The
 231 cementitious material was added to water and then it was mixed at the slow speed (140 r/min) for
 232 30 s. Over the next 30 s, the fine aggregate was added. The speed was changed to medium speed
 233 (285 r/min) and mixed the mortar for 30 s. The mixer was stopped for 90 s, in this duration the
 234 bowl and the paddle were scrapped down. Then the mixing was finished by mixing it for 60 s at
 235 medium speed.

236 3.3. Tests on Cementitious Pastes

237 3.3.1. Isothermal calorimetry

238 Heat release was measured using isothermal calorimetry (TAM Air, TA Instruments) according to
239 ASTM C1679-17. Cementitious pastes were mixed using a vacuum mixer as described in the
240 mixing procedure. After mixing, 6-7 g of the cementitious paste was transferred to a glass ampoule
241 and sealed. The glass ampoules were then lowered into the isothermal calorimeter which was pre-
242 conditioned at 23 ± 0.05 °C. Data was not collected for the first 45 minutes. Heat flow and heat
243 release were measured, and the data was collected for 7 days. Two replicates of all mixtures were
244 tested for each mixture, and the average of the two replicates was reported [41, 77]. Replicate
245 testing for all mixtures showed variability of less than 2% between the replicates.

246 3.3.2. Ball-on-three-ball (B3B) flexural strength

247 The cementitious paste mixture prepared was placed in 50 mm (diameter) \times 100 mm (length)
248 cylindrical molds in two layers and each layer was vibrated to ensure adequate compaction of the
249 material. The molds were sealed, and the samples were placed on a roller for 24 hours to minimize
250 the potential effect of bleeding. After 24 hours, the samples were removed from the roller and
251 cured under sealed conditions at 23 ± 1 °C until sample preparation began for flexural strength
252 testing.

253 Flexural strength testing was performed using the B3B test at 7 and 28 days according to ASTM
254 C1904-20 [78]. A detailed procedure for B3B flexural strength testing can be found in the literature
255 [78, 79]. At the age of testing, the cylinder was demolded, and the top and bottom of the cylinder
256 were discarded to avoid end effects (approximately 20 mm from each end). The central portion of
257 the cylinder was cut into disks that were 2.65 ± 0.15 mm thick. These samples were tested on a
258 B3B testing frame [79]. The flexural strength was calculated based on the equation described in
259 literature [79, 80]. The testing was carried out within 15 minutes of cutting the sample. At least six
260 replicates were tested for all mixtures at each age of testing, and the coefficient of variation (COV)
261 was less than 10% except in one mixture, whose COV was 12%.

262 3.3.3. Thermogravimetric analysis (TGA)

263 Immediately after flexural strength testing at 28 days, the central portion of each disk was obtained
264 and ground into a fine powder using a mortar and pestle. The powdered sample was then sieved
265 using a 75 μ m sieve (#200 sieve). The samples were then immediately double sealed in plastic
266 bags to minimize carbonation.

267 Calcium hydroxide and non-evaporable water content for the cementitious powders were obtained
268 using thermogravimetric analysis (TGA). The testing consisted of placing approximately 30-50
269 mg of samples on a platinum pan, and the sample was then loaded into the TGA (TGA 5500, TA

270 Instruments). The TGA chamber was heated at the rate of 10°C/minute to 1000°C in a nitrogen
 271 atmosphere. Calcium hydroxide content (normalized to per g of binder) and non-evaporable water
 272 content (per g of binder) were calculated using equations 1 and 2a, respectively. The onset and end
 273 temperatures were obtained using the tangential method described in Kim and Olek [81]. Replicate
 274 testing for the mixtures showed that the variability was less than 2%.

$$275 \quad m_{CH} = 4.11 \cdot \frac{m_{CH,start} - m_{CH,end}}{m_{init,anhyd}} + 0.74 \cdot \left(2.27 \cdot \frac{m_{CC,start} - m_{CC,end}}{m_{init}} - m_{CC,init} \right) \quad (\text{Eq. 1})$$

276 where, m_{CH} is the mass of calcium hydroxide, $m_{CH,start}$ is the onset temperature of calcium
 277 hydroxide mass decomposition, $m_{CH,end}$ is the end point of calcium hydroxide decomposition,
 278 $m_{CC,start}$ and $m_{CC,end}$ are the onset and end points of calcium carbonate decomposition, $m_{CC,init}$ is the
 279 calcium carbonate present in the binder, $m_{init,anhyd}$ is the anhydrous sample mass in the TGA.

$$280 \quad w_{ne} = \frac{A \cdot m_{105} - B \cdot m_{1000}}{m_{1000}} \quad (\text{Eq. 2a})$$

281 where, w_{ne} is the non-evaporable water content, m_{105} and m_{1000} are the sample masses at 105
 282 oC and 1000 °C respectively obtained from the TGA, A and B are constants calculated from
 283 equations 2b and 2c, respectively to account for the loss on ignition.

$$284 \quad A = \left[(1 - r_{LS})(1 - LOI_{cem}) + (r_{SCM} \cdot (1 - LOI_{LS})) + (D_{CNC} \cdot \rho_{CNC} \cdot k_{CNC} \cdot \left(\frac{1 - r_{LS}}{\rho_{cem}} - \frac{r_{LS}}{\rho_{LS}} \right)) \right]$$

285 (Eq. 2b)

$$286 \quad B = \left[1 + D_{CNC} \cdot \rho_{CNC} \cdot k_{CNC} \cdot \left(\frac{1 - r_{LS}}{\rho_{cem}} + \frac{r_{LS}}{\rho_{LS}} \right) \right] \quad (\text{Eq. 2c})$$

287 LOI_{OPC} and LOI_{LS} are the loss on ignition for OPC and LS used in the study, r_{LS} is the LS
 288 replacement level, D_{CNC} is the CNC suspension dosage by volume percentage of binder, ρ_{CNC} , ρ_{cem} ,
 289 and ρ_{LS} are the specific gravities of CNCs, OPC, and LS respectively. k_{CNC} is the weight percentage
 290 of the CNC solids (11% solids by weight).

291 3.3.4. Porosity and bulk resistivity of cementitious pastes

292 Porosity and bulk resistivity were measured using 50 mm × 100 mm cylinders at 7 and 28 days.
 293 The cylinders were cured in sealed condition after casting until testing. The bulk resistivity was
 294 measured on vacuum saturated samples in accordance with AASHTO TP 119-20 [82].

295 The demolded samples were placed under vacuum at 7 ± 2 Torr for 3 hours. After this, a simulated
 296 pore solution containing 7.6 g/L of sodium hydroxide, 10.64 g/L of potassium hydroxide, and 2
 297 g/L of calcium hydroxide was allowed to saturate the samples under vacuum for one hour.
 298 Simulated pore solution was utilized to vacuum saturate the samples to maintain uniform pore
 299 solution resistivity across all samples for formation factor calculations. After vacuum saturation,
 300 the samples were stored in the simulated pore solution for 24 ± 4 hours at 23°C . The samples were
 301 then measured for electrical impedance to calculate resistivity value. The bulk resistivity was
 302 calculated according to equations 3a and 3b. Appropriate corrections for temperature and sample
 303 geometry were applied as detailed in Ref. [83]. Two replicates of each mixture were tested and the
 304 average data was reported.

$$305 \quad \rho_{sat} = R_{sat} \frac{A}{L} \quad (\text{Eq. 3a})$$

$$306 \quad \rho_{sat-corrected} = \rho_{sat} \cdot e^{\left[\frac{E_{A-cond}}{R} \left(\frac{1}{T} - \frac{1}{T_0} \right) \right]} \quad (\text{Eq. 3b})$$

307 where, $\rho_{sat-corrected}$ is the temperature corrected saturated bulk resistivity, ρ_{sat} is the saturated bulk
 308 resistivity (in $\Omega\text{-m}$), R_{sat} is the vacuum saturated resistance (in Ω), A is the cross-sectional area of
 309 the sample (in m^2), L is the length of the sample, E_{A-cond} is the activation energy of conduction
 310 (considered as 15 kJ/mol based on [84]), R is the universal gas constant (8.314 kJ/mol-K), T is
 311 the sample temperature at the time of measurement (in K), and T_0 is the reference temperature
 312 (298.15 K).

313 For the same cylinders, the saturated weight and the apparent weight were obtained immediately
 314 after the bulk resistivity measurement. The cylinders were then dried at 105°C until a constant
 315 mass was achieved (i.e., the difference between two successive mass measurements is less than
 316 0.1%) [85]. The porosity of the cylinders (in accordance with AASHTO TP 135) was calculated
 317 according to equation 4 and reported as an average of two samples for all the mixtures.

$$318 \quad \Phi_{paste} = \frac{w_{sat} - w_{dry}}{w_{sat} - w_{app}} \quad (\text{Eq. 4})$$

319 where, Φ_{paste} is the porosity of the cementitious paste, w_{sat} is the vacuum saturated sample mass,
 320 w_{dry} is the constant mass obtained after drying the samples at 105°C , w_{app} is the apparent mass of
 321 the samples.

322 The saturated formation factor (F_{sat}) of the mixtures was calculated according to equation 5

$$323 \quad F_{sat} = \frac{\rho_{sat-corrected}}{\rho_{ps}} \quad (\text{Eq. 5})$$

324 where, $\rho_{sat-corrected}$ is the temperature corrected saturated bulk resistivity and ρ_{ps} is the resistivity of
325 the simulated pore solution (0.127 Ω -m). Since the samples were vacuum saturated and stored in
326 simulated pore solution, it is assumed that the pore solution resistivity is uniform for all samples.

327 The pore connectivity (a combination of tortuosity and constriction), β of the paste samples is
328 calculated from equation 6.

$$329 \quad \beta = \frac{\rho_{ps}}{\phi_{paste} \cdot \rho_{sat-corrected}} \quad (\text{Eq. 6})$$

330 where, ρ_{ps} is the resistivity of the simulated pore solution (0.127 Ω -m).

331 3.3.5. Dynamic vapor sorption (DVS)

332 Dynamic vapor sorption (DVS) measurements were made on two samples (LS20-CNC0.0 and
333 LS20-CNC0.2) that were seal cured for 28 days to determine if CNCs have an effect on the pore
334 size distribution of paste samples. The samples were demolded at 28 days, broken into small
335 chunks that weigh ~70-80 mg. These chunks were vacuum saturated with limewater. They were
336 placed under vacuum for 3 hours, and saturated calcium hydroxide solution for an hour under
337 vacuum. The samples were then placed under the solution for three days in a 23 °C chamber to
338 allow for the sample chunks to get completely saturated. At three days, an assumption of full
339 saturation (i.e. degree of saturation of 100%) is made due to the small sample size.

340 DVS measurements were carried out using a Q5000 vapor sorption equipment (TA Instruments)
341 in an inert nitrogen atmosphere. The steps for ramping down the relative humidity to 0% is as
342 follows:

- 343 1. The saturated sample was equilibrated at 23.00 °C
- 344 2. The relative humidity was set to 97.50 % and held for 2880 minutes
- 345 3. The relative humidity was ramped down to 90%, 80%, 50%, 11%, and 0% in consecutive
346 steps over a duration of 5880 minutes for each step.
- 347 4. Each step was maintained until the mass change recorded was <0.001% for 15 minutes.
- 348 5. After reaching 0% RH, the sample was held at isothermal condition for 1440.00 min to
349 equilibrate

350 The pore radius at each RH was calculated using equation 7 and 8. The pore radius is assumed to
351 be the sum of Kelvin radius and thickness of water adsorbed film [86]. Kelvin radius can be
352 determined using equation 7 and t-curve can be determined using equation 8 [87, 88].

$$353 \quad r_k = -\frac{2\gamma V_m}{RT \ln(RH)} \quad (\text{Eq. 7})$$

$$354 \quad t = \left(\frac{AV_m}{6\pi RT(RH)} \right)^{1/3} \quad (\text{Eq. 8})$$

355 where, r_k is Kelvin radius (m), t is thickness of water adsorbed film, γ is surface tension of the pore
356 solution ($= 72 \times 10^{-3}$ N/m), V_m is the molar volume of the pore solution, R is the ideal gas constant
357 with a value of 8.314 J/(mol.K), T is the absolute temperature (K), and A is Hamaker constant for
358 the interaction of solid-liquid-gas (considered to be -19×10^{-20} J). The degree of saturation (DOS)
359 at each RH is calculated using equation 9.

$$360 \quad \text{DOS}_{\text{RH},x} = (M_{\text{RH},x} - M_{\text{RH},0}) / (M_{\text{RH},100} - M_{\text{RH},0}) \quad (\text{Eq. 9})$$

361 where, $\text{DOS}_{\text{RH},x}$ is the degree of saturation at $x\%$ RH, $M_{\text{RH},x}$ is mass of the sample at $x\%$ RH, $M_{\text{RH},0}$
362 is mass of the sample at 0% RH, and $M_{\text{RH},100}$ is mass of the sample at 100% RH.

363 3.4. Tests on Cementitious Mortars

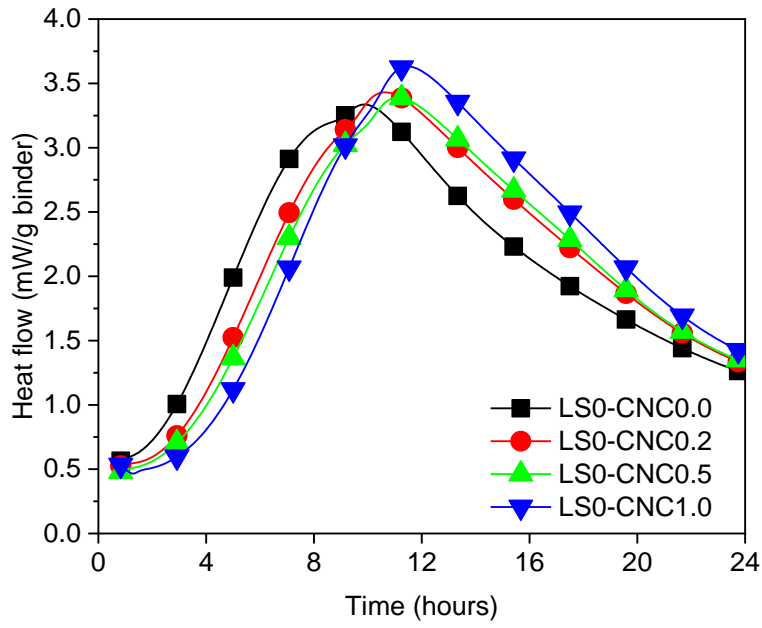
364 3.4.1. Drying shrinkage

365 Mortar samples of dimensions 25 mm (width) x 25 mm (height) x 285 mm (length) were prepared
366 for four different mixtures (OPC, OPC-0.2% CNC, LS30, LS30-0.2% CNC). The curing and drying
367 shrinkage measurement procedures for the mortar specimens were followed according to ASTM
368 C596-18. Three specimens were cast for each mixture, and the average and standard deviation of
369 the drying shrinkage strain measured over the drying period were reported.

370 3.5. Experimental Results and Discussion

371 3.5.1. Heat release

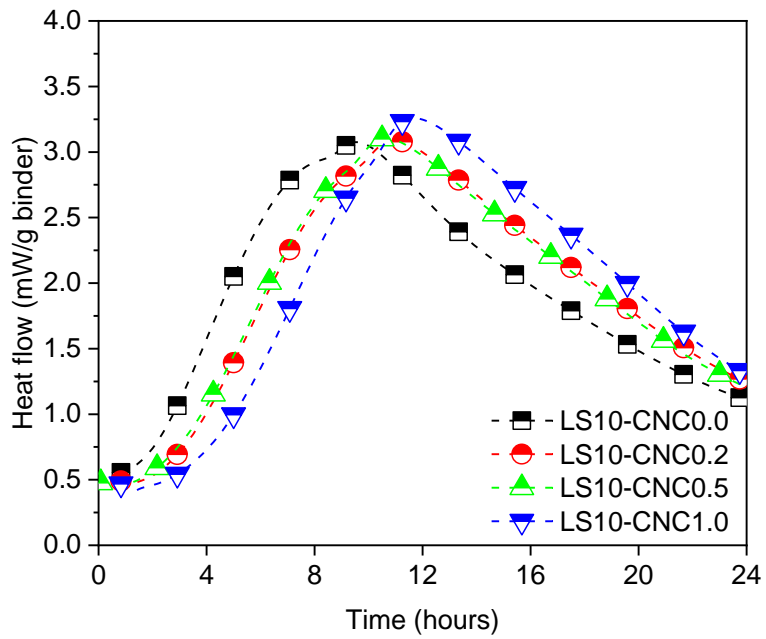
372 Figure 1 shows the variation of heat flow (the derivative of the heat release) for the first 24 hours
373 with a change in CNC dosage. At all LS replacement levels, the heat release was retarded by
374 approximately 2-3 hours (indicated by the curve shifting to the right) with the addition of CNCs.
375 This retardation causes a delay in the onset of the acceleration period, which was approximately
376 similar for 0.2% and 0.5% CNC dosages and higher for 1.0% CNC dosage in all cases. This trend
377 of retardation due to increased CNC dosage is consistent with literature. Based on the Parrot-Killoh
378 (PK) model [89], the heat flow curve can be divided into three phases, namely, the nucleation and
379 growth phase, the diffusion in three dimensions, and the reduction in transport of ionic species at
380 later ages, which was discussed in detail in [89, 90]. For mixtures with CNCs, the rate of reaction
381 of OPC-LS mixtures in the nucleation and growth phase (~6 hours) was slower compared to the
382 mixtures without CNCs. However, the diffusion phase occurs for a longer duration in mixtures
383 containing CNCs compared to the mixtures without added CNCs. This was evident from the higher
384 heat flow for mixtures with CNCs at all LS replacement levels. A similar trend of retardation with
385 CNC addition was observed by Fu et al. [23] and Cao et al. [17]. Cao et al. [17] attributed this
386 retardation to the adsorption of CNCs on the cement grains, resulting in fewer surfaces undergoing
387 hydration. A similar retardation effect was explained in the literature for superplasticizers and
388 other chemical admixtures interacting with cementitious mixtures [6, 17, 91].



389

390

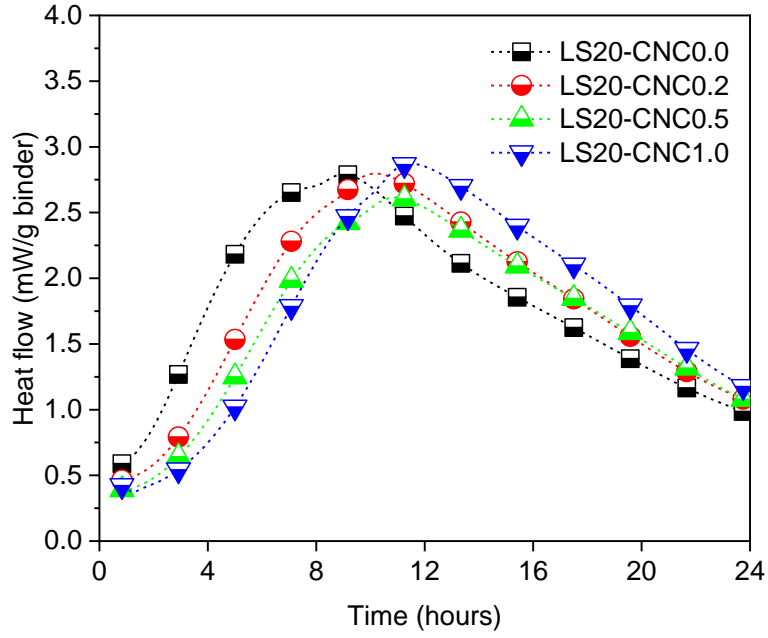
(a)



391

392

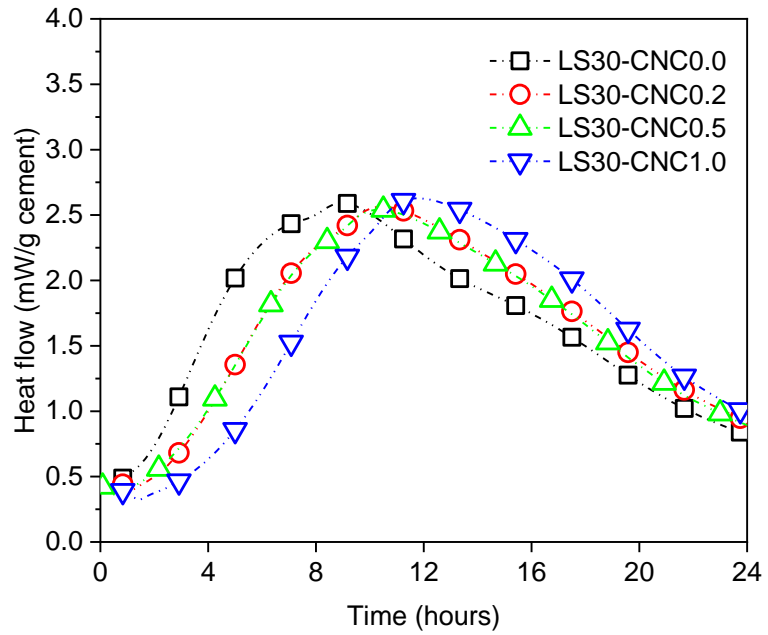
(b)



393

394

(c)



395

396

(d)

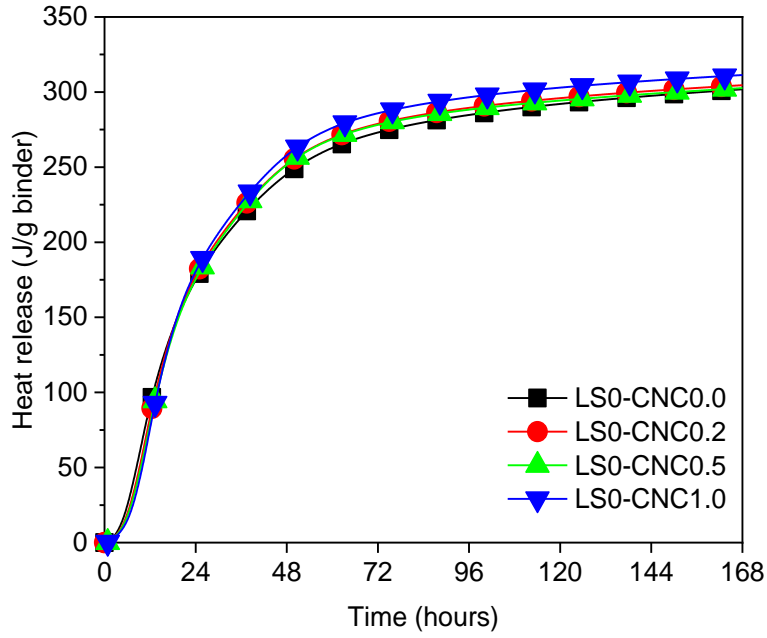
397

398

Figure 1. Change in heat flow with varying CNC dosage – (a) LS0 (b) LS10 (c) LS20 (d) LS30

399 CNCs addition appeared to affect the heat flow peak associated with silicate hydration in the
400 mixture as well as the aluminate peak (or sulfate depletion peak), as shown in Figure 1. The heat
401 flow in the mixtures without CNCs (shown in black and square markers) was characterized by two
402 distinct peaks occurring at approximately 7 (LS30) to 8.25 (LS0) hours and approximately 8.5
403 (LS20) to 10 (LS0) hours, respectively for silicate and aluminate peaks. However, for the mixtures
404 containing CNCs, these peaks mostly overlap. The overlapping peaks likely correspond to silicate
405 and aluminate reactions occurring at approximately the same time, and as a result, the peak heat
406 flow rate appeared to be higher with added CNCs. Similar observations in peak overlap were made
407 by others in literature for cementitious mixtures containing fly ash [92, 93]. It was reported that
408 the optimal sulfate level in OPC-fly ash mixtures caused an offset between the C₃S hydration peak
409 and the aluminate peak [93]. In this case, the addition of CNCs to OPC-LS mixtures could have
410 an influence on the sulfate balance. The change in sulfate balance may be due to the adsorption of
411 sulfate ester end groups of CNCs on C₃A phase of OPC. However, additional studies are needed
412 to examine this. The higher rate of heat flow in the deceleration phase is likely due to short circuit
413 diffusion [17].

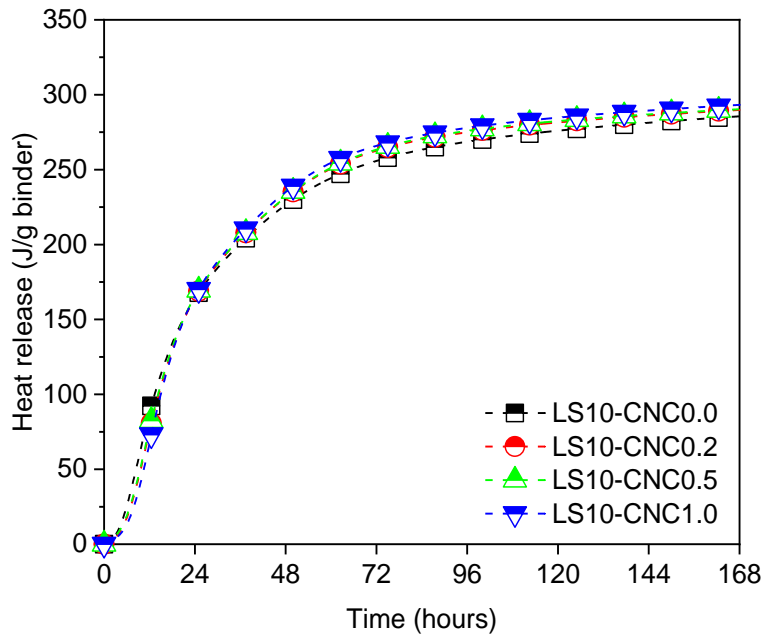
414 Figure 2 shows the 7-day heat release for the mixtures studied here. The heat release values ranged
415 from 302 J – 311 J/g binder (LS0), 285 J – 293 J/g of binder (LS10), 261 J – 274 J/g binder (LS20),
416 and 247 J – 252 J/g binder (LS30) for the various mixtures as in Fig. 2a-d. Up to the first 24 hours,
417 the heat release of the mixtures with CNCs lagged behind the mixtures without CNCs, indicating
418 the retardation due to CNC addition. After approximately 24 hours, there was a cross-over in the
419 heat release curves, indicating an increased rate of hydration for mixtures with CNCs due to short
420 circuit diffusion. For mixtures with no CNCs, dilution and filler effects can explain the results
421 [94]. However, with the addition of CNCs, there was a slight increase in the 7-day heat release.
422 For a given LS replacement level, the addition of CNCs resulted in 2-3% increase in heat release
423 per g of binder compared to mixtures with no added CNCs.



424

425

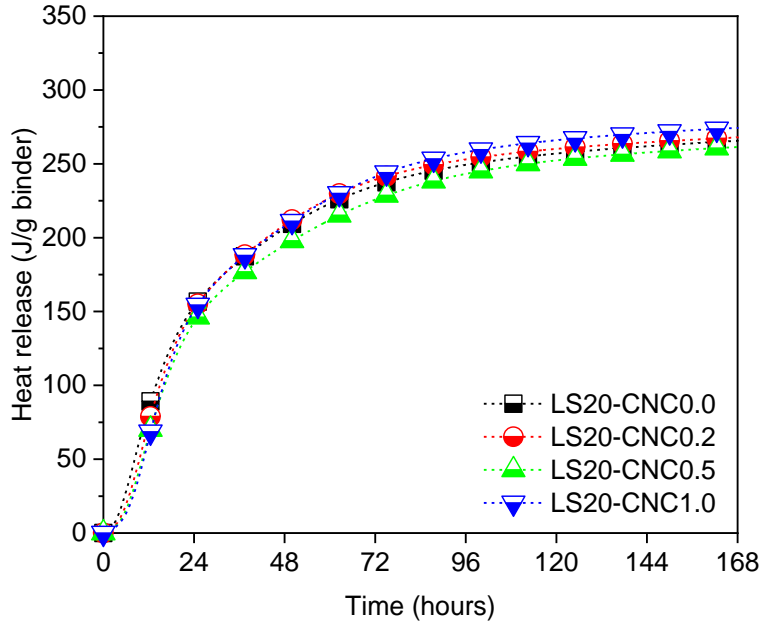
(a)



426

427

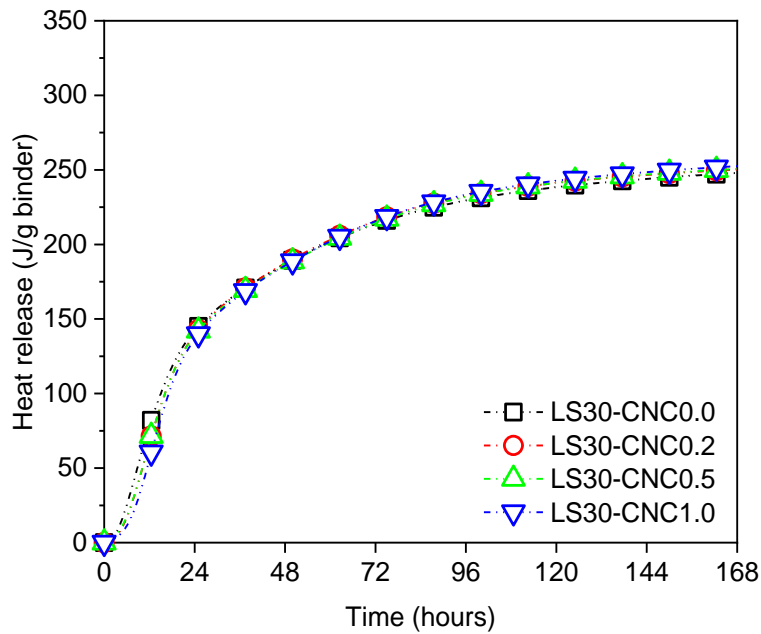
(b)



428

429

(c)



430

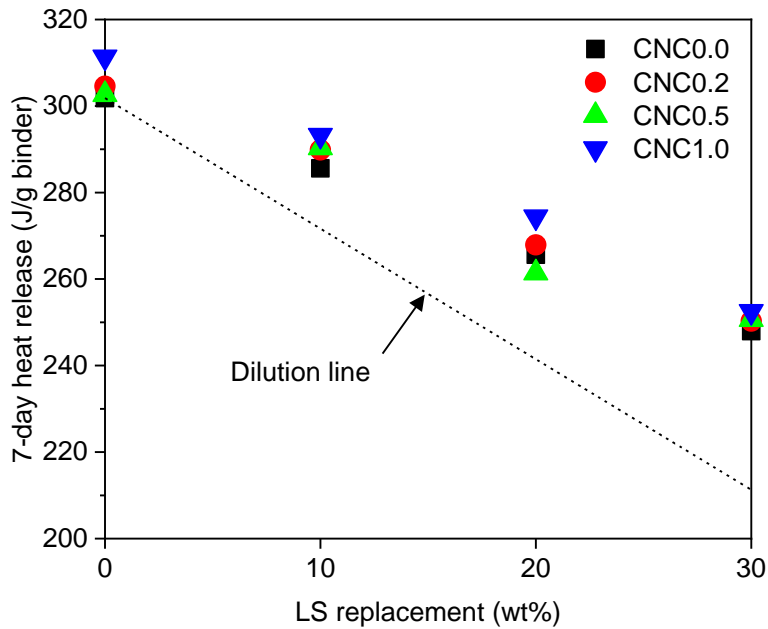
431

(d)

432 Figure 2. Representative 7-day heat release of mixtures at different CNC dosages for
433 LS30 mixtures

434 The replacement of OPC with LS in the mixtures causes a proportional decrease in the 7-day heat
435 release values due to the dilution effect. The dilution effects are offset by addition of LS and CNCs.

436 The combined effect of LS and CNCs was evident from Figure 3, where it was observed that the
 437 7-day heat release of the mixtures with added CNCs and LS lie above the dilution line. This
 438 increase in heat release was likely due to enhanced hydration of the cement clinker resulting from
 439 a combination of short circuit diffusion (SCD) and nucleation effect due to the presence of CNCs
 440 and LS, respectively [17, 44, 45]. This increase in hydration may also be due to other factors.
 441 Some have speculated that this may be due to changes in pore solution chemistry; however, studies
 442 [95] have evaluated the changes in pore solution chemistry and reported little change in ions during
 443 the first 12 hours, and changes on the order of 20% or less after that (CNC having a slightly higher
 444 Na^+ , OH^- concentration and a slightly lower K^+ , SO_3 concentration). Similar improvements in the
 445 heat of hydration were observed in literature for OPC pastes with CNC addition. Fu et al. [23]
 446 observed an approximately 5% increase in the degree of hydration of Type I/II clinker up to 7
 447 days. It is likely that the use of clinkers with low C_3A contents could result in further enhancement
 448 in the clinker hydration [6, 29, 96]. The formation of carboaluminate phases due to the added LS
 449 [97] could also contribute to the increase in the heat release.



450

451

Figure 3. Effect of CNC dosage on 7-day heat release

452

3.5.2. Thermogravimetric analysis – calcium hydroxide and non-evaporable water content

453

454

455

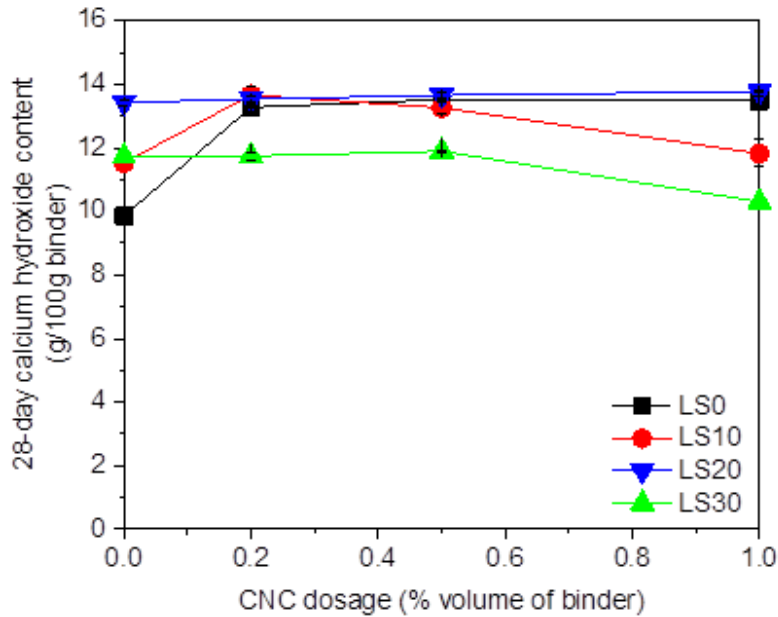
456

457

458

The 28-day calcium hydroxide content of the mixtures is shown in Figure 4. The 28-day calcium hydroxide content of the mixtures varied from 9.9 g - 11.7 g /100 g binder for CNC0.0 mixtures, 11.7 g – 13.7 g/100g binder for CNC0.2 mixtures, 11.9 g – 13.5 g/100g binder for CNC0.5 mixtures, and 10.3 g – 13.5 g / 100g binder for CNC1.0 mixtures. When CNCs were added (up to 0.5% by binder volume) to the mixture, there was an increase in the 28-day calcium hydroxide content of the mixtures that can be explained by the increase in the clinker hydration. The average

459 increase in calcium hydroxide content at low CNC dosage (0.5% CNCs by volume) was ~36%
 460 (LS0), ~17% (LS10), and ~1% (LS30). The increase in calcium hydroxide content on the addition
 461 of low doses of CNCs is consistent with reported data in the literature [6, 15]. At lower CNC
 462 dosages, steric stabilization may allow for greater diffusion of water through the matrix to the
 463 cement grains, resulting in enhanced hydration of the clinker [6]. At 1.0% CNC dosages, however,
 464 there was no significant influence of CNCs on the calcium hydroxide content of the OPC-LS
 465 mixtures. This is probably due to the reduced impact of CNCs on cement hydration as CNCs tend
 466 to agglomerate at higher CNC dosages [17, 19].



467

468

Figure 4. 28-day calcium hydroxide content of different mixtures

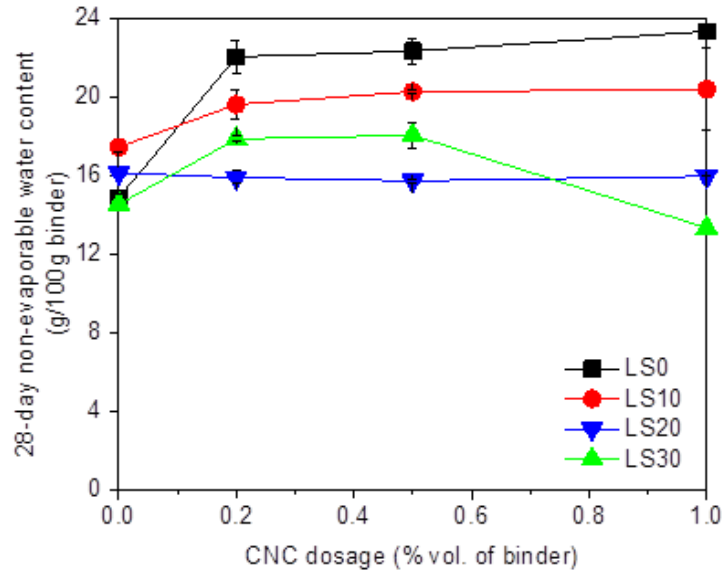
469

470

471

472

The later-age degree of hydration can be computed by calculating the non-evaporable water content (w_n). It was observed that the increase in w_n from 7 to 28 days was generally higher for mixtures containing CNCs compared to those without. Figure 5 shows the 28-day non-evaporable water content of the different mixtures at different CNC dosages.



473

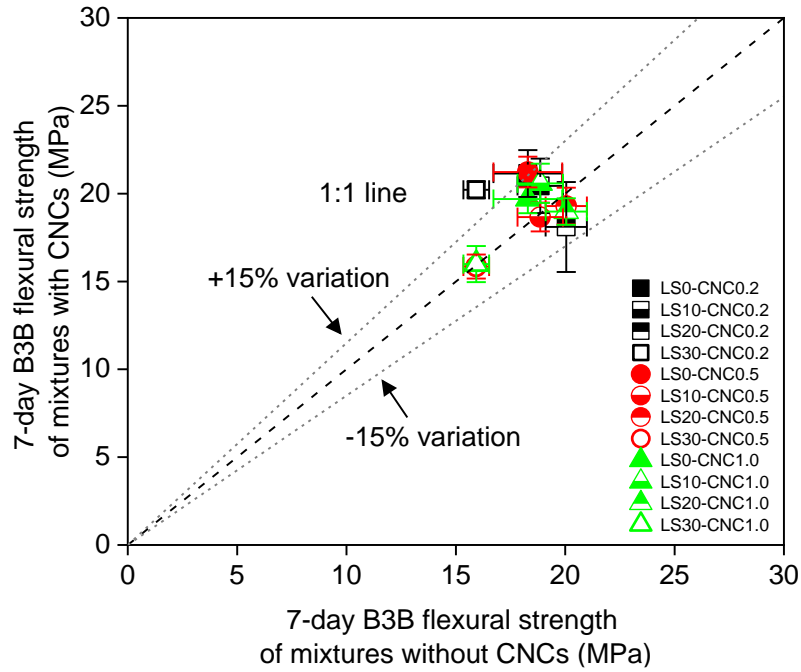
474

Figure 5. 28-day non-evaporable water content of the mixtures

475 It was evident that the addition of small amounts of CNCs (up to 0.5% by volume of binder)
 476 resulted in an increase in the non-evaporable water content when compared to the mixtures with
 477 no CNCs. The increase in w_n ranged from 14% (LS10) – 47% (LS0) and 16% (LS10) – 48% (LS0)
 478 with 0.2% and 0.5% CNC addition, respectively. LS10-CNC0.0 was observed to be an exception
 479 as the w_n was higher than LS0-CNC0.0 mixture. Increased bound water content for high LS
 480 mixtures up to 0.5% CNC dosage indicated a more “effective” clinker usage i.e., more cement
 481 participates in the hydration reaction. This indicated that CNCs could be added to OPC-LS
 482 mixtures to improve clinker efficiency while reducing the clinker content. Cao et al. [17, 18]
 483 reported similar increases in the non-evaporable water content of mixtures containing CNCs.

484 3.5.3. B3B flexural strength

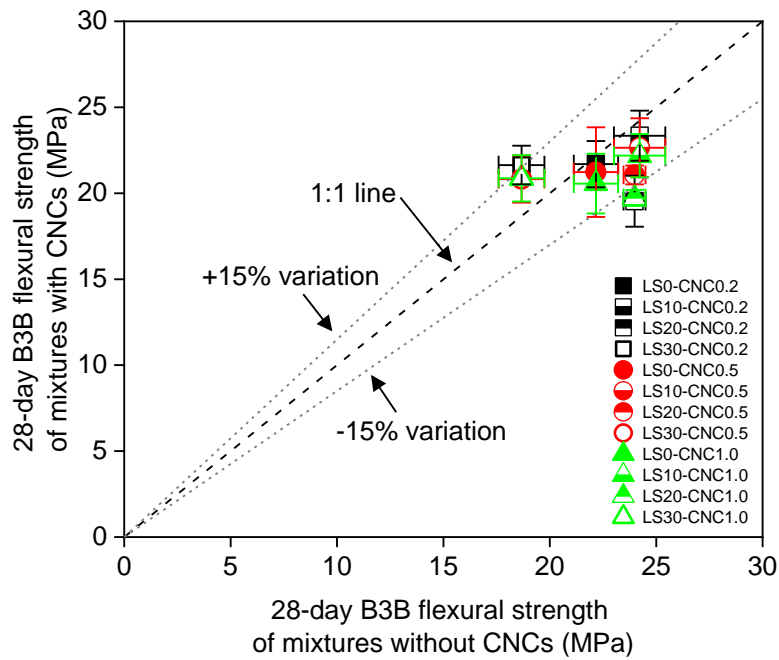
485 Figure 6 shows a parity plot for the 7-day and 28-day B3B flexural strengths for the mixtures with
 486 and without CNCs. The 7-day B3B flexural strengths of mixtures range from 20.2 MPa (LS30) –
 487 21.1 MPa (LS0), 15.9 MPa (LS30) – 21.2 MPa (LS0), and 16 MPa (LS30) – 20.6 MPa (LS10) at
 488 0.2%, 0.5%, and 1.0% CNC dosage, respectively. It should be noted that the B3B flexural strengths
 489 indicate characteristic strength of the mixtures, and they are higher than flexural strength
 490 determined using conventional flexural strength testing due to the size effect. A detailed discussion
 491 of the size effect of samples on B3B flexural strength can be found in literature [79].



492

493

(a)



494

495

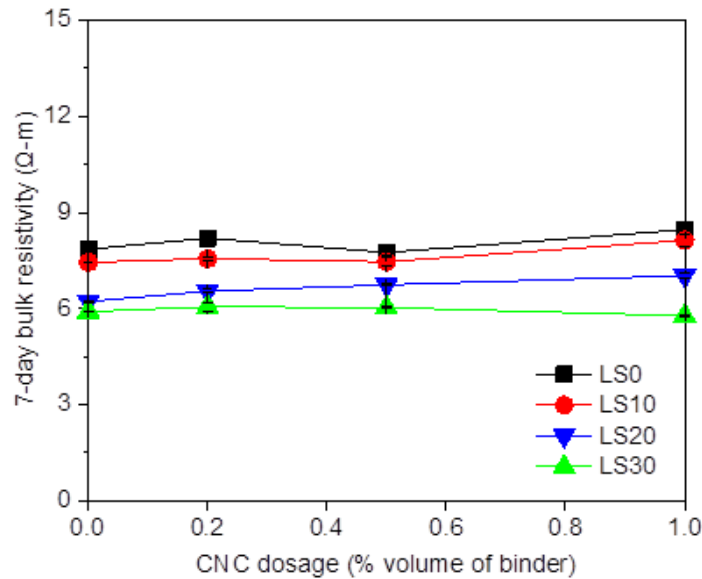
(b)

496 Figure 6. Effect of CNC dosage on B3B flexural strength – (a) 7 days (b) 28 days. A data point
 497 on the 1:1 line indicates similar performance, and a data point above the 1:1 line indicates better
 498 performance for mixtures with added CNCs (i.e., the measurement on the Y-axis). 1 MPa =
 499 145.04 psi.

500 Comparing the mixtures with and without CNCs at 7 days, it was observed that CNCs do not have
501 adverse effects on early-age strength development. Clear effects of dilution due to high LS
502 replacement was seen in the early age flexural strength for mixtures without CNCs consistent with
503 the literature, where reduction in early age mechanical properties was seen with an increase in LS
504 replacement [46]. However, the addition of CNCs compensates for this dilution effect (along with
505 the nucleation effect of LS) and the increase in strength was generally within 15% of the mixtures
506 without CNCs with the exception of LS30-CNC0.2, which showed a 27% increase. A similar trend
507 was observed for 28-day B3B flexural strength; there were no adverse effects on the strength
508 development of mixtures due to CNC addition. The 28-day flexural strength of the mixtures with
509 CNCs was within 15% of the mixtures without CNCs.

510 3.5.4. Bulk resistivity and pore structure characteristics

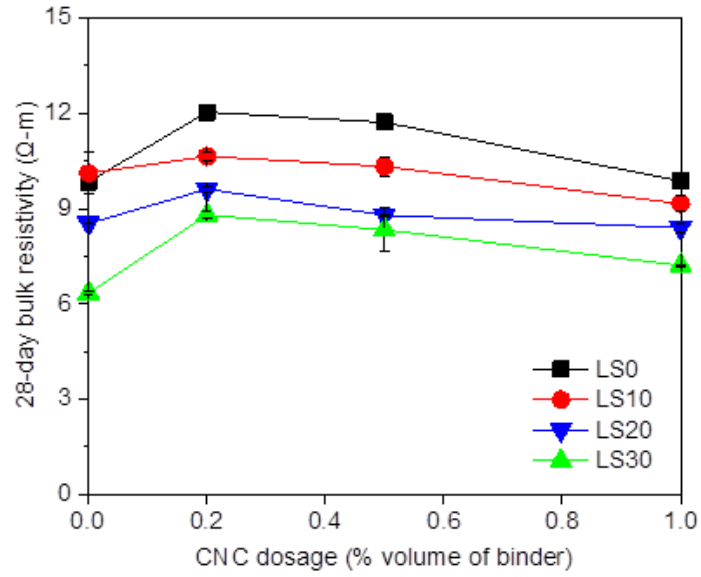
511 The 7-day and 28-day bulk resistivity and saturated formation factor values of the mixtures with
512 different LS replacement levels is shown in Figure 7 and Figure 8 respectively. CNCs did not
513 substantially impact the 7-day bulk resistivity (and saturated formation factor) of the mixtures,
514 seen from Figure 7a and Figure 8a. Only dilution and filler effects on account of LS replacement
515 predominated at this age, which was consistent with literature for OPC-LS mixtures [46].



516

517

(a)



518

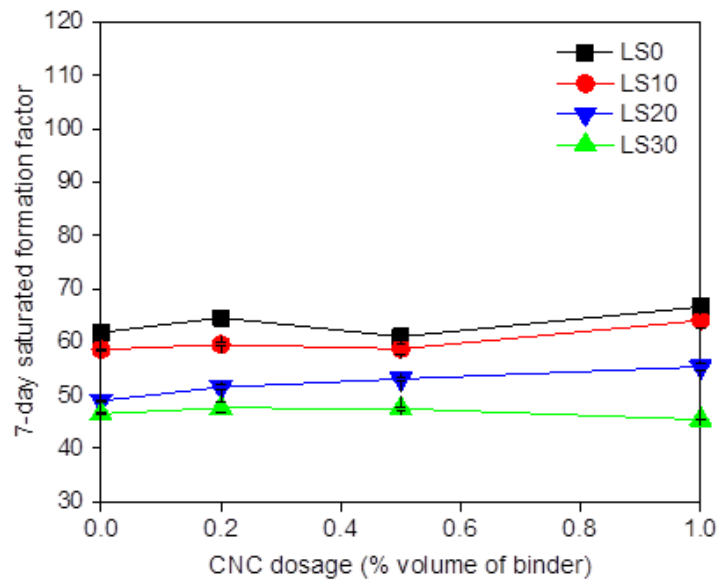
519

(b)

520

Figure 7. Effect of CNC dosage on saturated bulk resistivity (a) 7-days (b) 28-days

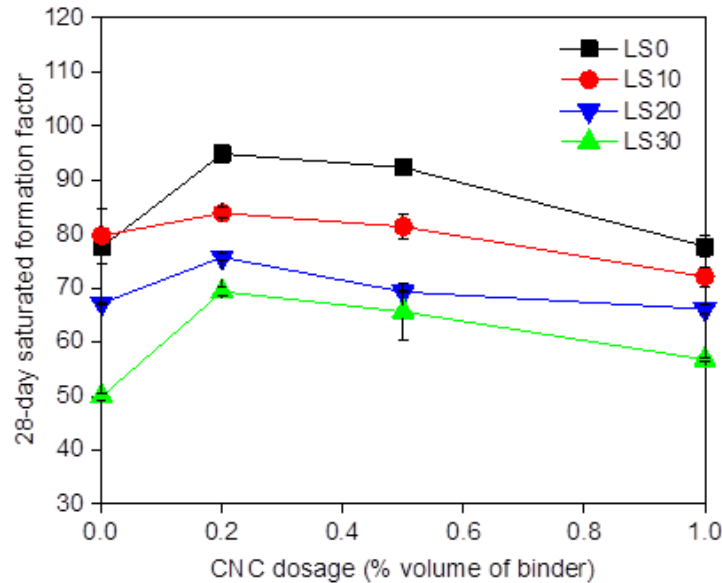
521



522

523

(a)



524

525

(b)

526

Figure 8. Effect of CNC dosage on saturated formation factor (a) 7-days (b) 28-days

527

528

529

530

531

532

533

534

535

536

The effect of CNC addition on the bulk resistivity (and saturated formation factor) of the different mixtures was seen at 28 days (Figure 7b and Figure 8b). CNC dosages of up to 0.5% by binder volume resulted in an increase in the 28-day saturated bulk resistivity compared to the mixtures without CNCs for a given LS replacement level. The increase in bulk resistivity values ranged from 5% (LS10) - 38% (LS30) and 2% (LS10) - 31% (LS30) at 0.2% and 0.5% CNC dosage by binder volume, respectively. The dilution effect due to LS addition was compensated by a combination of LS and CNC dosages up to 0.5% by binder volume. However, no such compensation was observed at higher CNC dosage. When the CNC dosage was 1.0% by binder volume, the effect was pure dilution, and the 28-day bulk resistivity was similar to mixtures with no added CNCs.

537

538

539

540

541

542

543

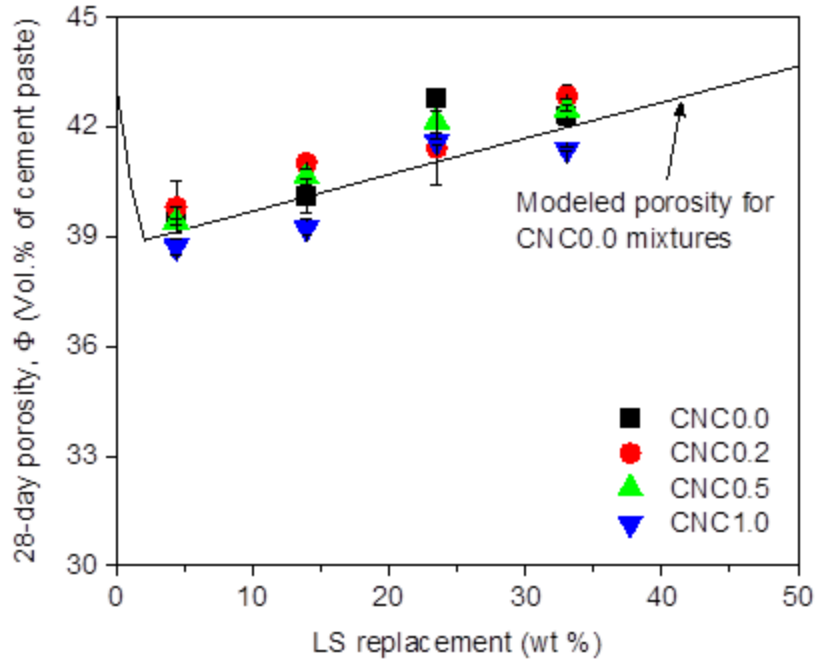
544

545

546

547

The 28-day porosity data for the different mixtures with and without CNCs is shown in Figure 9. A thermodynamic modeling approach [98] (briefed in Chapter 1) was used to provide an idea of how porosity of mixtures varies with LS replacement. The porosity of CNC0.0 mixtures determined from thermodynamic modeling [98] is shown in Figure 9 as a baseline to compare the porosity of mixtures with and without CNCs. The experimental results were in good agreement with the modeling results for CNC0.0 mixtures. At all CNC dosages, the porosity of the mixtures was the lowest for LS0 mixtures and increased with increase in LS content. This was consistent with literature for mixtures without CNCs [98, 99], where the porosity of mixtures decreased first (up to 2% LS addition) and then increased with an increase in LS replacement. No significant changes in total porosity of the samples were observed when CNCs were added and the variation was less than 1% when compared to the corresponding mixtures without CNCs.

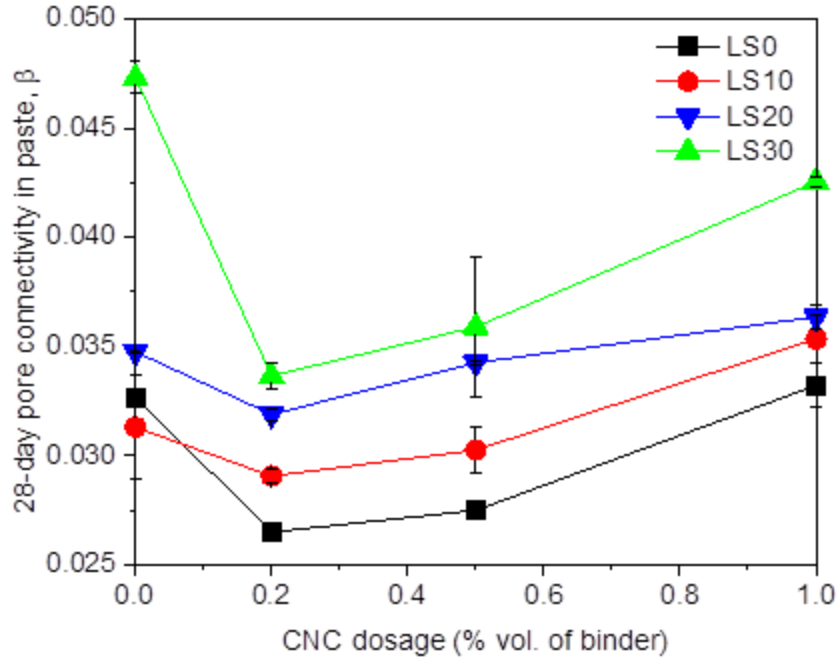


548

549 Figure 9. 28-day porosity of mixtures with and without CNCs. The ends of the error bars shown
 550 here represent the measured values and the markers show the average value of the two samples.

551 The limestone replacement percentages also account for the limestone present in the cement
 552 clinker (4.1% for this cement).

553 While the porosity of the mixtures did not significantly vary, differences were observed in the pore
 554 connectivity (β) of the mixtures (shown in Figure 10). The pore connectivity of the mixtures
 555 without CNCs generally increased with an increase in LS replacement level and ranged from 0.03
 556 (LS0 and LS10) - 0.05 (LS30), consistent with literature [98]. It was seen that low dosages of
 557 CNCs up to 0.5% by volume of binder caused a decrease in pore connectivity (indicating increased
 558 performance), and the lowest pore connectivity was observed for mixtures with 0.2% CNCs by
 559 volume of binder. For CNC0.2 and CNC0.5 mixtures, the decrease in pore connectivity ranged
 560 from 7% (LS10) - 29% (LS30) and 3% (LS10) - 24% (LS30) respectively compared to the CNC0.0
 561 mixtures with the same LS replacement levels. At 1.0% CNC dosage, only LS30 showed decreased
 562 pore connectivity (compared to its 0% CNC counterpart i.e., LS30CNC0.0), whereas LS0, LS10,
 563 and LS20 mixtures did not follow the trend (compared to LS0CNC0.0, LS10CNC0.0, and
 564 LS20CNC0.0 respectively). This could be due to agglomeration of CNCs at higher CNC dosages
 565 as discussed in the previous section on B3B flexural strength. This decrease in pore connectivity
 566 with CNC addition was likely due to increased cement hydration resulting in pore filling and
 567 consequently increasing the bulk resistivity of the mixtures [14, 17, 21, 100].

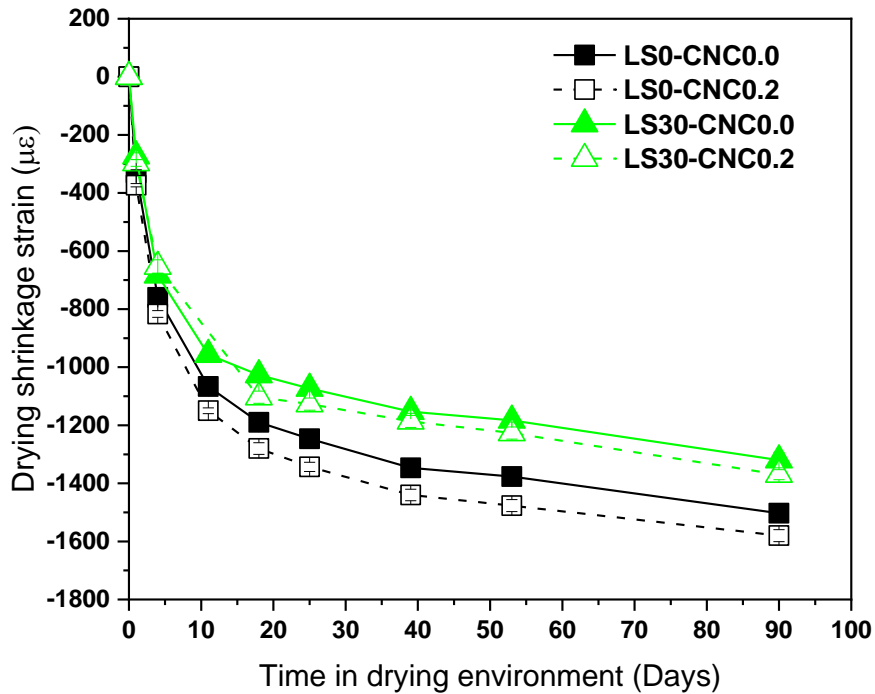


568

569 Figure 10. Pore connectivity in mixtures with and without CNCs at 28 days. The ends of the
 570 error bars shown here represent the measured values and the markers show the average value of
 571 the two samples.

572 3.5.5. Drying shrinkage

573 The drying shrinkage test results of the mixtures LS0-CNC0.0, LS0-CNC0.2, LS30-CNC0.0, and
 574 LS30-CNC0.2 are shown in Figure 11.



575

576

Figure 11. Drying shrinkage results of the mortar specimens

577

It was observed that LS0 mixtures with CNC had a slightly higher shrinkage strain than the mixture without CNC. After 90 days of exposure to the drying environment, a maximum difference of 5% of average shrinkage strain was observed between the LS0 mixtures with and without CNCs. The observed slightly higher shrinkage strain could probably be due to higher clinker hydration with the CNCs addition. For LS30 mixtures, there was no statistically significant difference in drying shrinkage strain between the mixtures with and without CNCs.

578

579

580

581

582

583

3.5.6. Dynamic vapor sorption

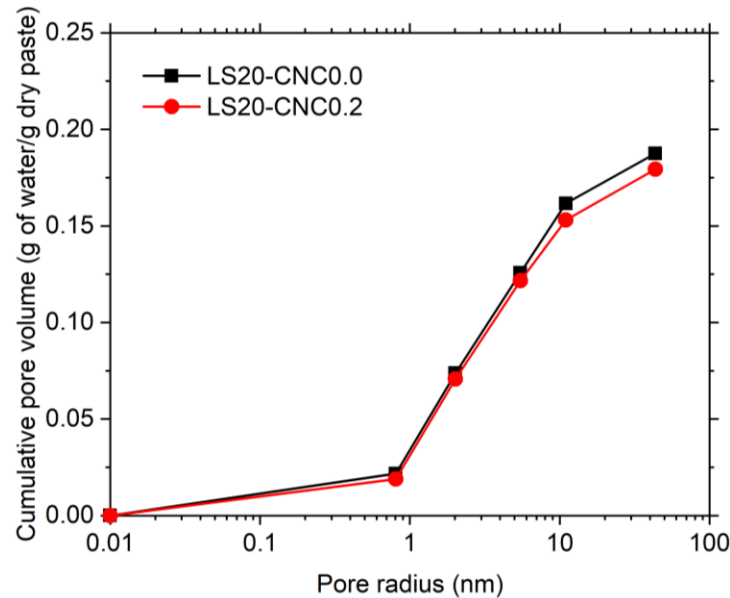
584

Figure 12 shows the cumulative pore volume determined for the LS20 paste samples with and without CNC. It was observed that the cumulative pore volumes are similar for the LS20 samples and not affected by the CNC addition. Figure 13 shows the pore size distribution of LS20 samples with and without CNC.

585

586

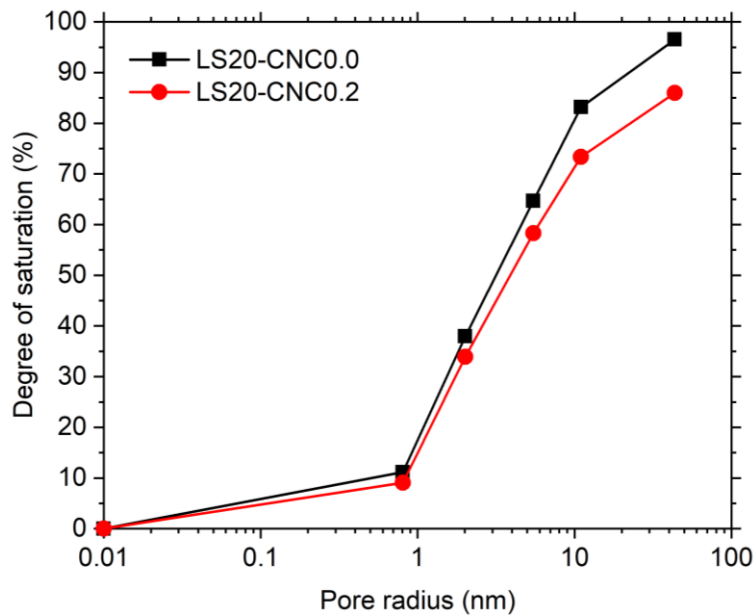
587



589

590

Figure 12. Cumulative pore volume of LS20 paste samples with and without CNC



591

592

Figure 13. Pore size distribution of LS20 paste samples with and without CNC

593 The pores in the sample can be classified as capillary pores (with pore radius ≥ 5 nm) and gel pores
 594 (with pore radius < 5 nm) [86]. From Figure 13, it was observed that the degree of saturation of
 595 LS20-CNC0.2 mixture is slightly lower than LS20-CNC0.0 mixture indicating higher fraction of
 596 capillary pores (and any entrapped air voids) in the LS20-CNC0.2 mixture. Despite the higher

597 fraction of capillary pores in LS20-CNC0.2 when compared to LS20-CNC0.0, it should be noted
598 that the pore connectivity (β) in LS20-CNC0.2 mixture was 8% lower than LS20-CNC0.0 mixture.

599 3.5.7. Thoughts on developing “greener” mixtures with CNCs

600 The approach studied here has two components with respect to making concrete greener. The first
601 component is to replace a part of OPC in the mixture by LS as it would reduce the GHG emissions.
602 The second component is to add CNCs to the mixture to augment the properties of mixtures with
603 LS. Replacing OPC with LS (>15%) can result in a decrease in bulk resistivity at high replacement
604 levels due to dilution effects (45). However, with CNC addition, an increase in bulk resistivity was
605 observed and compensated for the dilution effects. The following assumptions are made to
606 calculate the GHG emissions using the life cycle inventory (LCI) calculation tool developed by
607 Miller et al [41, 101]:

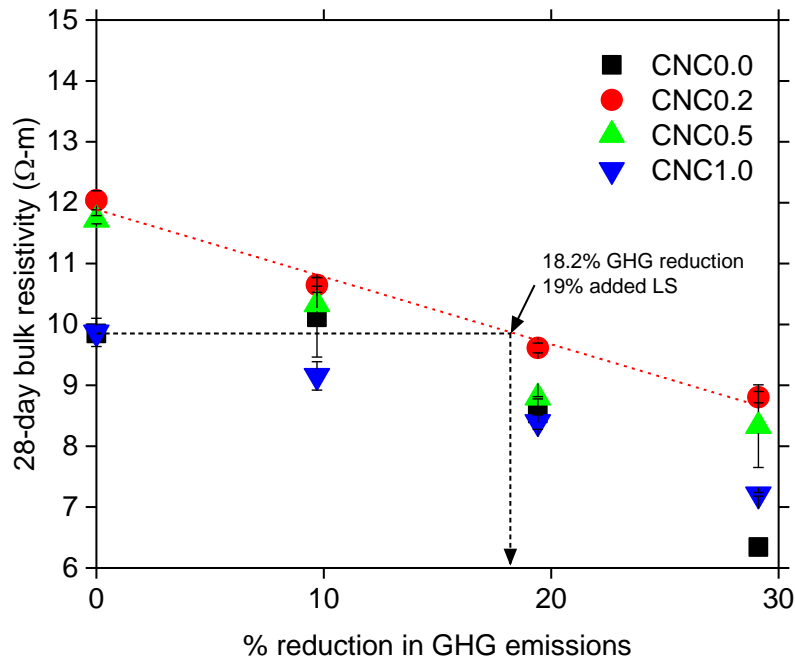
- 608 • The transportation distances for ingredients were assumed based on previous research
609 conducted [41, 101].
- 610 • All mixtures contain the same quantities of aggregates and chemical admixtures.
- 611 • A cradle-to-gate option (A1 to A3) was considered for evaluating emissions associated.
612 Only the emissions associated with raw material transport, manufacturing, batching, and
613 end of life were included here. In terms of life cycle assessment (LCA) modules, for the
614 raw materials and concrete production stage, LCA modules A1-A3 were considered.
615 Batching raw materials for concrete was considered the boundary for this phase.
616 Additionally, for end-of-life emissions associated, LCA modules C1-C4 was considered.
617 The emissions associated with the “in use” phase of concrete (i.e. B1-B7) and recycling
618 (i.e. LCA module D) was not considered here. LCA modules A4 and A5, associated with
619 the use phase of concrete were not considered here.
- 620 • Since CNCs are derived from carbon neutral sources, it was assumed that CNCs have
621 negligible CO₂ emissions. It is acknowledged that CNC manufacturing and CNC
622 dispersion in the construction phase (LCA modules A4 and A5) contributes to minor CO₂
623 emissions. The emissions associated with CNCs in a full-scale production environment
624 will depend on the distance of the plant from the raw materials, type of raw materials, and
625 the processing used to manufacture the CNC [102]. Additional research is needed on the
626 LCA of CNC when commercially produced. Work is in progress to evaluate the full LCA
627 of CNCs; however, it is anticipated as lab and pilot plants move to full scale the full LCA
628 of these materials will become more clearly understood. It should be noted that in this paper
629 refrigeration is used to limit fungal growth in the CNCs over the duration of the research
630 project. However, refrigeration is not necessary for full scale applications.
631

632 Figure 14 shows the plot of 28-day bulk resistivity as a function of GHG emissions. A general
 633 form of the linear equation is shown in equation 10 and the parameters m and b for the different
 634 CNC dosages is shown in Table 2.

635
$$\rho_{28\text{-day}} = m_i(f, CNC).GHG + b_i(f, CNC) \quad (\text{Eq. 10})$$

636 where, $\rho_{28\text{-day}}$ is the saturated bulk resistivity at 28 days, m is the slope, GHG is the % GHG
 637 emissions reduced, and b is the intercept on the Y-axis.

638



639

640 Figure 14. 28-day saturated bulk resistivity versus GHG emissions for OPC-LS mixtures with
 641 and without CNCs. The ends of the error bars shown here represent the measured values and the
 642 markers show the average value of the two samples.

643 Maximum reduction in GHG emissions possible with optimal LS and CNC contents was calculated
 644 based on m and b from Table 2. It was found that equivalent performance (in terms of resistivity)
 645 could be achieved by 19% LS addition (22% total LS) with 0.2% dosage of CNCs and this
 646 corresponded to 18.2% reduction in GHG emissions compared to the LS0-CNC0.0 mixture.
 647 Therefore, 20% LS addition with 0.2% CNC dosage was considered, which corresponded to a
 648 19.4% decrease in GHG emissions. A comparison of the other cementitious paste properties is
 649 shown in Table 3, where it was seen that LS20 mixtures with 0.2% CNC addition had similar
 650 performance compared to a 100% OPC mixture with no added CNCs. Further reduction in GHG
 651 emissions (~29%) can be achieved by adding 30% LS and 0.2% CNCs with similar 28-day B3B
 652 flexural strength and slightly lower (~10.6%) 28-day saturated bulk resistivity compared to 100%
 653 OPC mixture. It should be noted that single-operator variability of bulk resistivity measurement

654 according to ASTM C1876-19 should be within 12%, implying that the reduction in bulk resistivity
 655 due to 30% LS and 0.2% CNC addition is not significant compared to 100% OPC mixture.

656 Table 2. Slope (m_i) and intercept (b_i) values for best fit lines

i	CNC dosage (% volume of binder)	m_i	b_i
1	0.0	-0.12	10.53
2	0.2	-0.11	11.89
3	0.5	-0.12	11.55
4	1.0	-0.09	9.97

657 Table 3. Comparison of properties between LS20-CNC0.2 and LS0-CNC0.0 mixtures

Property evaluated	Testing age	LS0-CNC0.0	LS20-CNC0.2	% change
Heat of hydration of clinker (J/g cement)	7 days	301.84	334.86	+10.9%
Non-evaporable water content (g/100g binder)	28 days	14.87 ± 0.00	15.79 ± 0.32	+6.2%
B3B flexural strength (MPa)	28 days	22.17 ± 1.04	19.56 ± 1.48	-11.7%
Saturated formation factor, F_{sat}	28 days	77.57 ± 0.00	75.70 ± 0.63	-2.4%
Overall porosity, Φ	28 days	39.45 ± 0.36%	43.30 ± 0.00%	+3.8%
Pore connectivity, β	28 days	0.0327	0.0305	-6.7%

658
 659 Past research showed that the performance of PLCs (confirming to ASTM C595) was similar to
 660 OPC [37, 38, 42, 98] in terms of mechanical properties and durability and hence is an acceptable
 661 substitute in the push towards sustainability in the concrete industry. The use of PLCs could result
 662 in reducing the GHG emissions by ~10%. Any further LS replacement without added reactive
 663 SCMs would result in a significant reduction in mechanical and transport properties rendering the
 664 possibility of using high LS dosages unfeasible. The addition of CNCs to OPC-LS mixtures
 665 resulted in improved transport properties (which would result in reduced diffusion of deleterious
 666 species) without compromising mechanical properties. The increased degree of hydration at 28
 667 days in OPC-LS mixtures with CNCs indicated that the OPC clinker is utilized more effectively.
 668 Therefore, the addition of CNCs to mixtures containing higher amounts of LS (up to 22%,
 669 including the LS content in OPC) could push this envelope further and pave way for ternary blends
 670 and result in “greener” mixtures without compromising on the performance.

671 3.6. Conclusions

672 OPC-LS-CNC mixtures were studied as a possible method to reduce GHG emissions. The addition
673 of up to 0.5% CNCs to OPC-LS mixtures resulted in an increased degree of hydration of binder at
674 all ages. At early ages, the increase in degree of hydration was attributed to the combined effect of
675 LS and CNCs. At later age, the increased degree of hydration was due to the CNCs.

676 The addition of low dosages of CNCs up to 0.5% resulted in a decrease in pore connectivity of the
677 mixtures and an increase in bulk resistivity of up to 38%. CNCs addition did not have a significant
678 impact on the overall porosity and B3B flexural strength of the mixtures at both 7 and 28 days.
679 Also, the addition of CNCs did not have a significant impact on the drying shrinkage strain of the
680 mortar specimens made with limestone. There was slightly higher (~5%) drying shrinkage strain
681 after 90 days in drying environment for the mixture with OPC and CNC when compared to mixture
682 without CNC, probably due to higher clinker reaction in the presence of CNCs.

683 The addition of 20% LS and 0.2% CNCs together resulted in mixtures with ~19% reduced GHG
684 emissions with comparable mechanical and transport properties to the conventional 100% OPC
685 mixture. Higher GHG emission reductions up to ~29% can be achieved by adding 30% LS and
686 0.2% CNCs resulting in mixtures with similar mechanical properties and slightly lower (~11%)
687 bulk resistivity. These findings pave way to explore the use of CNCs to achieve further lower GHG
688 emissions and develop “greener” mixtures.

689

690 **4. CHAPTER 3: Performance of Mixtures with SCMs and CNCs**

691 As shown in Chapter 2, CNCs can be used to improve the performance of mixtures with limestone
692 by increasing the degree of hydration and providing a way to reduce GHG emissions. To further
693 reduce the GHG emissions, this research also evaluated the use of SCMs to replace the cement
694 along with using CNCs. Therefore, the extended goal of this project, and the objective of this
695 chapter, is to evaluate the performance of CNCs in mixtures with SCMs.

696 **4.1. Constituent Materials and Characterization Procedures**

697 **4.1.1. Materials**

698 Commercially available Type II OPC and a PLC made using the same clinker as OPC were used
699 for this study. SCMs considered in this study were fly ash (FA), slag (SL), and silica fume (SF).
700 The chemical composition and particle size parameters of the OPC, PLC, and the SCMs are shown
701 in Table 4. X-ray fluorescence was used to determine the chemical composition of the materials,
702 LOI was determined using a furnace, and particle size parameters were determined using laser
703 diffraction technique. The detailed procedures for the material characterization and testing were
704 described in Chapter 2. CNCs that were obtained in the form of suspension with 11% w/w CNC
705 solids were used. The CNCs were manufactured by Forest Products Laboratory using sulfuric acid
706 hydrolysis process. Four CNC concentrations used were 0%, 0.2%, 0.5%, and 1.0% solid volume
707 by volume of binder.

708
709

Table 4. Chemical composition and particle size parameters of the OPC, PLC, and SCMs (NA: not applicable)

%	Cement		SCMs		
	OPC	PLC	Fly Ash (FA)	Slag (SL)	Silica Fume (SF)
SiO ₂	19.95	18.38	51.86	31.58	95.88
Al ₂ O ₃	3.95	3.62	21.70	12.13	0.69
Fe ₂ O ₃	2.28	2.07	5.04	0.55	0.12
CaO	63.32	61.69	8.61	41.34	0.70
MgO	1.43	1.33	2.58	6.97	0.26
SO ₃	2.55	2.48	0.78	3.75	0.15
LOI	2.71	6.42	1.42	0.00	4.30
Na ₂ O	0.21	0.22	2.58	0.24	0.16
K ₂ O	0.48	0.44	1.45	0.28	0.49
TiO ₂	0.19	0.18	1.19	0.47	0.01
P ₂ O ₅	0.10	0.10	0.23	0.00	0.05
ZnO	0.01	0.01	0.02	0.00	0.06
Mn ₂ O ₃	0.07	0.07	0.03	0.19	0.04
Cl	0.003	0.003	0.01	0.00	0.01
Limestone	4.31	13.32	NA	NA	NA
d ₅₀ (μm)	10.52	15.70	13.01	29.08	4.96
d ₉₀ (μm)	27.89	59.18	44.62	87.81	11.28

710

711 Several binder combinations that are currently accepted by CALTRANS were used in this study.
712 The OPC and PLC were used with 50% SL, 20% FA + 5% SF, and 25% FA + 25% SL. All the
713 considered binder combinations were evaluated with and without CNCs.

714 **4.1.2. Paste mixing and sample preparation**

715 The cementitious materials were dry mixed for 90 s using a vacuum mixer at 400 rpm and 70%
716 vacuum. The CNC dispersed mix water was placed in a mixing bowl, and the dry mixed
717 cementitious materials were added, and mixed using a vacuum mixer (Renfert Inc. model
718 18281000) for 90 s at 400 rpm and a 70% vacuum level. The mixing cup was scraped using a
719 silicone spatula for 15 s, and vacuum mixing was carried out for an additional 90 s. Pastes were
720 prepared at a water to binder ratio of 0.40. The prepared pastes were cast in 50 mm diameter and
721 100 mm length cylinder molds. The cylinder molds with the fresh pastes were rotated on a roller
722 at 60 rpm for 12 hours to prevent any bleeding and they were kept sealed until testing.

723 **4.1.3. Tests on cementitious pastes**

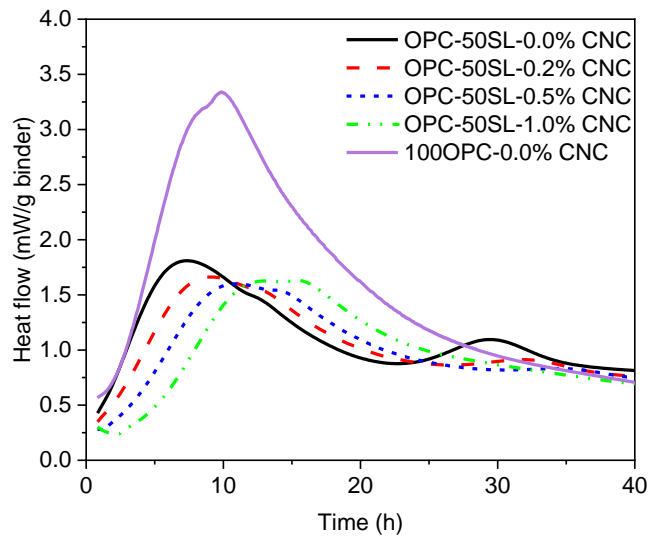
724 All the paste mixtures were tested for heat release (and heat flow), B3B flexural strength, porosity,
725 and saturated bulk resistivity. Heat release (and heat flow) were measured using isothermal
726 calorimetry for seven days. The samples were tested for B3B flexural strength at 28 and 56 days.
727 Samples were tested for porosity and bulk resistivity at 28 and 56 days. All samples were sealed
728 after casting until the age of testing. The detailed procedures for testing the samples were reported
729 in Chapter 2 and not repeated here for brevity.

730 **4.2. Experimental Results and Discussion**

731 **4.2.1. Heat flow**

732 Figure 15a-f shows the heat flow (rate of heat release) for the OPC-SCM and PLC-SCM mixtures
733 up to first 40 hours. For all the SCM mixtures, CNC addition resulted in a slight retardation
734 (indicated by the curve shifting to the right) compared to mixtures without CNC. This retardation
735 causes a delay in the set time and the onset of the acceleration period. A higher CNC dosage
736 caused a longer retardation. Similar observation was made in Chapter 2 where CNCs were used
737 along with OPC and limestone. The heat flow peak intensity of the PLC-SCM mixtures is lower
738 compared to OPC-SCM mixtures because of additional reduction of clinker from LS replacement.
739 A secondary peak after approximately 24 hours was observed that requires further study.

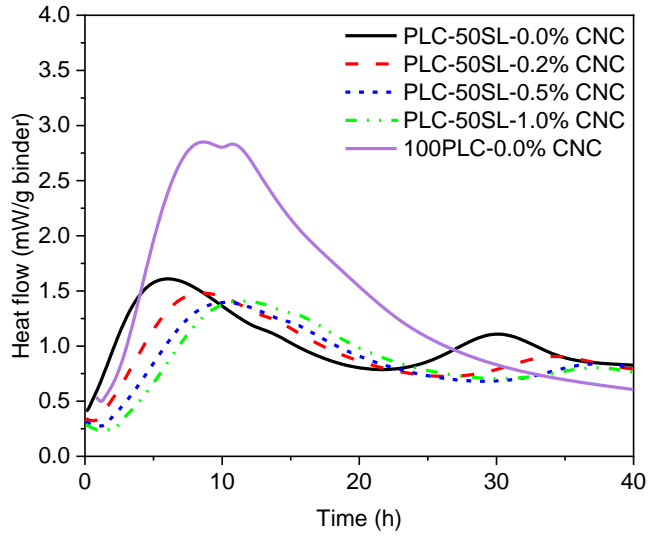
740



741

742

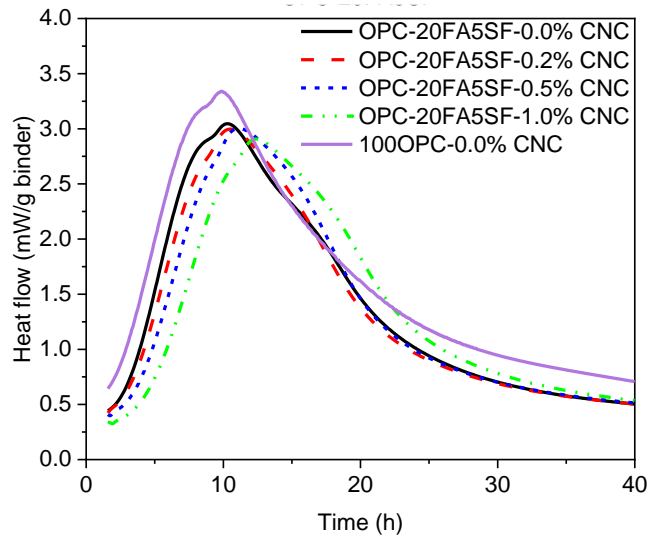
(a)



743

744

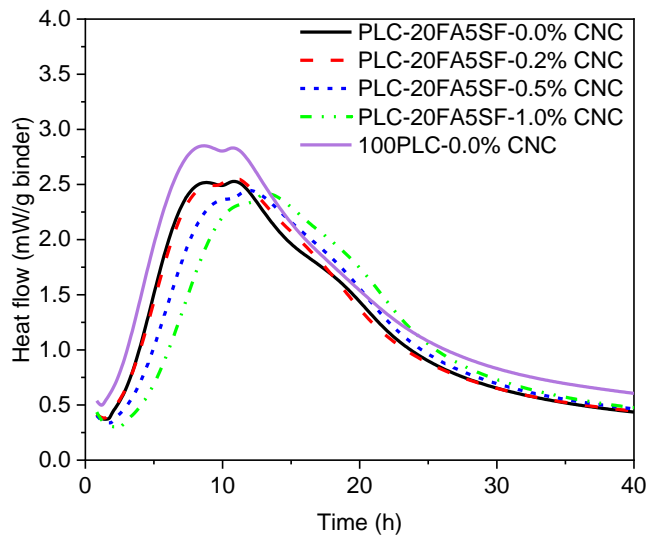
(b)



745

746

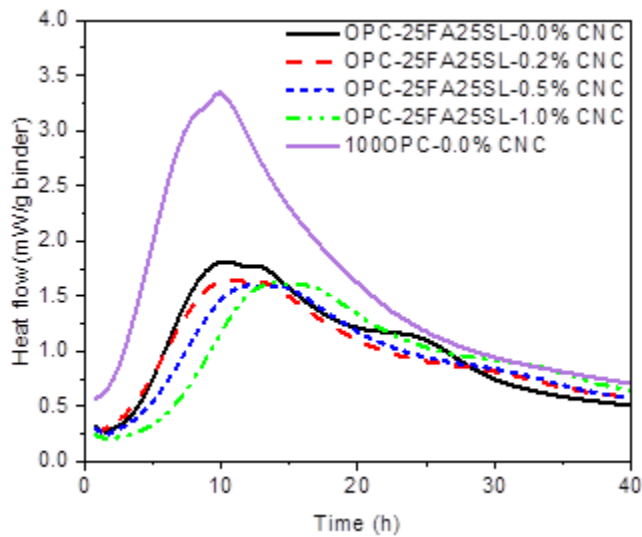
(c)



747

748

(d)

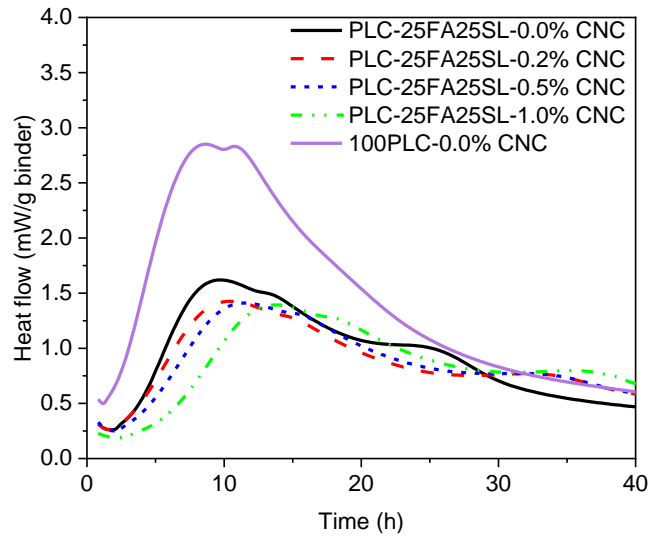


749

750

751

(e)



(f)

752

753

754 Figure 15. Change in heat flow with varying CNC dosage – (a) OPC-50SL (b) PLC-50SL (c)
755 OPC-20FA5SF (d) PLC-20FA5SF (e) OPC-25FA25SL (f) PLC-25FA25SL

756 In case of OPC-SL50 mixture (Figure 15a), the shift in the silicate peak ranged from 1.5 hours
757 (0% CNC) to 6.5 hours (1% CNC). In case of PLC-SL50 mixtures (Figure 15b), the filler effect
758 of LS in the PLC caused an acceleration in the 0% CNC mixture (compared to the 100OPC-
759 CNC0.0 mixture), but with increase in CNC dosage, the peak shifted with CNC content to later
760 ages (i.e., from 2 hours (0% CNC) to 5 hours (1% CNC)). In both OPC-SL50 and PLC-SL50
761 mixtures, the slag hydration peak, characterized by the third peak (after approximately 24 hours)
762 had lower intensity with CNC addition. For instance, in OPC-SL50-0.0% CNC mixture the slag
763 hydration peak intensity was 1.2 mW/g binder occurring at 30 hours, whereas for the mixtures
764 with CNC, the peak was shifted to 35 hours with a lower heat flow intensity of 1 mW/g binder. A
765 similar trend was observed for PLC-SL50. It appears that addition of CNCs to OPC/PLC-SL
766 mixtures resulted in retardation of slag hydration.

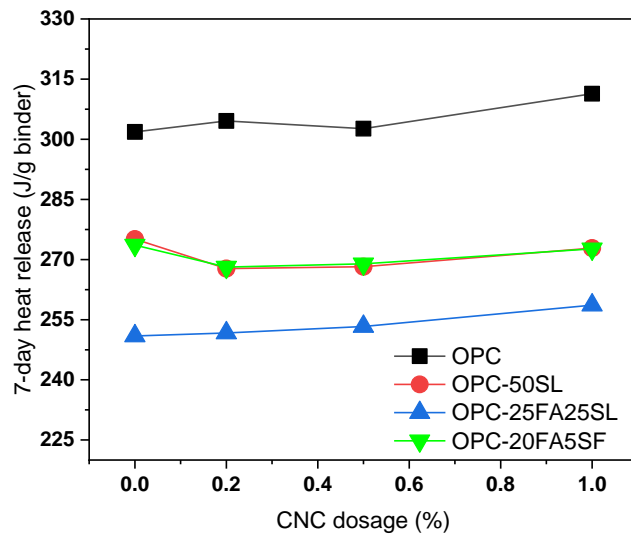
767 For OPC-20FA-5SF (Figure 15c) and PLC-20FA-5SF (Figure 15d) mixtures, the observed trends
768 are similar. Any retardation in the pastes due to the presence of fly ash is compensated by the
769 presence of SF in 0% CNC mixtures. In case of mixtures with CNC, there appears to be a
770 retardation by 3 hours (OPC mixtures) and 5 hours (PLC mixtures). For mixtures with OPC-25FA-
771 25SL (Figure 29e) and PLC-25FA-25SL (Figure 29f), similar trends are observed; with increase
772 in CNC dosage, there is a shift in the silicate hydration peak to the right by a maximum of three
773 hours. However, a much longer retardation (as long as 10 hours) of the peak associated with the
774 slag hydration was observed at higher CNC dosage.

775 In all cases, the aluminate peak (or the sulfate depletion peak) for the mixtures with CNC had a
776 higher intensity compared to mixtures without CNCs. In case of FA mixtures, the silicate and the

777 aluminate peaks overlapped, indicating that CNC addition may be close to causing a sulfate
778 imbalance like conditions, similar to the observations made for mixtures with LS and CNCs.

779 Figure 16 shows the 7-day heat release for the mixtures studied here. The 7-day heat release values
780 for OPC-SCM ranged from 302 – 311 J/g binder for OPC mixtures, 268 – 275 J/g binder for OPC-
781 50SL mixtures, 251 – 259 J/g binder for OPC-25FA25SL mixtures, and 268 – 274 J/g binder for
782 OPC-20FA5SF mixtures when CNC dosages were varied from 0 – 1% by volume of binder. The
783 7-day heat release values for the PLC-SCM mixtures ranged from 285 – 287 J/g binder for PLC
784 mixtures, 247 – 258 J/g binder for PLC-50SL mixtures, 233 – 241 J/g binder for PLC-25FA25SL
785 mixtures, and 248 – 251 J/g binder for PLC-20FA5SF mixtures when CNC dosages varied from 0
786 – 1% by volume of binder.

787



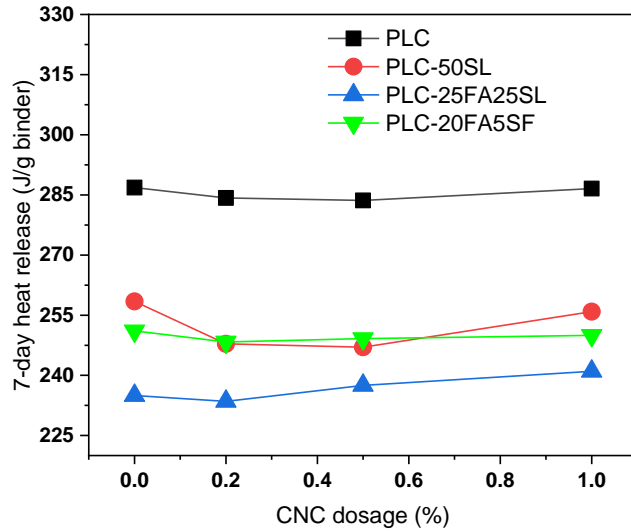
788

789

(a)

790

791



(b)

792

793

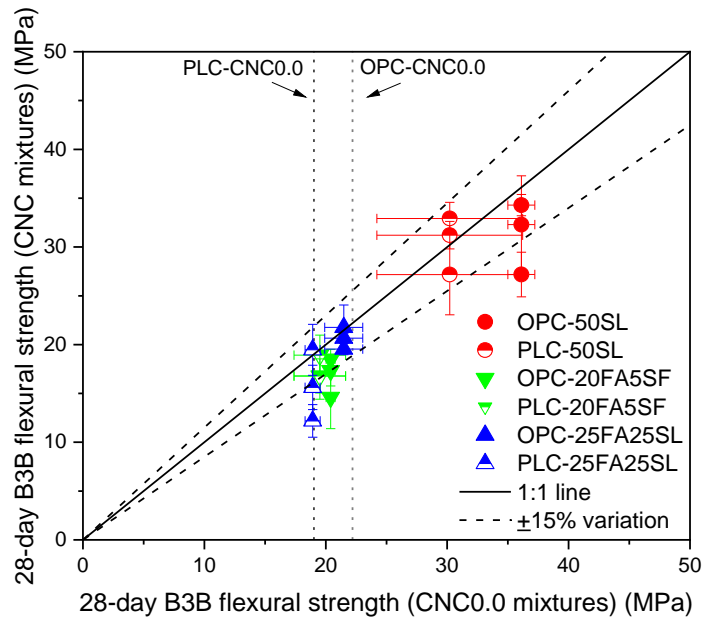
794 Figure 16. Effect of CNC dosage on 7-day heat release (a) OPC mixtures (b) PLC mixtures

795 It was observed that overall, the CNCs addition did not significantly affect the 7-day heat release
 796 value of the mixtures with SCMs. The 7-day heat release values of the mixtures with CNCs were
 797 usually within $\pm 2\%$ of the 7-day heat release values of the respective mixtures without CNCs.
 798 When CNCs were added at low dosages of 0.2 and 0.5% to PLC-50SL mixture, it was observed
 799 that the 7-day heat release was reduced by 4.1 and 4.4%, respectively, and this needs to be further
 800 investigated. When CNCs were added at 1.0% dosage to OPC-25FA25SL and PLC-25FA25SL
 801 mixture, the 7-day heat release values were increased by 3.1 and 2.6%, respectively. The
 802 adsorption behavior of CNCs on SCMs is not known, and it could be playing an important role in
 803 terms of reaction rate of SCMs. More research work is needed to explain possible mechanisms for
 804 the role of CNCs in hydration of SCM mixtures.

805 **4.2.2. B3B flexural strength**

806 Figure 17 shows a parity plot for the 28-day and 56-day B3B flexural strength for the mixtures
 807 with and without CNCs. It should be noted that the B3B flexural strengths indicate characteristic
 808 strength of the mixtures, and they are higher than flexural strength determined using conventional
 809 flexural strength testing due to the size effect.

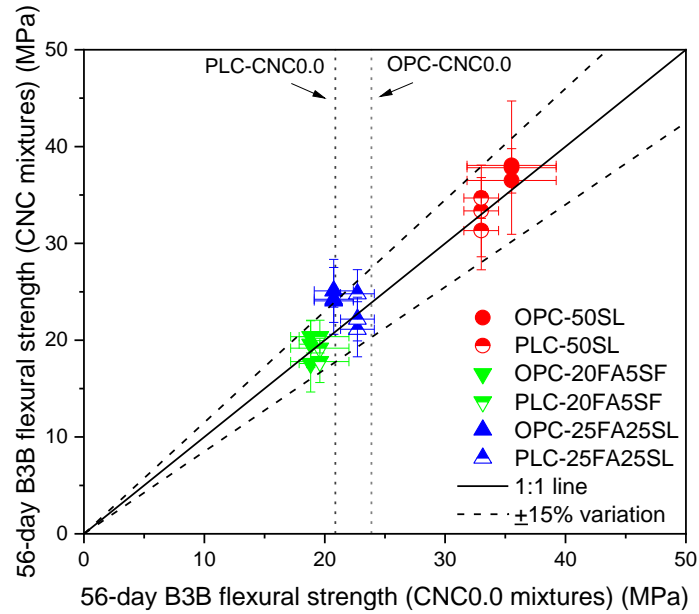
810



811

812

(a)



813

814

(b)

815 Figure 17. Effect of CNC dosage on B3B flexural strength – (a) 28 days (b) 56 days. A data
816 point on the 1:1 line indicates similar performance, and a data point above the 1:1 line indicates
817 better performance for mixtures with added CNCs (i.e., the measurement on the Y-axis).

818 With CNC addition, B3B flexural strength of the most mixtures were within 15% of the flexural
819 strength of the mixtures without CNC. The 28-day B3B flexural strengths of the mixtures that had
820 lower than 15% of the B3B flexural strengths of the mixtures without CNC were OPC-50SL-
821 CNC1.0, OPC-20FA5SF-CNC0.5, and PLC-25FA25SF-CNC0.5. With the exception of the three
822 mixtures, it can be said that the addition of CNCs did not have an adverse effect on the 28-day
823 flexural strengths of the mixtures with SCMs.

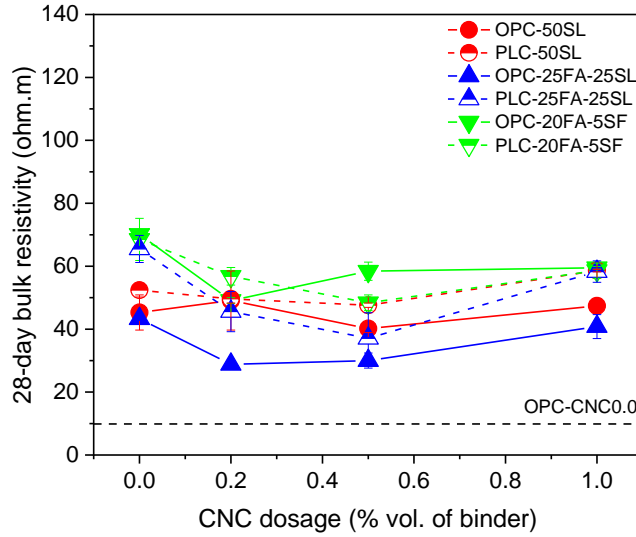
824 It was observed that the mixtures with PLC and SL, PLC-50SL and PLC-25FA25SL, had
825 improved strength from 28 days to 56 days. No adverse effects of adding CNCs in terms of flexural
826 strength was seen at 56 days, as none of the mixtures with CNCs had lower than 15% of the flexural
827 strength of the mixtures without CNCs. It was observed that 56-day B3B flexural strength of OPC-
828 25FA25SL mixtures with CNC had slightly higher (by 1 to 6%) than 15% of the B3B flexural
829 strength of the OPC-25FA25SL-CNC0.0.

830 **4.2.3. Bulk resistivity and pore structure characteristics**

831 The 28-day and 56-day saturated bulk resistivity values of the mixtures with OPC, PLC, and
832 different SCMs are shown in Figure 18. Bulk resistivities of the SCM mixtures with and without
833 CNCs were significantly higher than the OPC-CNC0.0 mixtures at both 28 and 56 days as seen in
834 Figure 18. Overall, the mixtures with 20FA5SF had the highest bulk resistivity among the mixtures
835 tested, likely due to the inclusion of finer material like silica fume that contributed to a reduction
836 in pore connectivity. At 28 days, the bulk resistivity of the SCM mixtures, except OPC-50SL,
837 decreased with the addition of CNCs at low dosages (0.2 and 0.5%) and increased at higher dosage
838 of 1.0% CNC. Only OPC-50SL and PLC-50SL had slightly higher 28-day resistivities (4.6 and
839 11.8%, respectively) at 1.0% CNC dosage when compared to the respective mixtures without
840 CNC. For OPC-50SL, the 28-day bulk resistivity of the mixtures were between 40.2 ohm.m and
841 47.4 ohm.m with varying CNC dosage.

842

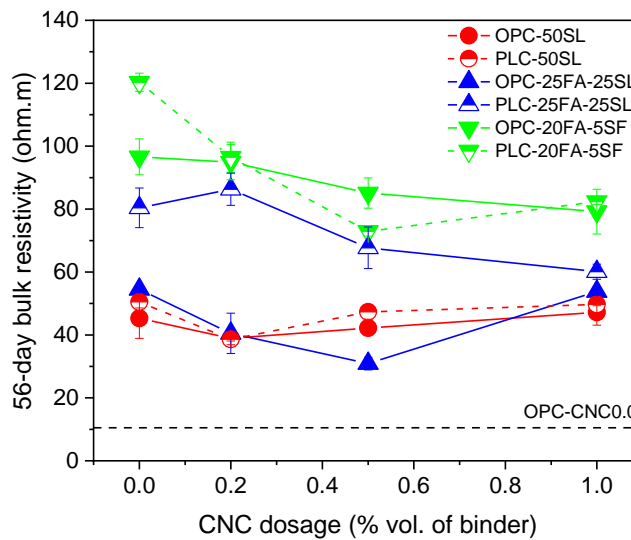
843



844

845

(a)



846

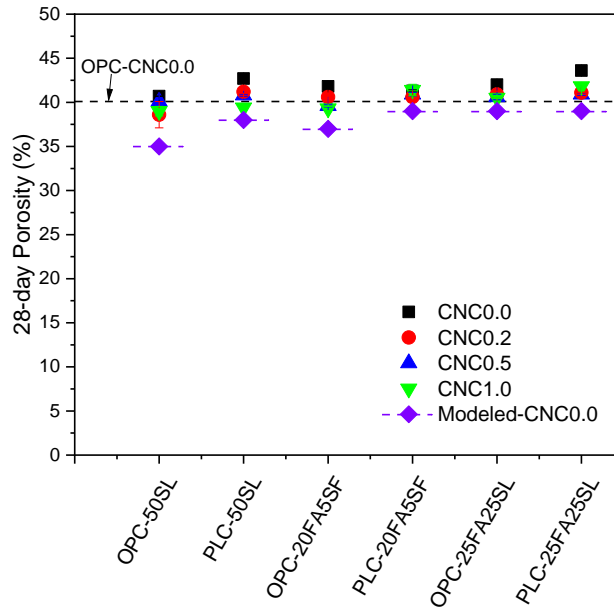
847

(b)

848 Figure 18. Effect of CNC addition on saturated bulk resistivity of the mixtures with SCMs (a) 28
849 days (b) 56 days.

850 At 56 days, it was observed that with the addition of CNCs, the bulk resistivities were decreased
851 for most of the mixtures. The decrease in bulk resistivity with CNC addition ranged from 1.3% to
852 43.3%. The two mixtures that had higher bulk resistivity compared to their respective mixtures
853 without CNC were OPC-50SL-CNC1.0 (higher by 4.2%) and PLC-25FA25SL-CNC0.2 (higher
854 by 7.3%). The possible reasons for the overall trend of reduction in bulk resistivities with the
855 addition of CNCs to the SCM mixtures include agglomeration of CNCs when SCMs are present
856 and possible adsorption of CNCs on SCMs resulting in slower reaction of SCMs. A comparison

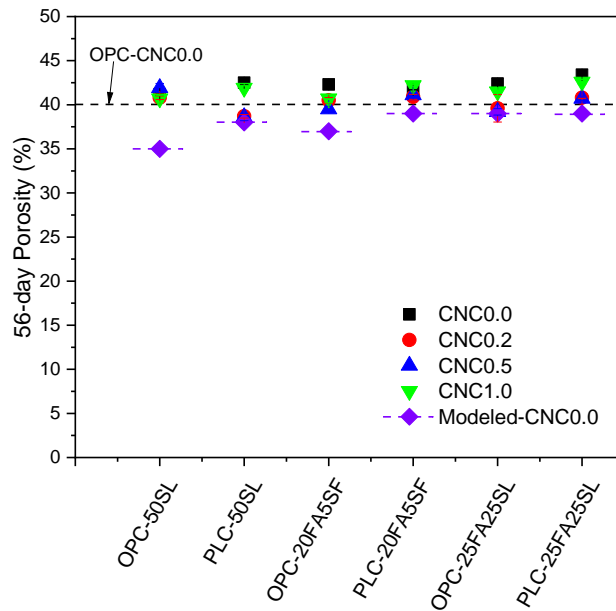
857 study is underway evaluating the long-term resistivity and chloride transport properties. The 28-
 858 day and 56-day porosity data for the different mixtures with and without CNCs is shown in Figure
 859 19. A thermodynamic modeling approach was used to provide an idea of how much porosity of
 860 the samples would vary with different SCMs and SCM contents.



861

862

(a)



863

864

(b)

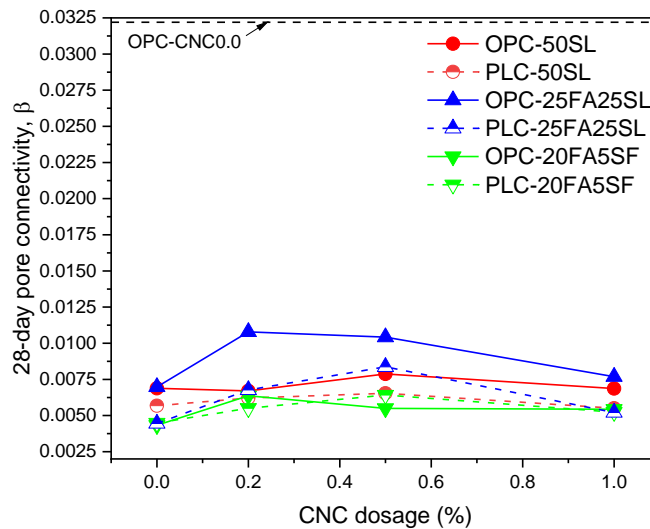
865

Figure 19. Porosity of the paste samples at (a) 28 days (b) 56 days

866 The porosity of CNC0.0 mixtures determined from thermodynamic modeling is shown in Figure
 867 19 as a baseline to compare the porosity of mixtures with and without CNCs. The porosity of the
 868 mixture OPC-CNC0.0 is also shown in Figure 19 as a reference. Minimal changes in total porosity
 869 of the samples were observed when CNCs were added, and the variation was less than 3% for the
 870 most mixtures and less than 4% for all the mixtures when compared to the corresponding mixtures
 871 without CNCs. The mixtures that had more than 3% difference in porosity between the mixtures
 872 with CNC and without CNC were PLC-50SL (CNC1.0 mixture at 28 days with 3.3% difference
 873 and 56 days with 3.9% difference) and OPC-25FA25SL (CNC0.5 mixture at 56 days with 3.2%
 874 difference).

875 The pore connectivity (β) of the mixtures determined at 28 days and 56 days are shown in Figure
 876 20. It was observed that the pore connectivity of the SCM mixtures was significantly lower than
 877 the OPC-CNC0.0 mixture as SCMs are known to improve the pore refinement. With the addition
 878 of CNCs to the SCM mixtures, differences in the determined pore connectivity values were
 879 observed. It was observed that the pore connectivity of the mixtures with CNCs were generally
 880 higher than the respective mixtures without CNCs. Again, it is important to remember that SCMs
 881 are even more effective at later ages so longer-term testing is still needed.

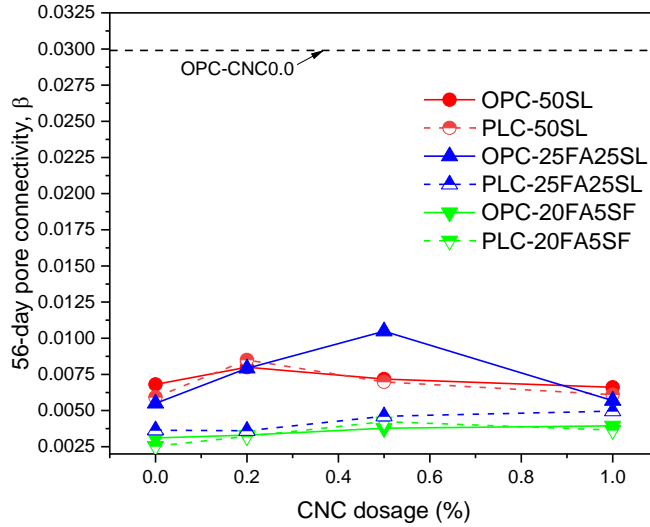
882



883

884

(a)



885

886

(b)

887 Figure 20. Effect of CNC dosage on pore connectivity (β) in the pastes (a) 28 days (b) 56 days

888 At 28 days, except the OPC-50SL mixture, the pore connectivity values peak at 0.2 or 0.5% CNC
 889 dosage and reduce at 1.0% CNC dosage. In the case of OPC-50SL mixture, the 28-day pore
 890 connectivity values were very similar at all CNC dosages except at 0.5% CNC dosage. Similar
 891 trend was observed with 56-day pore connectivity values where it peaks at either 0.2 or 0.5% CNC
 892 dosage and slightly reduces at 1.0% CNC dosage, with the exception of OPC-20FA5SF and PLC-
 893 25FA25SL mixtures where the pore connectivity increased with increase in CNC dosage. The 28-
 894 day pore connectivity values of the SCM mixtures ranged from 0.0045 to 0.0108, which are
 895 significantly lower (by 66 - 86%) when compared to pore connectivity value (0.0322) of OPC-
 896 CNC0.0 mixture. The 56-day pore connectivity values of the SCM mixtures ranged from 0.0025
 897 to 0.0105, which are significantly lower (by 65 - 92%) when compared to pore connectivity value
 898 (0.0299) of OPC-CNC0.0 mixture. The general increase in pore connectivity values with the CNC
 899 dosage can explain the general decrease in saturated bulk resistivity of the SCM mixtures with
 900 CNCs as the porosity did not significantly change with the CNC addition.

901 4.3. Conclusions

902 OPC-SCM-CNC and PLC-SCM-CNC mixtures were evaluated for CNCs use in the mixtures with
 903 SCMs. Overall, CNCs addition to the SCM mixtures did not significantly affect the 7-day heat
 904 release values, except the 25FA25SL mixtures where a reduction of up to 4.4% in 7-day heat
 905 release at low CNC dosages. In the mixtures with 25FA25SL, there was up to 3.1% increase in 7-
 906 day heat release at 1.0% CNC dosage. The interaction between CNCs and SCMs need to be
 907 understood to clearly explain the effect of CNCs on the degree of hydration of the SCM mixtures,
 908 and ongoing work is currently underway.

909 The 28- and 56-day B3B flexural strength of the majority of the SCM mixtures with CNC were
910 within $\pm 15\%$ of the flexural strength of the respective mixtures without CNC. At 56 days, the
911 addition of CNCs improved the flexural strength of OPC-25FA25SL mixtures by 16 (at 1.0%
912 CNC) – 21% (at 0.5% CNC).

913 The addition of low dosages of CNCs up to 0.5% resulted in an overall increase in pore
914 connectivity of the SCM mixtures and reduction in bulk resistivity measured at 28 and 56 days. It
915 was noted that the 28-day pore connectivity values of the SCM mixtures ranged from 0.045 to
916 0.0108, which were significantly lower than the 28-day pore connectivity value of 0.0322 for OPC-
917 CNC0.0 mixture. The 56-day pore connectivity values of the SCM mixtures ranged from 0.025 to
918 0.0104, which were again significantly lower than the 56-day pore connectivity value of 0.0299
919 for OPC-CNC0.0 mixture. The 56-day saturated bulk resistivity values ranged from 30.9 to 120.3
920 ohm.m for the mixtures with SCMs depending on type of SCM and CNC dosage, which were
921 significantly higher than the 56-day bulk resistivity value of 10.5 ohm.m for OPC-CNC0.0
922 mixture.

923 The overall trend of reduction in bulk resistivities and increase in pore connectivity with the
924 addition of CNCs to the SCM mixtures could be due to the agglomeration of CNCs, alteration of
925 the pore structure due to delayed early hydration, and possible adsorption of CNCs on SCMs
926 resulting in lower reaction of SCMs. Further research is needed to understand the adsorption
927 behavior of CNCs on SCMs and evaluate the resulting effect on the performance of the SCM-CNC
928 mixtures. Future research shall also include studying the effect of reduction in pH of the pore
929 solution in the SCM mixtures on CNCs performance in the mixtures.

930 **5. CHAPTER 4: Full Scale Field Trials of Slabs Placement using Mixtures with**
931 **Limestone and CNCs at UC Davis Pavement Research Center**

932 This chapter of the report summarizes the results of the implementation of the use of cellulose
933 nanocrystals (CNC) in portland cement concrete (PCC) pavement. In this experiment, the use of
934 CNC is evaluated in combination with portland-limestone cement (PLC) and compared with
935 ordinary portland cement (OPC) concrete in a set of pilot slabs built on the research site of the
936 University of California Pavement Research Center (UCPRC) in Davis, California.

937 **5.1. Test Sections Preparation**

938 Three test sections were built for three mixtures. The three mixtures were i) OPC mixture with
939 30% slag (labelled as OPC), ii) PLC mixture with 30% slag (labelled as PLC), and iii) PLC mixture
940 with 30% slag and 0.1% CNC (labelled as CNC). The location of the test sections is shown in
941 Figure 21 (picture taken after the application of the curing compound on the lean concrete base)
942 and Figure 22 (picture taken after the construction of the concrete slabs).



943

944 Figure 21. Location of test sections (white path at the bottom of the picture; picture taken after
945 the application of the curing compound on the lean concrete base).



946

947

Figure 22. Test sections (from picture bottom to top: PLC, CNC, and OPC)

948

5.1.1. Test sections configuration

949

The test sections were designed to study mixture constructability and mid-term (less than a year) ambient environmental response. While mechanical and durability characteristics of the mixtures are important as well, they do not constitute the main focus of the test sections experiment. Mechanical properties were evaluated based on laboratory testing of specimens prepared from mixtures sampled during the test sections construction. Limited durability laboratory testing was conducted on specimens also prepared from the construction mixtures.

950

951

952

953

954

955

One of the goals of the experiment is to evaluate the ambient environmental response, focused on moisture-related shrinkage and thermal deformations. To maximize those deformations, the concrete slab thickness was set to a low value, 4 inches and slab width was set to 8 feet, rather than the conventional 12 feet, so that the consolidation could be achieved with a vibrating rolling screed while maintaining the 4-inch slump of the mixtures.

956

957

958

959

960

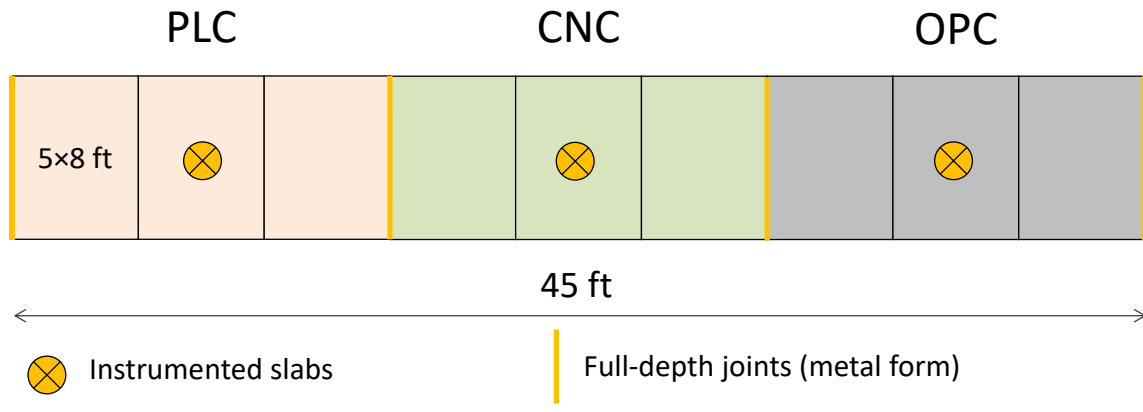
The location of the test sections was selected to build a walking path at the UCPRC site in Davis. The total length of the walking path is approximately 70 feet, with an approximately 45 feet useful length that is not affected by shading from nearby buildings so that uniform solar exposure could be obtained. The three test sections, one per mixture type, were built along the useful length. Each section consists of three 5 foot long slabs as shown in Figure 23.

961

962

963

964

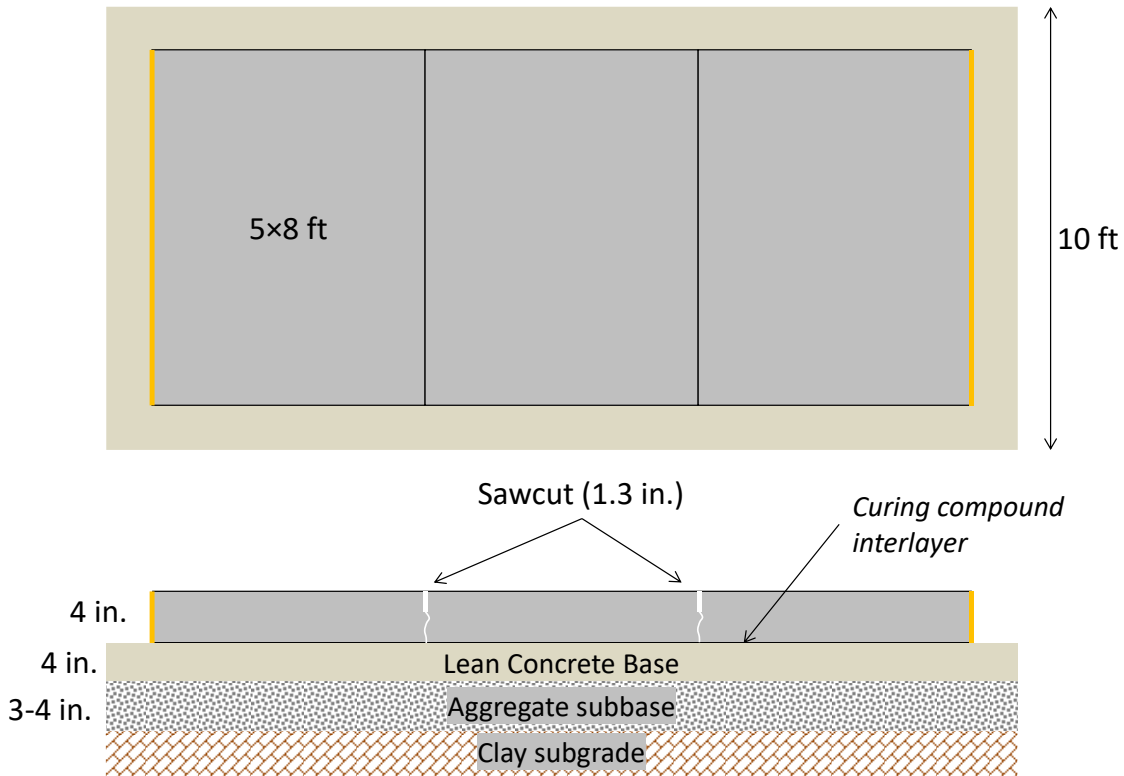


965

966

Figure 23. Test sections layout

967 Beneath the 5x8 ft (length x width) and 4 inch thick slabs is a lean concrete base that is 4 inch
 968 thick, which in turn was placed on a 3 to 4 inch thick aggregate subbase (Figure 24). The subgrade
 969 is clay. The shoulder was backfilled with loose aggregates after the construction of the concrete
 970 slabs.



971

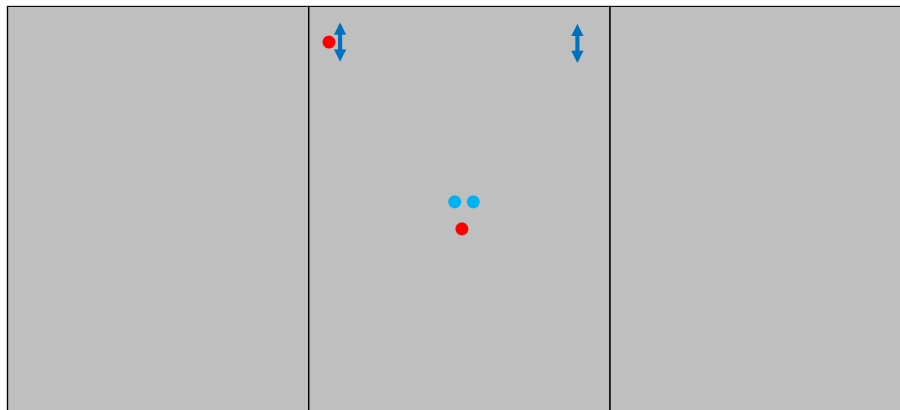
972

Figure 24. Test section configuration

973 **5.1.2. Test section instrumentation**

974 The instrumentation installed in each of the sections, shown in Figure 25, focuses on measuring
975 the response to the ambient environment loading. The instrumentation of each section includes:

- 976 • Two thermocouples on rods for measuring temperature profile in the slabs and base.
- 977 • Two relative humidity (RH) sensors. The RH sensors are Sensirion SHT85, housed in
978 a porous plastic tube.
- 979 • Two pairs of GeoKon 4200 vibrating wire strain gages (VWSGs), located at two of the
980 slab corners, 10 in. from the shoulder edge of the slabs. Each pair includes a VWSG
981 close to the top of the slab (0.8 in. from top) and another VWSG close to the bottom of
982 the slab (0.8 in. from bottom).



- Thermocouples rod; five depths: 0.2 in. / 0.8 in. / 2 in. / 4 in. (slab bottom) / 6 in. (lean concrete base)
- RH sensor (0.8 in. Depth)
- ↕ VWSGs; two depths: 0.8 in. / 3.2 in. (0.8 in. above slab bottom)

983

984 Figure 25. Test section instrumentation (Not to scale)

985 In addition to the instrumentation embedded in the test sections, three prisms per concrete mixture
986 were fabricated and instrumented with a VWSG each (Figure 26 left). The prisms are 20×6×1.6
987 in. in size and they are referred as unrestrained shrinkage prisms (USP) in this report. The concrete
988 for the prisms' fabrication was the same used for the construction of the slabs (sampled from the
989 ready-mix trucks) although screened through 3/4 in. sieve to remove the largest aggregates. These
990 prisms were cured the same as the slabs and left outdoors by the test sections so that they were
991 subjected to the same ambient environmental conditions (Figure 26 right). These prisms measure
992 the unrestrained deformations of the concrete as they are not bonded to any support.



993

994

Figure 26. Unrestrained shrinkage prisms

995 **5.2. Materials and Mixtures**

996 The chemical composition and fineness of OPC, PLC, and Ground granulated blast furnace slag
 997 used are shown in Table 5. As expected, the PLC has higher fineness than OPC [38]. The mill
 998 certificates of the cementitious materials are attached in the Appendix section. The three mixtures
 999 were i) OPC mixture with 30% slag (OPC), ii) PLC mixture with 30% slag (PLC), and iii) PLC
 1000 mixture with 30% slag and 0.1% CNC (CNC).

1001 Table 5. Chemical composition and fineness of OPC, PLC, and Slag used (NA: not available)

%	OPC	PLC	GGBFS
SiO ₂	20.3	18.4	NA
Al ₂ O ₃	4.1	3.5	17.5
Fe ₂ O ₃	3.9	3.0	NA
CaO	62.4	58.4	NA
MgO	4.9	4.2	NA
SO ₃	3.1	3.0	2.5
LOI	2.6	10	NA
Na ₂ O	0.19	0.24	0.45
K ₂ O	0.41	0.30	(Na ₂ O _e)
Limestone	3.4	14	NA
Blaine Fineness, cm ² /gm	4184	5470	4780

1002

1003 **5.2.1. OPC mixture**

1004 The OPC mixture design and materials were supplied by Cemex (Perkins plant, in Sacramento
 1005 area). This mixture is used for concrete paving in regular applications where high early strength is

1006 not required. The mixture is designed to achieve the strength needed to open to traffic (550 psi
1007 flexural strength) in 10 days. The mixture design is shown in Table 6.

1008 Table 6. OPC mixture design (1 cy)

Material	Description	Design quantity
Coarse Aggregate	Gravel	1900 lb
Fine Aggregate	Sand	1313 lb
Cement	Type II/V ordinary portland cement (OPC), ASTM C150	413 lb
Ground granulated blast furnace slag (GGBFS)	Slag, Grade 120, ASTM C989	177 lb
Water reducer	Master Glenium 7500	4 oz/cwt
Water	-	34.0 gal

1009

1010 The Type II/V cement was produced by the Cemex Victorville plant (California). The slag was
1011 produced in Rizhao (China); slag content is 30% of total cementitious materials.

1012 For water-reducing admixture, the Master Glenium 7500 was selected after showing acceptable
1013 compatibility with the CNC suspension. The Master Glenium 7500 is a high-range water-reducing
1014 admixture, based on polycarboxylate technology, meeting ASTM C494 Types A and F
1015 specifications. The water-reducer content was based on trial batching conducted with the PLC
1016 mixture by UCPRC. All three mixtures were batched with 4 oz/cwt of Master Glenium 7500
1017 following the mix design.

1018 The water-reducer typically used by the supplier for this mixture, based on lignosulphonate
1019 technology, was assumed to be incompatible with a CNC slurry produced by sulfuric hydrolysis
1020 evaluated in the preliminary phase of this experiment.

1021 Some other properties of the OPC mixture are listed below:

- 1022 • Crushed alluvial aggregates, mainly siliceous
- 1023 • Water/total cementitious ratio is 0.481
- 1024 • Non-air-entrained concrete
- 1025 • Design slump: 4 inches

1026 5.2.2. PLC mixture

1027 The PLC mixture is the same as the OPC mixture except for replacement of the Type II/V cement
1028 with portland-limestone cement (Type IL, ASTM C595), on a one-to-one basis. The Type IL
1029 cement was produced by the Cemex Victorville plant (California). All other materials and
1030 quantities in Table 1 remain the same in the PLC mix

1031 **5.2.3. CNC mixture**

1032 The CNC mixture is the same as the PLC mixture except for the addition of the cellulose
1033 nanocrystals. The added CNC content is 0.1% (CNC solids by weight of total cementitious
1034 materials); this is 0.590 lb of CNC solids per cy of concrete.

1035 The CNC was supplied by Forest Products Laboratory (FPL) and produced by sulfuric acid
1036 digestion (product name: 2022-FPL-CNC-213). According to FPL, from this production method,
1037 CNC has sulfuric half-esters on the surface. The CNC solids are rigid rods typically about 5 nm
1038 wide by 100-150 nm long. The product was supplied as a suspension with 10.4% CNC solids
1039 content.

1040 **5.3. Test Sections Construction**

1041 The subbase was prepared by the UCPRC team in April 2022. The lean concrete base (LCB) was
1042 supplied by Elite ready mix and placed and consolidated by Vanguard on May-6, 2022. The
1043 concrete was supplied by Cemex ready mix plant in Perkins, close to Sacramento, and placed,
1044 consolidated, and cured by UC Davis Facilities Construction team with support from UCPRC on
1045 June-27, 2022. The fresh concrete QC and specimen preparation were conducted by Twining with
1046 support from UCPRC team.

1047 The timing of the construction of the slabs (June-27, 2022) is summarized below:

- 1048 • Ready mix truck 1, CNC mixture: 12:50-12:55
- 1049 • Ready mix truck 2, PLC mixture: 13:55-14:00
- 1050 • Ready mix truck 3, OPC mixture: 14:45-14:50

1051 The weather conditions during paving were dry and warm, with air maximum temperature and
1052 minimum relative humidity (RH) approximately 105°F (40°C) and 15%, respectively. Wind speed
1053 was below 2 mph and the sky was clear. Air minimum temperature and maximum RH, during the
1054 first nights after construction, were approximately 60°F (15°C) and 80%, respectively. Days
1055 following construction had similar weather conditions, typical of Davis during summer.

1056 The concrete was consolidated with a vibrating rolling screed and finished with trowel. No surface
1057 texturing was applied. The curing was conducted with white pigmented, resign based, curing
1058 compound meeting ASTM C309 Type 2B specifications, applied at a nominal rate of 150 ft²/gal.

1059 A few construction pictures are shown in Figure 27 - Figure 29. Figure 28a shows the test section
1060 after the preparation and before the concrete placement. Figure 28b shows the placement of PLC
1061 mixture. Figure 28c shows the use of vibrating rolling screed for the CNC mixture and Figure 28d
1062 shows finishing of OPC mixture.



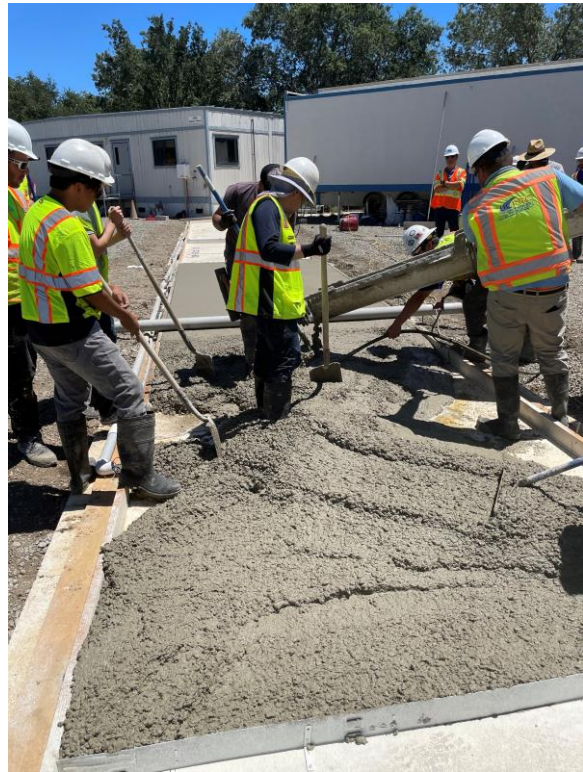
1063

1064
1065

Figure 27. Test section instrumentation; left: thermocouple rod and pair of VWSFs; right: thermocouple rod and two RH sensors



(a)



(b)



(c)



(d)

1066 Figure 28. Slabs construction pictures; (a) before concrete pouring; (b) placing PLC concrete; (c)
 1067 consolidating CNC concrete; (d) finishing OPC concrete section



1068

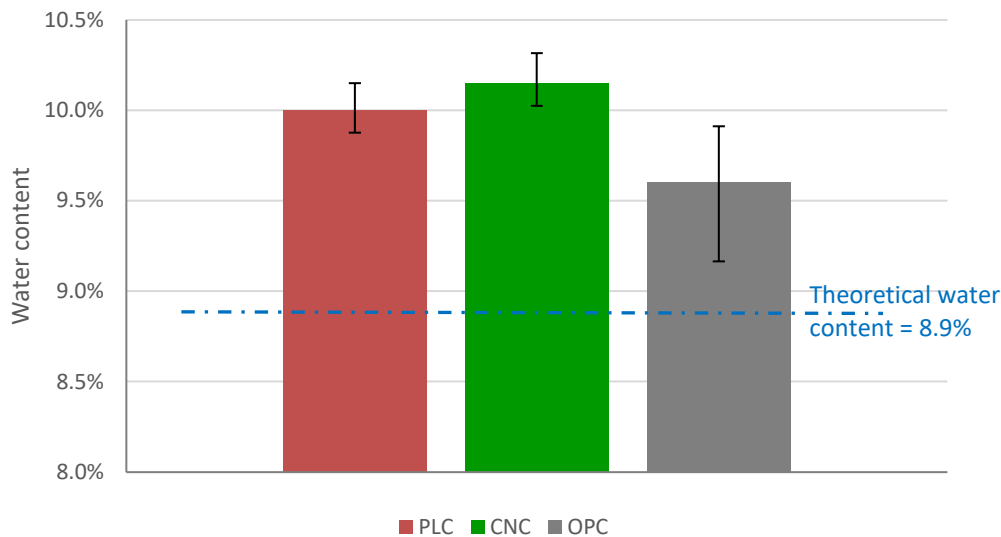
1069 Figure 29. Trowel finishing of PLC section (bottom of photograph); CNC section already
 1070 sprayed with curing compound (middle of photograph; note that white covering is from the
 1071 curing compound and not the CNC effect); rolling screed consolidation of OPC concrete
 1072 (middle-top of photograph).

1073 **5.3.1. Control of water content**

1074 The three mixtures (OPC, PLC, and CNC) all have a design water to cementitious materials ratio
1075 of 0.481, equivalent to 34.0 gal of water per cubic yard of concrete. The following steps were
1076 followed to ensure that the three mixtures would be produced with the same amount of mixing
1077 water:

- 1078 • The three mixtures were batched at the plant with a target of 31.0 gal of water/cy.
- 1079 • The actual amount of water added at the plant (batch water plus any water added by the
1080 truck driver) was noted in the truck dispatch.
- 1081 • The remaining water (to match exactly 34.0 gal/cy) was added at the construction site
1082 either directly from the truck tank or as part of the CNC suspension.

1083 The water content of the fresh concrete was measured following AASHTO T 318. Three specimens
1084 were tested per mixture type. The results are shown in Figure 30. The PLC and the CNC mixtures
1085 had similar measured water contents. For the three mixtures, the measured water contents were
1086 over the 8.9% theoretical water content (the theoretical water content is the same for the three
1087 mixtures).



1088

1089 Figure 30. Measured water content (evaporable water / dry weight of mixture, AASHTO
1090 T 318) (Note: The theoretical water content includes the design batch water plus the water
1091 absorbed by the aggregates in the saturated surface-dry (SSD) condition.)

1092 **5.3.2. CNC addition**

1093 The CNC were dispersed in their water suspension 4-5 hours before mixing into concrete (CNC
1094 solids content of the suspension was 3.33%). A high-shear blender (Waring CB15 Commercial

1095 Blender) was used for this purpose. The CNC suspension was blended at 4000 rpm for 60 seconds
1096 twice. When the concrete truck arrived at the construction site, the CNC suspension was added to
1097 the concrete ready-mix truck from the hopper (Figure 31). The concrete was then mixed at the
1098 maximum speed (14-16 rpm) for five minutes.



1099

1100 Figure 31. Addition of the CNC suspension to the ready-mix truck at the construction site

1101 5.4. Experimental Methods

1102 Fresh concrete mixtures were tested for consistency by measuring slump following ASTM
1103 C143/C143M-20, temperature following ASTM C1064/C1064M-17, air content using the
1104 pressure method following ASTM C231/C231M-17, and unit weight following ASTM
1105 C138/C138M-17. In addition, setting time of the concrete was measured following ASTM C403.
1106 Three specimens per mixture were tested for the setting time measurement.

1107 The concrete specimens were prepared with mixture sampled from the corresponding read-mix
1108 truck during the slabs construction. The specimens were cured in wooden boxes or covered with
1109 wet burlap, in the either case inside a room, until 24 hours (Figure 32). Then they were demolded
1110 and stored in lime water at 23°C until testing. The laboratory testing included several properties
1111 evaluated at different times as shown in Table 7. Three specimens were tested for each property
1112 measurement.



1113

1114

Figure 32. Specimen preparation and wooden boxes

1115

Table 7. List of hardened properties tested

Property	Standard	Specimen size (in.)	Testing times ⁽¹⁾
Flexural strength	ASTM C78	6×6×20 beams	10 days, 28 days, and 4 months
Compressive strength	ASTM C39	4×8 cylinders	10 days, 28 days, and 4 months
Modulus of elasticity	ASTM C469	6×12 cylinders	10 days, 28 days, and 4 months
Bulk electrical resistivity	ASTM C1876	4×8 cylinders	10 days, 28 days, and 4 months
Coefficient of thermal expansion (CTE)	AASHTO T 336	4×7 cylinders	42 days
Drying shrinkage	ASTM C157 ⁽²⁾	4×4×11 prims	Up to 4 months

1116

⁽¹⁾ A fourth set of specimens was prepared for testing at 1 year age. Testing results not included in this report.

1117

⁽²⁾ Except for the water immersion period; in this research, the specimens were subjected to drying at 7-day age.

1118

1119 5.5. Experimental Results

1120 5.5.1. Fresh properties

1121 Fresh concrete testing results are presented in Table 8.

1122

Table 8. Fresh concrete testing results

Mixture	Slump (in.)	Temp	Air Content (%)	Unit Weight (lb/ft ³)
PLC	6.50	88.2 °F (31.2 °C)	2.2	146.6
CNC	5.75	85.5 °F (29.7 °C)	1.9	147.8
OPC	7.75	88.9 °F (31.6 °C)	1.9	149.8

1123

1124 The slump of the mixtures with Type IL cement (PLC and CNC) was slightly lower than the slump
 1125 of the mixture with Type II/V cement (OPC) with similar water content, indicating a higher water
 1126 demand of the Type IL cement versus the Type II/V, for the same consistency. Most likely, this
 1127 outcome is due to the higher fineness of the Type IL cement (Blaine 5470 cm²/g) compared to the
 1128 Type II/V cement (Blaine 4184 cm²/g) used in this experiment (Blaine fineness from Cemex
 1129 cement mill test reports).

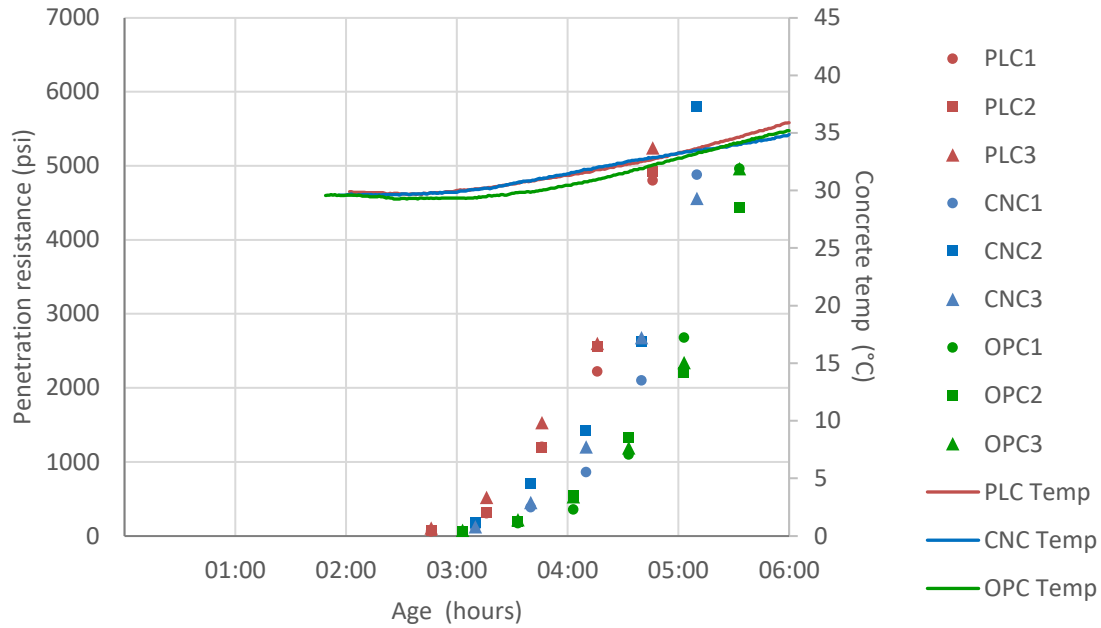
1130 The small temperature differences between mixtures are most likely due to the different time of
 1131 the day when each mixture was placed (CNC at approximately 1:00 pm, PLC at approximately
 1132 2:00 pm, and finally OPC at approximately 3:00 pm).

1133 The construction workers and industry experts present at the construction site commented on the
 1134 "creamy" consistency of the two mixtures with Type IL cement (CNC and PLC) compared to the
 1135 mixture with Type II/V (OPC). The creamy consistency, based on construction workers and
 1136 industry experts' opinion, would improve the constructability and reduce the segregation of the
 1137 mixture. Most likely, this outcome is also due to the higher fineness of Type IL compared to the
 1138 Type II/V cement used in this experiment.

1139 Construction workers and industry experts did not observe consistency or workability differences
 1140 between the two mixtures with Type IL cement (CNC versus PLC).

1141 **5.5.2. Setting time**

1142 The setting time of the concrete was measured following ASTM C403. Three specimens were
 1143 tested per mixture type. Penetration resistance evolution and set times are shown in Figure 33 and
 1144 Table 9, respectively.



1145

1146 Figure 33. Penetration resistance (ASTM C403); temperature in the plot is measured in a dummy
 1147 penetration resistance specimen

1148

Table 9. Setting time results (ASTM C403)

Mixture	Initial Set (*) (500 psi)	Final Set (*) (4000 psi)
PLC	3:25	4:30
CNC	3:45	4:55
OPC	4:05	5:25

1149 (*) Set time is measured from the ready-mix truck batching time. For example, 4:30 means 4.5
 1150 hours after the ready-mix truck batching.

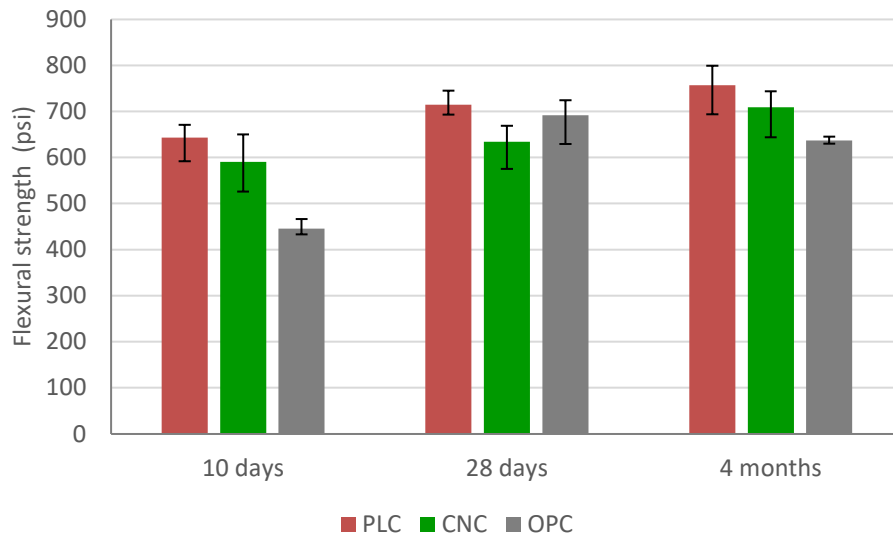
1151 The OPC mixture's initial and final setting times were longer than the setting times of the two
 1152 mixtures with Type IL, most like due to the lower fineness of the Type II/V compared to the Type
 1153 IL. The setting time of the mixture with CNC was slightly delayed compared to the PLC mixture
 1154 without CNC. It has been shown previously that CNC delays the set time of the cement, most
 1155 likely by electrostatic dispersion of the cement [103] or the coating of clinker (primarily aluminate
 1156 phases with CNC [6].

1157 5.5.3. Hardened properties

1158 The testing results are included in Figure 34 to Figure 39. Overall, the two mixtures with Type IL
 1159 cement (CNC and PLC) were similar to each other for all properties (strength, modulus of

1160 elasticity, electrical resistivity, CTE, and shrinkage), with differences being either approximately
1161 10% or less (flexural and compressive strength) or not statistically significant at the 5%
1162 significance level (modulus of elasticity, electrical resistivity, CTE, and drying shrinkage).

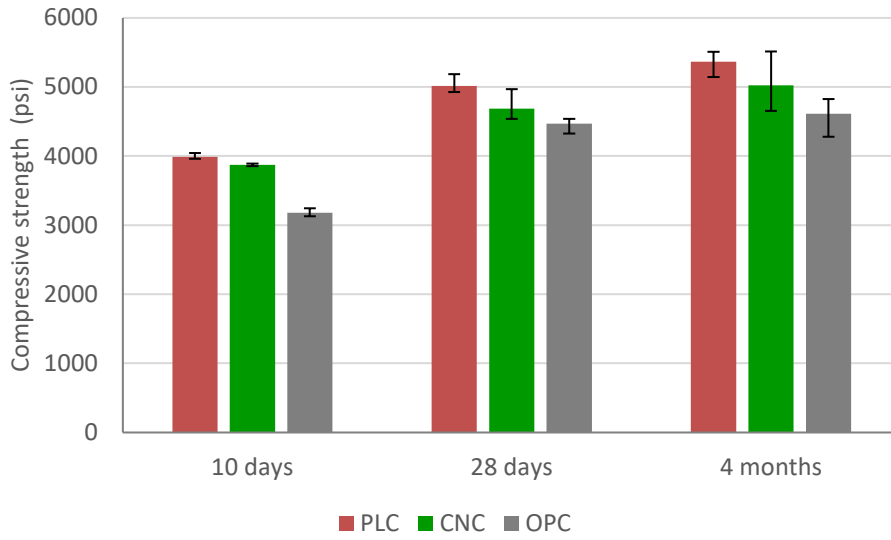
1163 The two mixtures with Type IL (CNC and PLC) presented approximately 10-15% higher strength
1164 than the mixture with Type II/V (OPC). The resistivity of these two mixtures was also considerably
1165 better (higher) than the resistivity of the mixture with Type II/V. On the contrary, the mixtures
1166 with Type IL presented higher CTE than the mixture with Type II/V. Regarding drying shrinkage,
1167 the Type IL resulted higher strains in the short term (6 days drying) which is consistent with a
1168 more rapid hydration but lower strains after 4 months of drying, compared to the mixture with
1169 Type II/V. Overall, the differences between the two mixtures with Type IL versus the mixture with
1170 Type II/V were statistically significant.



1171

1172

Figure 34. Flexural strength of the different mixtures

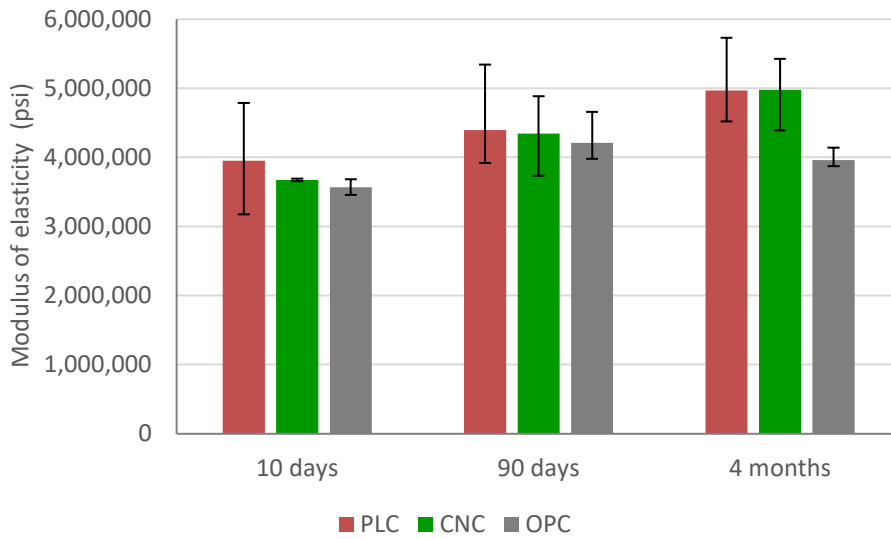


1173

1174

Figure 35. Compressive strength of the different mixtures.

1175

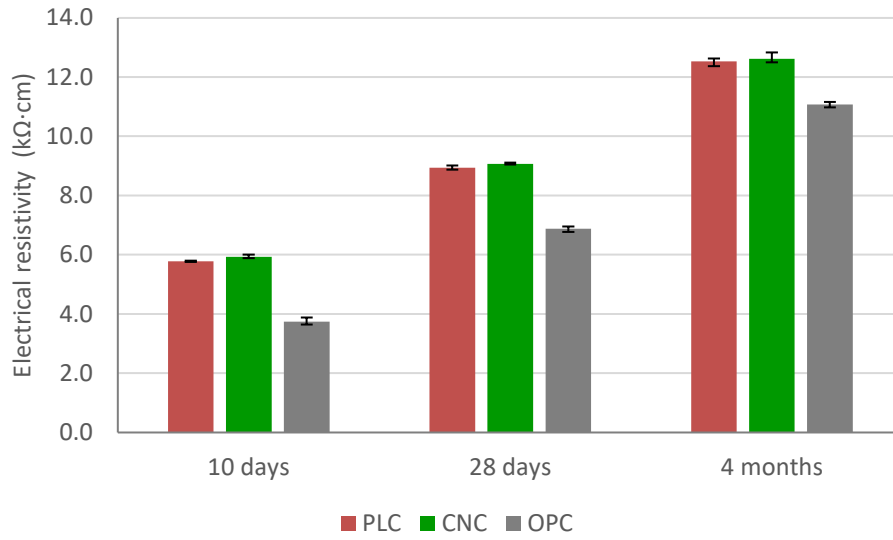


1176

1177

Figure 36. Modulus of elasticity of the different mixtures.

1178

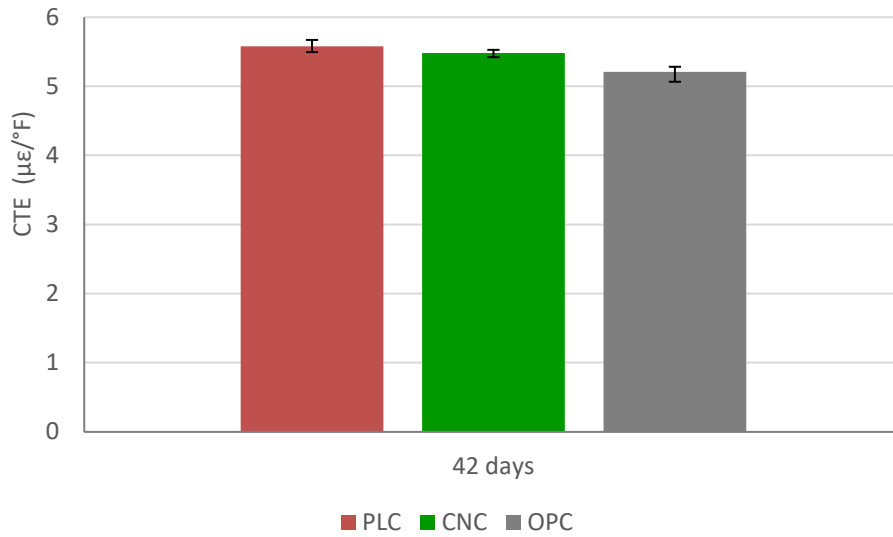


1179

1180

Figure 37. Bulk electrical resistivity of the different mixtures.

1181

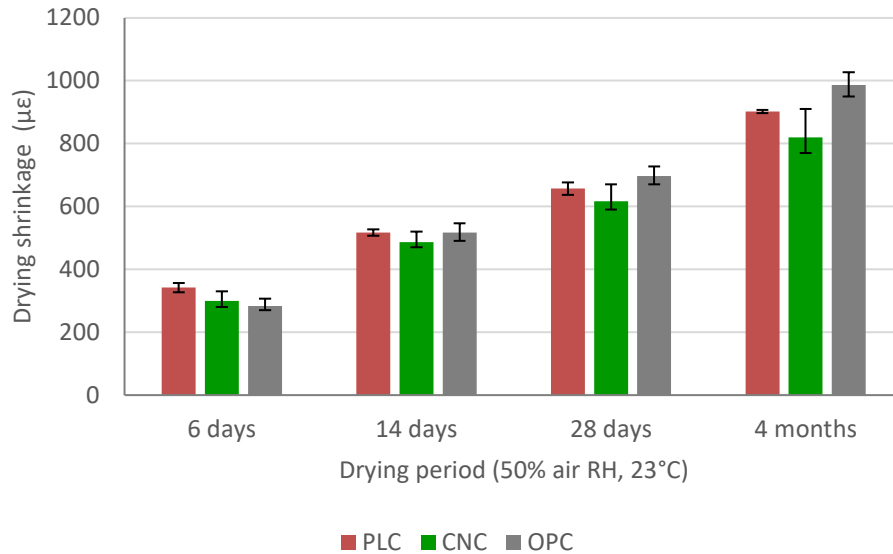


1182

1183

Figure 38. CTE of the different mixtures.

1184



1185

1186

Figure 39. Drying shrinkage of the different mixtures.

1187

1188 5.5.4. Hygrothermal deformation of the slabs

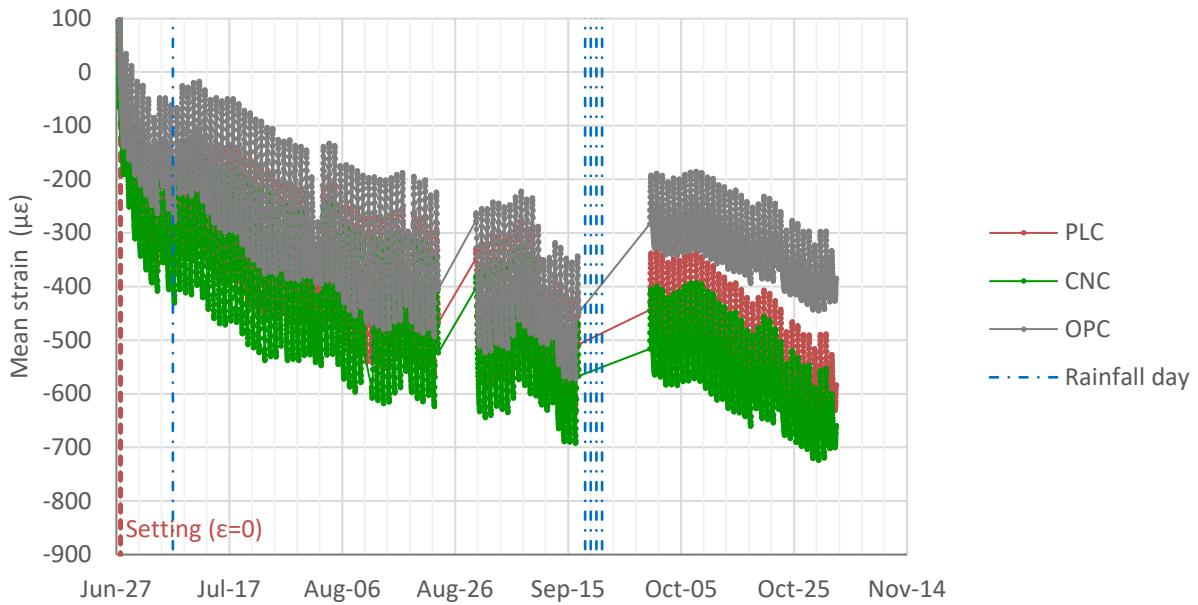
1189 One of the goals of the experiment is to evaluate the impact of the CNC addition on the moisture-
 1190 related shrinkage and thermal deformations of the concrete. This evaluation was based on the
 1191 strains measured with VWSGs in the two corresponding sets of slabs (CNC versus PLC sections).
 1192 A secondary goal is to compare the mixture with Type II/V cement versus the mixture with Type
 1193 II/V cement (PLC versus OPC sections).

1194 The strains measured with VWSGs in the three sections are presented in Figure 40 (ϵ_{MEAN} : mean
 1195 strain, i.e. average of top and bottom of the slab) and Figure 41 (ϵ_{DIFF} : differential strain, i.e. top
 1196 versus bottom of the slab). In all sections, a "field setting time" of 5 hours has been adopted as
 1197 reference for strain calculation (ϵ is set to zero at the "field setting time"). The adoption of 5 hours
 1198 is based on the setting time testing results presented in Table 9. The strain measured in the
 1199 unrestrained shrinkage prisms is presented in Figure 42.

1200 Note that there are two periods with missing data in Figure 40 and Figure 41: Aug-22 to Aug-30,
 1201 and Sep-16 to Sep-30. In both cases, the problem was a failure in the data acquisition system
 1202 electrical supply.

1203 The average of all sensors per mixture type is shown In Figure 40 to Figure 42: the average of two
 1204 pairs of VWSGs (located at each of the two instrumented corners in each section) in Figure 40 and
 1205 Figure 41 and the average of three unrestrained shrinkage prisms per mixture type in Figure 42.

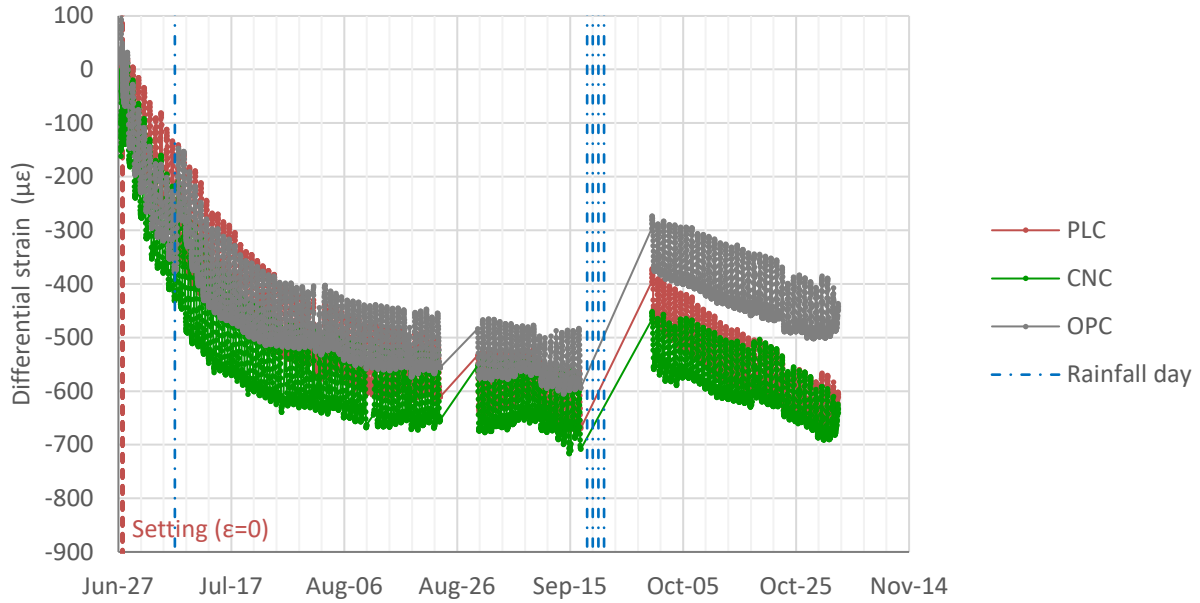
1206 Figure 43 shows an example of variability of strain measured within pairs of VWSGs. In this
1207 figure, the diurnal variations of the strain and temperature can be also observed.



1208

1209 Figure 40. Mean strain measured in the slabs (average of top and bottom VWSGs; for each
1210 section, the average of two pairs of VWSGs is shown)

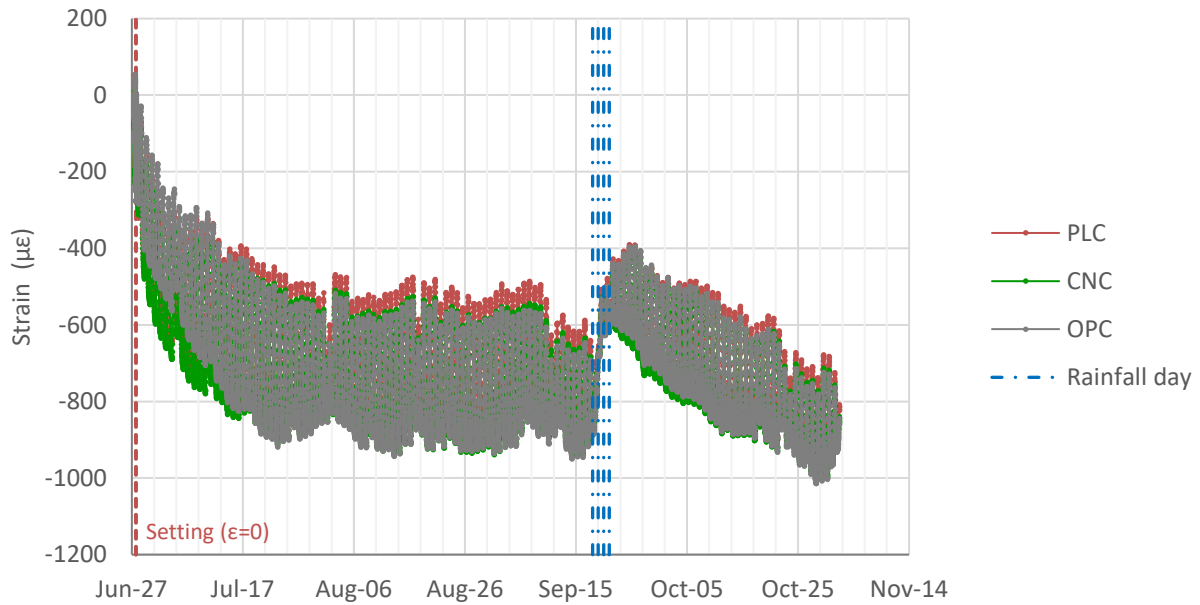
1211



1212

1213 Figure 41. Differential strain measured in the slabs (difference between top and bottom VWSGs
 1214 multiplied by H/D , where H is slab thickness [4 in.] and D is distance between VWSGs [2.4 in.];
 1215 for each section, the average of two pairs of VWSGs is shown)

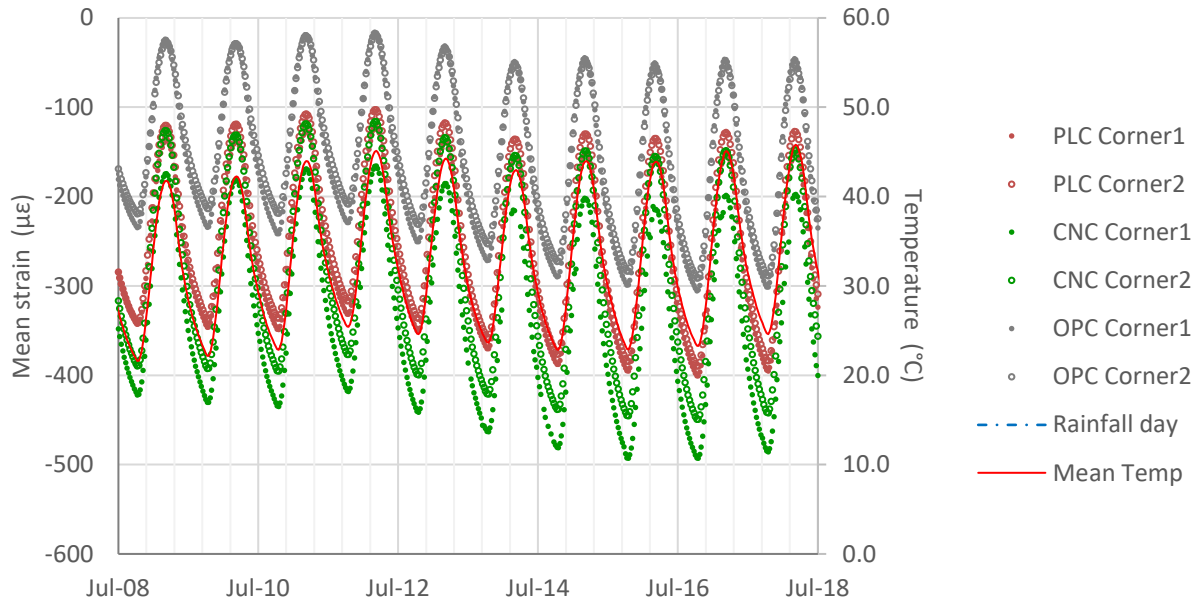
1216



1217

1218 Figure 42. Strain measured in the unrestrained shrinkage prisms (for each mixture, the average of
 1219 three unrestrained shrinkage prisms shown; one of the PLC prisms was regarded an outlier and
 1220 discarded)

1221



1222

1223 Figure 43. Example of diurnal variation of mean strain measured in the slabs (average of top and
 1224 bottom VWSGs; Corner1 and Corner2 correspond to each of the two instrumented corners in
 1225 each section; Mean Temp is the mean temperature of the slabs)

1226

1227 Based on the strains measured in the sections (Figure 40 and Figure 41) and in the unrestrained
 1228 shrinkage prisms (Figure 42), it is evident that the CNC and PLC mixtures have similar
 1229 hydrothermal deformations (moisture-related shrinkage and thermal strains).

1230 Further analysis of the strains measured in the sections and unrestrained shrinkage prisms was
 1231 conducted to determine which part of the measured strain is related to the moisture-related
 1232 shrinkage and which part is related to the thermal action. The strain data were fitted with the
 1233 models shown in equations 11 and 12 below, following the methodology described in reference
 1234 [104].

$$\Delta\varepsilon_{\text{MEAN}} = \Delta\varepsilon_{\text{MEAN,Hyg}} + \alpha \cdot \text{CTE1}(t) \cdot \Delta T_{\text{MEAN}} \quad (\text{Eq. 11})$$

1235 where: $\varepsilon_{\text{MEAN,Hyg}}$ is the component of $\varepsilon_{\text{MEAN}}$ that is caused by the hygral action (Mean drying shrinkage
 1236 shown in Figure 44)

1237 α is a coefficient that accounts for the restriction to slab expansion-contraction due to
 1238 slab weight and slab interaction with its base; it can be assumed to be 1 for the
 1239 VWSGs configuration used in this experiment

1240 $\text{CTE1}(t)$ is time-dependent equivalent CTE of the concrete slab in terms of mean expansion-
 1241 contraction

1242 t is time

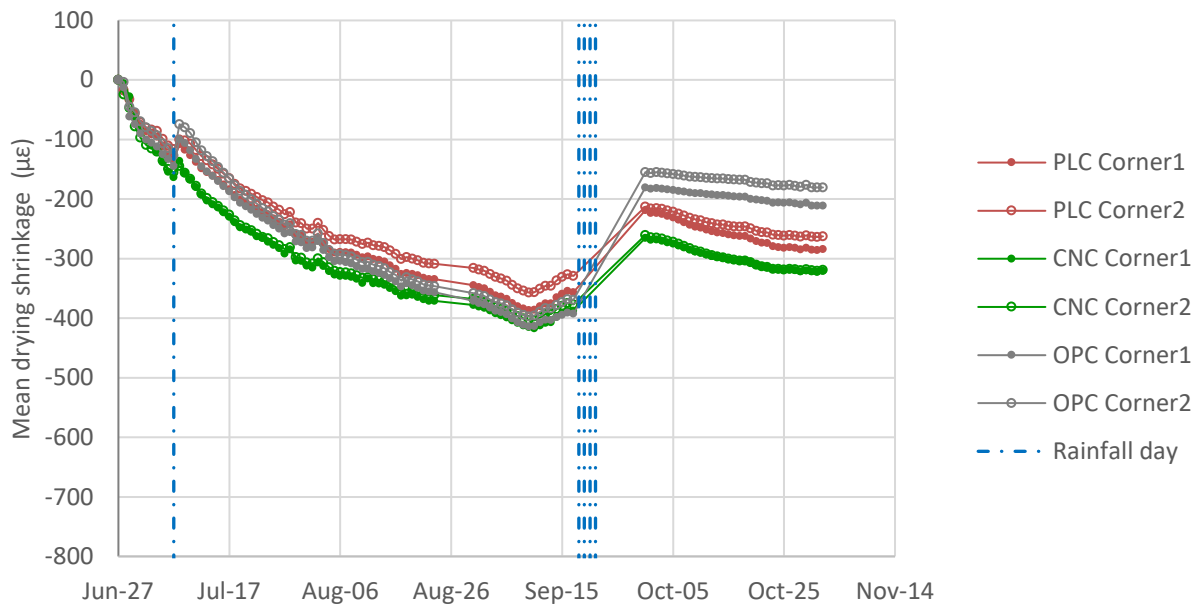
1243 T_{MEAN} is the mean slab temperature

1244

$$\Delta\varepsilon_{\text{DIFF}} = \Delta\varepsilon_{\text{DIFF,Hyg}} + \beta \cdot \text{CTE2}(t) \cdot \Delta\text{ELTD} \quad (\text{Eq. 12})$$

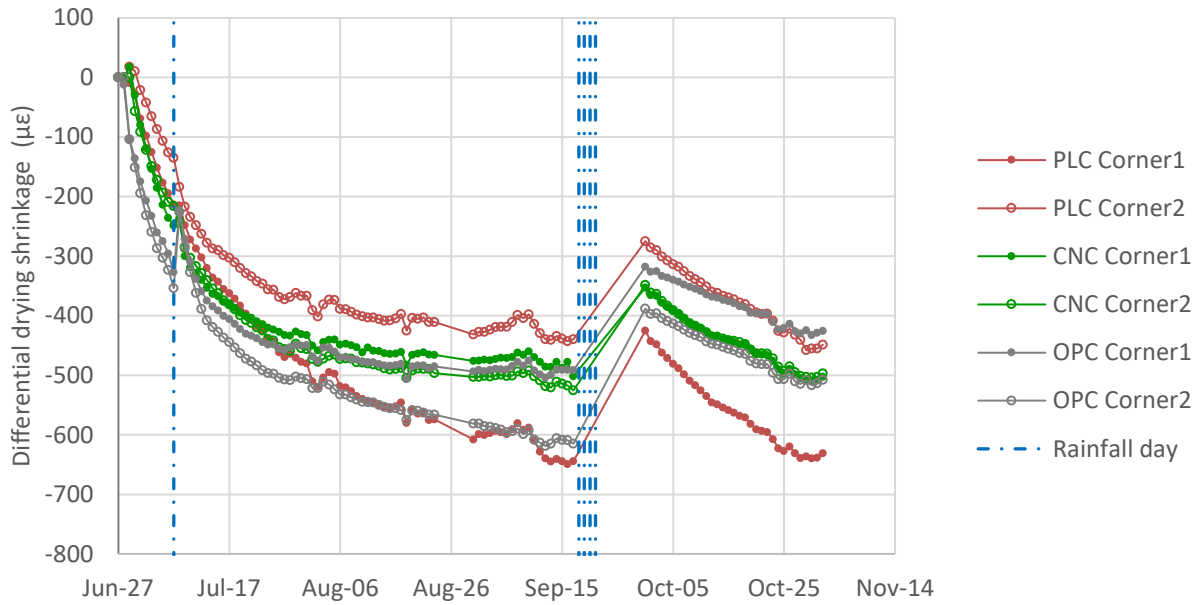
1245 where: $\varepsilon_{\text{DIFF,Hyg}}$ is the component of $\varepsilon_{\text{DIFF}}$ that is caused by the hygral action (Differential drying
 1246 shrinkage shown in Figure 45)
 1247 β is a coefficient that accounts for the restriction to slab bending due to slab weight, slab
 1248 interaction with its base, and transverse joint locking or lack of deployment; it can be
 1249 assumed to be 1 for the VWSGs configuration used in this experiment
 1250 $\text{CTE2}(t)$ is time-dependent equivalent CTE of the concrete slab in terms of bending
 1251 t is time
 1252 ELTD is the equivalent linear temperature difference in the slab (for a given temperature
 1253 profile, the ELTD is the temperature difference between the top and bottom of the slab
 1254 for the "equivalent linear temperature profile"; the "equivalent linear temperature
 1255 profile" is the temperature profile that is linear versus depth and produces the same
 1256 slab curvature produced by the actual vertical temperature profile)

1257 The moisture-related shrinkage estimated in the sections, based on equations 11 and 12, is
 1258 presented in Figure 44 (mean strain: average of top and bottom of the slab), Figure 45 (differential
 1259 strain: top versus bottom of the slab), and Figure 46 (unrestrained shrinkage prisms). Note that the
 1260 estimated moisture-related strain is referred to as "drying shrinkage" rather than "moisture-related
 1261 shrinkage" as it is due to external drying and wetting of the concrete rather than internal
 1262 desiccation. Internal desiccation and the consequent autogenous shrinkage are minimal in this
 1263 experiment due to the relatively high water to cementitious materials ratio of the mixtures.



1264
 1265 Figure 44. Mean drying shrinkage estimated in the slabs (Corner1 and Corner2 are each of the
 1266 two instrumented corners in each section)

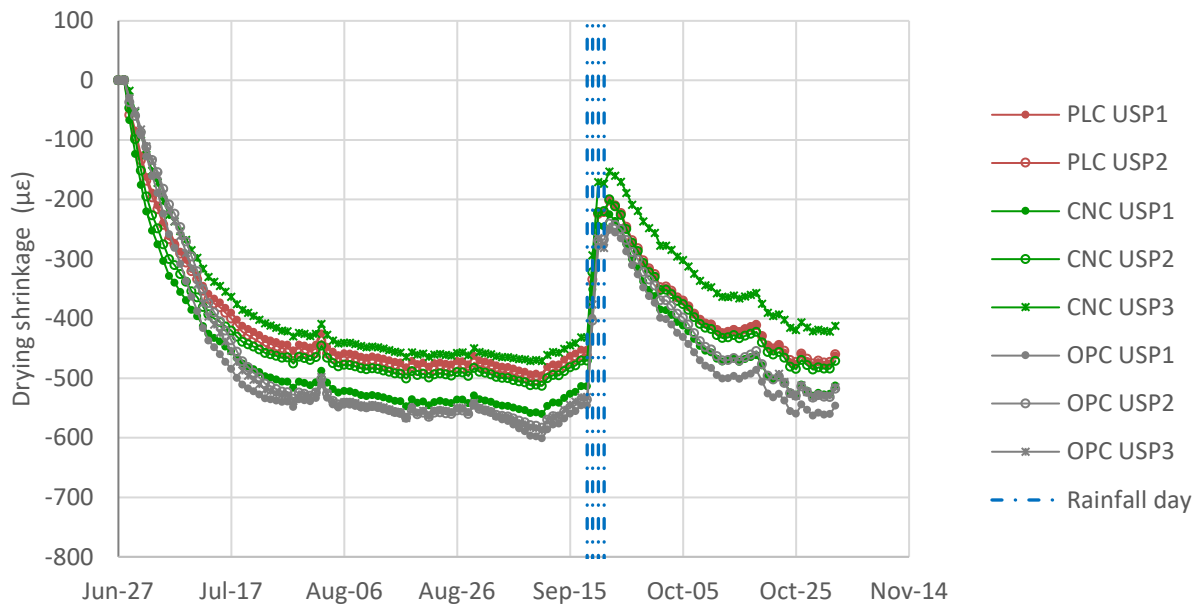
1267



1268

1269 Figure 45. Differential drying shrinkage estimated in the slabs (Corner1 and Corner2 are each of
 1270 the two instrumented corners in each section)

1271



1272

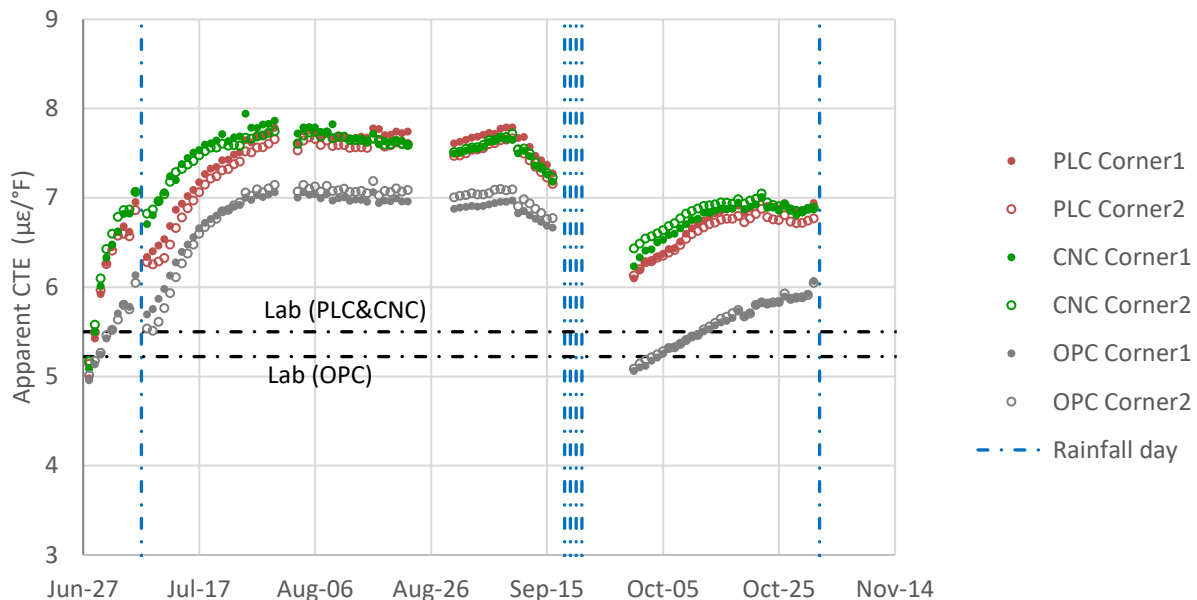
1273 Figure 46. Drying shrinkage estimated in the unrestrained shrinkage prisms (USP1, USP2, and
 1274 USP3 are the three prisms for each of the mixtures; PLC USP3 was regarded an outlier and
 1275 discarded)

1276

1277 Based on the estimated drying shrinkage of the sections and the unrestrained shrinkage prisms,
 1278 shown in Figure 44, Figure 45, and Figure 46, the CNC and PLC mixtures have similar
 1279 performance. Also, these two mixtures present drying shrinkage similar to that of the OPC mixture.

1280 The thermal deformations of the CNC and PLC mixtures are similar to each other. As an example,
 1281 the apparent CTE of the slabs in terms of expansion and contraction is shown in Figure 47. In this
 1282 figure, the increase in CTE as the concrete dries and the drop in CTE after rainfall are evident. In
 1283 the CNC and PLC sections, because of drying, the apparent CTE of the slabs reached values up to
 1284 40% higher than the CTE determined in the laboratory under saturated conditions (following
 1285 AASHTO T 336); the CTE increase is somewhat smaller in the OPC section. Similar changes in
 1286 CTE have been measured in other field experiments by UCPRC [104].

1287



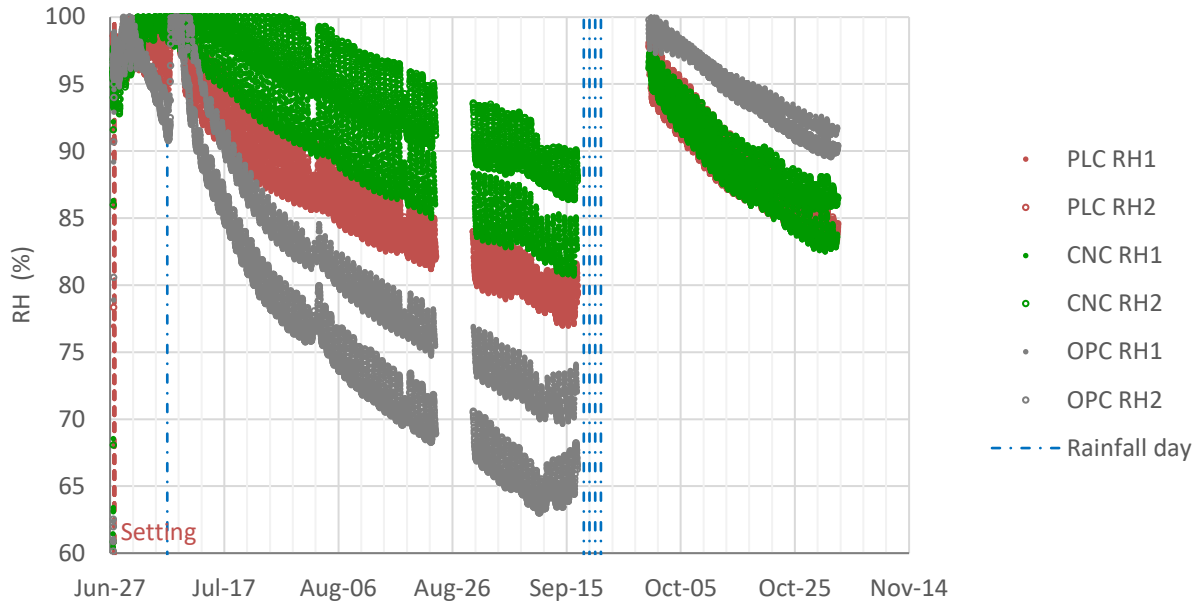
1288

1289 Figure 47. Apparent CTE of the slabs in terms of expansion-contraction (Corner1 and Corner2
 1290 are each of the two instrumented corners in each section); for a given day, the apparent CTE can
 1291 be defined as the ratio between changes in slab's horizontal strain and slab's mean temperature

1292 The RH measured at 0.8 inch depth in the sections can be also used to evaluate the effect of the
 1293 CNC addition on RH. The measured RH data are presented in Figure 48. While some CNC versus
 1294 PLC differences are observed in this figure, the differences are within the sensor-to-sensor
 1295 variability. Overall, the concrete internal RH was not affected much by the CNC addition. The RH
 1296 measured in these two mixtures is somewhat different from the RH measured in the OPC mixture.
 1297 Due to the dry and warm weather conditions of the summer, the RH in the OPC mixture dropped
 1298 faster than in the CNC and PLC mixtures. This outcome might be related to a greater porosity of
 1299 the OPC mixture compared to the other two mixtures, which needs to be confirmed.

1300 The diurnal variations of the concrete internal RH (variations within a day, mainly related to
1301 temperature changes) in the CNC and PLC mixtures are also similar to each other. Interestingly,
1302 the variations are somewhat higher for these two mixtures than for the OPC mixture (Figure 48
1303 and Figure 49). This outcome is believed to be the reason why the apparent CTE of the CNC and
1304 PLC mixtures increased upon drying somewhat more than the CTE of the OPC mixture (further
1305 investigation and explanation of this outcome is outside the scope of this report).

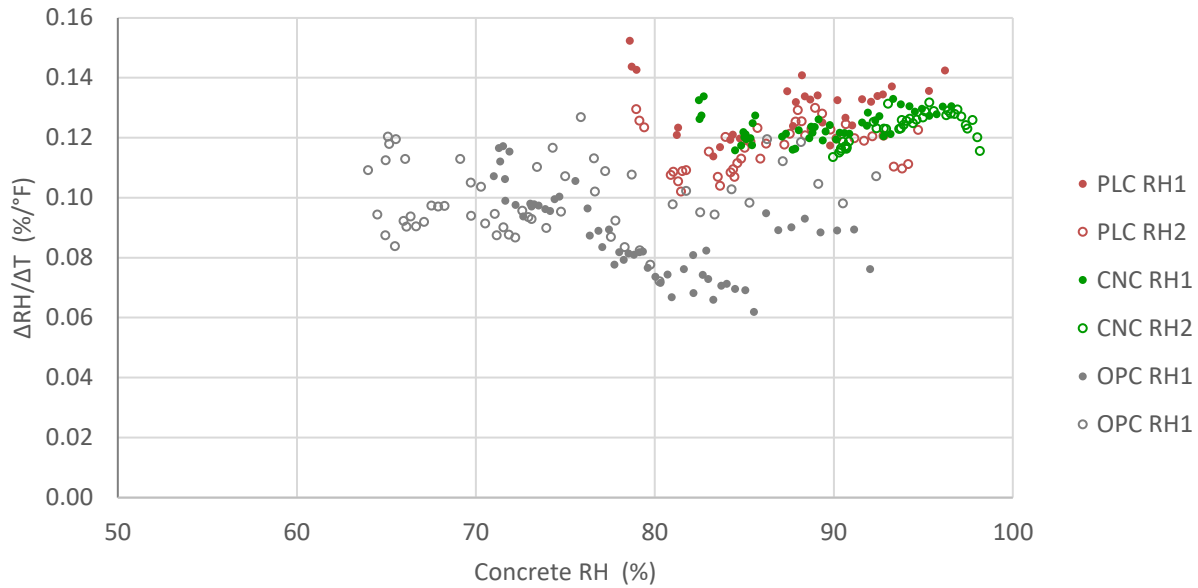
1306



1307

1308 Figure 48. RH measured in the concrete, at 0.8 in. depth (RH1 and RH2 are each of the two RH
1309 sensors embedded in each of the sections)

1310



1311

1312 Figure 49. Diurnal variation of RH versus temperature (for a given day, the ratio $\Delta RH/\Delta T$
 1313 indicates how much concrete internal RH changes versus temperature while the moisture of the
 1314 concrete remains essentially constant)

1315 **5.6. Discussion of Test Sections Experimental Results**

1316 The experiment presented in this chapter of the report was designed to evaluate the effects of the
 1317 addition of CNC on the constructability and properties of the portland-limestone cement concrete.
 1318 A secondary goal of the experiment was to compare the constructability and properties of the
 1319 portland-limestone cement concrete versus concrete made with Type II/V ordinary portland
 1320 cement. The control mixture, made with Type II/V cement, represents a typical concrete paving
 1321 mixture used in the Caltrans road network.

1322 The experiment includes the construction and monitoring of a set of slabs and the testing of the
 1323 mixtures sampled during the construction. Based on the collected experimental data, a number of
 1324 conclusions can be drawn regarding mixtures constructability, including fresh concrete properties,
 1325 hardened concrete mechanical properties, and concrete hygrothermal deformations (i.e., response
 1326 under ambient environmental actions).

1327 **5.6.1. Effects of the CNC addition**

1328 The effect of the CNC addition can be established by comparing the initial properties,
 1329 constructability, and several months of hydrothermal performance under the hot, dry
 1330 environmental conditions of the test section location of the CNC and PLC mixtures. The only
 1331 difference between the CNC and PLC mixtures is that the former includes 0.1% cellulose
 1332 nanocrystals (CNC solids by weight of total cementitious materials).

1333 Based on the collected experimental data, no important differences were found between the CNC
1334 and PLC mixtures:

- 1335 • Fresh concrete properties (slump, air content, and unit weight) were similar in the two
1336 mixtures.
- 1337 • The setting time was similar for the two mixtures, and the same applies to the concrete
1338 temperature recorded during the setting time experiment, which indicates similar early-age
1339 heat of hydration release.
- 1340 • Based on construction workers and Industry expert's observations, there were no
1341 consistency or workability differences between the two mixtures.
- 1342 • Mechanical properties of the two mixtures, based on laboratory testing of the hardened
1343 concrete, were similar for all properties (strength, modulus of elasticity, electrical
1344 resistivity, CTE, and shrinkage), with differences being either approximately 10% or less
1345 (flexural and compressive strength) or not statistically significant at the 5% significance
1346 level (modulus of elasticity, electrical resistivity, CTE, and drying shrinkage).
- 1347 • The hygrothermal responses of the slabs made with each of the two mixtures were very
1348 similar. The two groups of slabs presented similar drying shrinkage during the 4-month
1349 evaluation period and similar thermal deformations.

1350 Based on these results, it can be concluded that the CNC addition did not produce any significant
1351 effect on the fresh concrete properties, including constructability, and neither on the properties of
1352 the hardened-concrete.

1353 **5.6.2. Comparison of OPC and PLC**

1354 The effect of the substitution of the Type II/V ordinary portland cement by Type IL portland-
1355 limestone cement can be established by comparing the properties and performance of the PLC and
1356 OPC mixtures. The only difference between the PLC and OPC mixtures is that the former includes
1357 substituting Type IL instead of Type II/V cement. The cement content of both mixtures was the
1358 same.

1359 Based on the collected experimental data, some differences were found between the PLC and OPC
1360 mixtures:

- 1361 • The slump of the OPC mixture was slightly higher than the slump of the PLC mixture (7.75
1362 versus 6.50 in.), with similar water content. This outcome suggests a higher water demand

1363 of the Type IL cement versus the Type II/V, for the same consistency. The other fresh
1364 concrete properties (air content and unit weight) were similar for the two mixtures.

- 1365 • The PLC mixture set faster than the OPC mixture. Initial and final setting times of the OPC
1366 mixture, based on penetrating resistance, were 4:05 and 5:25 hours, respectively. The
1367 setting times of the PLC mixture were approximately 15% shorter (3:25 and 4:30 hours for
1368 the initial and final set, respectively). The temperature recorded during the setting time
1369 experiment was slightly higher, up to 2°F (1°C) higher, in the PLC than in the OPC mixture.
- 1370 • The construction workers and industry experts present at the construction site indicated a
1371 "creamy" consistency of the PLC mixture compared to the OPC mixture, which would
1372 improve the constructability and reduce the segregation of the PLC mixture compared to
1373 the OPC.
- 1374 • The PLC mixture presented around 10-15% higher strength than the OPC mixture
1375 regardless of the testing age (between 10 days and 4 months). The PLC mixture also
1376 presented higher electrical resistivity than the OPC mixture (around 50% higher after 10
1377 days and around 15% higher after 4 months). On the contrary, the CTE of the PLC mixture
1378 was 0.7 $\mu\epsilon/^\circ\text{C}$ higher than the CTE of the OPC mixture.
- 1379 • The PLC mixture presented 20% higher laboratory drying shrinkage (73°F (23°C), 50%
1380 air RH) than the OPC mixture in the short term (6 days drying) but 10% lower drying
1381 shrinkage after 4 months of drying.
- 1382 • The hygrothermal response of the slabs made with each of the two mixtures were similar
1383 to each other. The two groups of slabs presented similar drying shrinkage during the 4-
1384 month evaluation period and similar thermal deformations.

1385 Overall, the results indicate that PLC can be used interchangeably with OPC; however, the effect
1386 of differences in fineness of PLC and OPC should be noted. The mixtures with Type IL had better
1387 performance in terms of workability, mechanical, and durability properties than the mixture with
1388 Type II/V, mainly due to higher surface area of Type IL cement and synergistic behavior between
1389 the limestone and alumina. The mixtures with Type IL were observed to have higher water demand
1390 and somewhat higher CTE (0.7 $\mu\epsilon/^\circ\text{C}$) when compared to the mixture with Type II/V due to higher
1391 fineness of Type IL cement.

1392

1393 **6. CHAPTER 5: Conclusions**

1394 A comprehensive plan was undertaken to evaluate CNCs as a value-based additive for low-carbon
1395 footprint concrete. This project was aimed at evaluating the performance of mixtures with
1396 limestone and CNC to develop mixtures with a lower embodied carbon footprint. In addition, the
1397 project included the implementation of the use of CNC in a set of pilot slabs built on the research
1398 site of the University of California Pavement Research Center (UCPRC) in Davis, California.

1399 OPC-LS-CNC mixtures were evaluated for various limestone additions ranging from 0 – 30% by
1400 weight and various CNC dosages ranging from 0 – 1% of CNC solids per volume of cementitious
1401 materials. The heat of hydration using isothermal calorimetry, B3B flexural strength, CH content,
1402 non-evaporable water content, porosity, pore connectivity, and bulk resistivity of the mixtures
1403 were determined. GHG emissions of the mixtures were calculated using the life cycle inventory
1404 (LCI) calculation tool.

1405 The addition of CNCs to the OPC-LS mixtures resulted in slight retardation by approximately 2-3
1406 hours, depending on the CNC dosage. When CNCs are added, there was an increase in heat release
1407 measured at seven days by about 2-3% for OPC-LS mixtures due to increased clinker hydration.
1408 The increase in the degree of hydration at early ages was due to the combined effect of LS and
1409 CNCs. When the degree of hydration at later ages (28 days) was determined by measuring non-
1410 evaporable water content, it was found that mixtures with CNCs at lower dosages up to 0.5% had
1411 a higher degree of hydration, which was mainly attributed to CNCs.

1412 CNCs addition to OPC-LS mixtures did not have a significant impact on the porosity of the paste
1413 samples. B3B flexural strength of the OPC-LS-CNC mixtures measured at 28 days was within
1414 $\pm 15\%$ of the flexural strength of the OPC-LS mixtures. Also, CNCs did not have a significant
1415 impact on the drying shrinkage strain of mortar samples. The drying shrinkage strain of the mortar
1416 mixtures with CNC was statistically similar or slightly higher ($\sim 5\%$) than mixtures without CNCs
1417 after 90 days of exposure to a drying environment.

1418 The addition of CNCs to OPC-LS mixtures had an impact on pore connectivity (β). Lower dosages
1419 of CNC addition resulted in a decrease in pore connectivity by up to 29% and improved bulk
1420 resistivity by up to 38%. The addition of 20% LS and 0.2% CNC resulted in similar mechanical
1421 and transport properties to the conventional mixture; this resulted in the development of an OPC-
1422 LS-CNC mixture with 19.4% lower GHG emissions than 100% OPC mixture without
1423 compromising on the strength and transport properties.

1424 The performance of OPC-SCM and PLC-SCM mixtures with CNC were evaluated. The 7-day heat
1425 of hydration, 28- and 56-day B3B flexural strength, 28- and 56-day porosity, 28- and 56-day pore
1426 connectivity, and 28- and 56-day bulk resistivity were determined. The addition of CNC to SCM
1427 mixtures resulted in slight retardation due to the CNC covering the clinker, primarily aluminite
1428 phase. The 7-day heat release of the SCM mixtures with CNCs were within $\pm 5\%$ of the heat release

1429 of the mixtures without CNC. Overall porosity and B3B flexural strength did not vary significantly
1430 with the CNC dosage. Unlike what was observed for the plain and limestone mixtures, the CNC
1431 addition at low dosages resulted in an increase in pore connectivity and a decrease in bulk
1432 resistivity for the majority of the SCM mixtures. Additional research is needed to understand the
1433 role of the CNCs on the performance when SCMs are used. Specifically, research is needed to
1434 understand what surfaces the CNC are absorbed on. Work is underway to evaluate the long-term
1435 transport properties.

1436 The demonstration of the use of CNCs and PLCs was successfully done in field trials in California
1437 at the UC Davis Pavement Research Center. With the addition of CNCs, no significant difference
1438 in fresh concrete properties, including constructability, was observed. In addition, the compression
1439 and flexural strength of the mixtures with and without CNC were similar. CNCs addition had no
1440 statistically significant effect on the measured modulus of elasticity, electrical resistivity, and
1441 drying shrinkage. The hygrothermal responses of the slabs with and without CNC were very
1442 similar as well. The results indicated that PLC could be used alternative to OPC.

1443 Overall, in this project, comprehensive testing was done to evaluate CNCs as a value-based
1444 additive to mixtures with limestone to lower GHG emissions. Through this project, it was
1445 demonstrated that designing lower embodied carbon footprint mixtures with limestone and CNCs
1446 is possible without compromising on the mechanical and transport properties of concrete.

1447 **ACKNOWLEDGEMENTS**

1448 The authors would like to acknowledge and thank Larry Swan and Michael Goergen for valuable
1449 discussions on CNC amount calculations shown in section 8.1.

1450 7. References

- 1451 1. Moon, R.J., et al., *Cellulose nanomaterials review: structure, properties and*
1452 *nanocomposites*. Chemical Society Reviews, 2011. **40**(7): p. 3941-3994.
- 1453 2. Moon, R.J., G.T. Schueneman, and J. Simonsen, *Overview of cellulose nanomaterials,*
1454 *their capabilities and applications*. Jom, 2016. **68**(9): p. 2383-2394.
- 1455 3. Fu, T., et al., *Cellulose nanomaterials as additives for cementitious materials,* in *Cellulose-*
1456 *Reinforced Nanofibre Composites*. 2017, Elsevier. p. 455-482.
- 1457 4. Cuenca, E., et al., *Concept of ultra high durability concrete for improved durability in*
1458 *chemical environments: preliminary results*. 2019.
- 1459 5. Aziz, M.A., M. Zubair, and M. Saleem, *Development and testing of cellulose nanocrystal-*
1460 *based concrete*. Case Studies in Construction Materials, 2021. **15**: p. e00761.
- 1461 6. Cao, Y., *Nano-modification for high performance cement composites with cellulose*
1462 *nanocrystals and carbon nanotubes*. 2014: Purdue University.
- 1463 7. Peters, S.J., et al., *Nanocellulose and microcellulose fibers for concrete*. Transportation
1464 Research Record, 2010. **2142**(1): p. 25-28.
- 1465 8. Sun, X., et al., *Cellulose nanofibers as a modifier for rheology, curing and mechanical*
1466 *performance of oil well cement*. Scientific reports, 2016. **6**(1): p. 1-9.
- 1467 9. da Costa Correia, V., et al., *Nanofibrillated cellulose and cellulosic pulp for reinforcement*
1468 *of the extruded cement based materials*. Construction and Building Materials, 2018. **160**:
1469 p. 376-384.
- 1470 10. Haddad Kolour, H., et al., *An investigation on the effects of cellulose nanofibrils on the*
1471 *performance of cement paste and concrete*. Advances in Civil Engineering Materials, 2018.
1472 **7**(1): p. 15.
- 1473 11. Lee, H.-J. and W. Kim, *Long-term durability evaluation of fiber-reinforced ECC using*
1474 *wood-based cellulose nanocrystals*. Construction and Building Materials, 2020. **238**: p.
1475 117754.
- 1476 12. Montes, F., et al., *Rheological impact of using cellulose nanocrystals (CNC) in cement*
1477 *pastes*. Construction and Building Materials, 2020. **235**: p. 117497.
- 1478 13. Santos, R.F., et al., *Nanofibrillated cellulose and its applications in cement-based*
1479 *composites: A review*. Construction and Building Materials, 2021. **288**: p. 123122.
- 1480 14. Cuenca, E., A. Mezzena, and L. Ferrara, *Synergy between crystalline admixtures and nano-*
1481 *constituents in enhancing autogenous healing capacity of cementitious composites under*
1482 *cracking and healing cycles in aggressive waters*. Construction and Building Materials,
1483 2021. **266**: p. 121447.
- 1484 15. Kamasamudram, K.S., W. Ashraf, and E.N. Landis, *Cellulose nanofibrils with and without*
1485 *nanosilica for the performance enhancement of Portland cement systems*. Construction and
1486 Building Materials, 2021. **285**: p. 121547.
- 1487 16. Kamasamudram, K.S., et al., *Effects of ligno–and delignified–cellulose nanofibrils on the*
1488 *performance of cement-based materials*. Journal of Materials Research and Technology,
1489 2021. **13**: p. 321-335.
- 1490 17. Cao, Y., et al., *The influence of cellulose nanocrystal additions on the performance of*
1491 *cement paste*. Cement and Concrete Composites, 2015. **56**: p. 73-83.
- 1492 18. Cao, Y., et al., *Performance-enhanced cementitious materials by cellulose nanocrystal*
1493 *additions*. Production and Applications of Cellulose Nanomaterials, 2013. **2**.

- 1494 19. Cao, Y., et al., *The relationship between cellulose nanocrystal dispersion and strength*.
 1495 Construction and Building Materials, 2016. **119**: p. 71-79.
- 1496 20. Dousti, M.R., Y. Boluk, and V. Bindiganavile, *The effect of cellulose nanocrystal (CNC)*
 1497 *particles on the porosity and strength development in oil well cement paste*. Construction
 1498 and Building Materials, 2019. **205**: p. 456-462.
- 1499 21. Deze, E., et al., *Nanocellulose enriched mortars: Evaluation of nanocellulose properties*
 1500 *affecting microstructure, strength and development of mixing protocols*. Materials Today:
 1501 Proceedings, 2021.
- 1502 22. Haque, M.I., et al., *A comparative investigation on the effects of nanocellulose from*
 1503 *bacteria and plant-based sources for cementitious composites*. Cement and Concrete
 1504 Composites, 2022. **125**: p. 104316.
- 1505 23. Fu, T., et al., *The influence of cellulose nanocrystals on the hydration and flexural strength*
 1506 *of Portland cement pastes*. Polymers, 2017. **9**(9): p. 424.
- 1507 24. Flores, J., M. Kamali, and A. Ghahremaninezhad, *An investigation into the properties and*
 1508 *microstructure of cement mixtures modified with cellulose nanocrystal*. Materials, 2017.
 1509 **10**(5): p. 498.
- 1510 25. Claramunt, J., et al., *Effect of nanocelluloses on the microstructure and mechanical*
 1511 *performance of CAC cementitious matrices*. Cement and Concrete Research, 2019. **119**: p.
 1512 64-76.
- 1513 26. Cao, Y., et al., *The influence of cellulose nanocrystals on the microstructure of cement*
 1514 *paste*. Cement and Concrete Composites, 2016. **74**: p. 164-173.
- 1515 27. Bu, Y., et al., *The influence of accelerated curing on the properties used in the prediction*
 1516 *of chloride ingress in concrete using a Nernst–Planck approach*. Construction and
 1517 Building Materials, 2014. **66**: p. 752-759.
- 1518 28. Bu, Y., R. Spragg, and W. Weiss, *Comparison of the pore volume in concrete as*
 1519 *determined using ASTM C642 and vacuum saturation*. Advances in Civil Engineering
 1520 Materials, 2014. **3**(1): p. 308-315.
- 1521 29. Becerril, A.P., *The Influence of Cellulose Nanocrystals on Performance and Transport*
 1522 *Properties of Cementitious Materials and Gypsum*. 2020, Purdue University Graduate
 1523 School.
- 1524 30. Barnat-Hunek, D., et al., *Effect of eco-friendly cellulose nanocrystals on physical*
 1525 *properties of cement mortars*. Polymers, 2019. **11**(12): p. 2088.
- 1526 31. Washington, T., W.J. Weiss, and J. Youngblood, *Construction of full-scale concrete*
 1527 *elements containing cellulose nanocrystals (CNCs) in bridge decks and pavements*,
 1528 R.t.U.E.f.F.a. Communities, Editor. 2021.
- 1529 32. Ramanathan, S., et al., *Cellulose Nanocrystals as an Additive for Prestressed Box Girders*
 1530 *in ASPIRE - The Concrete Bridge Magazine*. 2023 (In Press): www.aspirebridge.org.
- 1531 33. Lothenbach, B., K. Scrivener, and R. Hooton, *Supplementary cementitious materials*.
 1532 Cement and concrete research, 2011. **41**(12): p. 1244-1256.
- 1533 34. Juenger, M.C. and R. Siddique, *Recent advances in understanding the role of*
 1534 *supplementary cementitious materials in concrete*. Cement and Concrete Research, 2015.
 1535 **78**: p. 71-80.
- 1536 35. Environment, U., et al., *Eco-efficient cements: Potential economically viable solutions for*
 1537 *a low-CO2 cement-based materials industry*. Cement and Concrete Research, 2018. **114**:
 1538 p. 2-26.

- 1539 36. Hawkins, P., P.D. Tennis, and R.J. Detwiler, *The use of limestone in Portland cement: a*
1540 *state-of-the-art review*. 1996: Portland Cement Association.
- 1541 37. Thomas, M.D. and R.D. Hooton, *The durability of concrete produced with portland-*
1542 *limestone cement: Canadian studies*. PCA R&D SN3142, Portland Cement Association,
1543 Skokie, IL, 2010: p. 28.
- 1544 38. Tennis, P., M. Thomas, and W. Weiss, *State-of-the-Art Report on Use of Limestone in*
1545 *Cements at Levels of up to 15%*. PCA R&D SN3148, Portland Cement Association, Skokie,
1546 IL, 2011.
- 1547 39. Barrett, T.J., *Performance of portland limestone cements: Cements designed to be more*
1548 *sustainable that include up to 15% limestone addition*. 2013, Purdue University.
- 1549 40. Hooton, R. and M. Thomas, *Sulfate resistance of mortar and concrete produced with*
1550 *portland-limestone cement and supplementary cementing materials*, in *Recommendation*
1551 *for ASTM C595/AASHTO M 240, PCA R&D SN3285a*. 2016, Portland Cement
1552 Association.
- 1553 41. Bharadwaj, K., et al., *CALTRANS: Impact of the Use of Portland-Limestone Cement on*
1554 *Concrete Performance as Plain or Reinforced Material - Final Report*. 2021.
- 1555 42. Bharadwaj, K., et al., *Predicting pore volume, compressive strength, pore connectivity, and*
1556 *formation factor in cementitious pastes containing fly ash*. Cement and Concrete
1557 Composites, 2021: p. 104113.
- 1558 43. Bentz, D.P., et al., *Limestone fillers conserve cement; Part I: an analysis based on Powers’*
1559 *model*. Concrete international, 2009. **31**(11): p. 41-46.
- 1560 44. Berodier, E. and K. Scrivener, *Understanding the Filler Effect on the Nucleation and*
1561 *Growth of C-S-H*. Journal of the American Ceramic Society, 2014. **97**(12): p. 3764-3773.
- 1562 45. Zajac, M., et al., *Influence of limestone and anhydrite on the hydration of Portland*
1563 *cements*. Cement and Concrete Composites, 2014. **46**: p. 99-108.
- 1564 46. Ramanathan, S., M. Croly, and P. Suraneni, *Comparison of the effects that supplementary*
1565 *cementitious materials replacement levels have on cementitious paste properties*. Cement
1566 and Concrete Composites, 2020. **112**: p. 103678.
- 1567 47. Association, P.C., *Roadmap to Carbon Neutrality*. 2021.
- 1568 48. Bharadwaj, K., *Towards the Development of Performance-Based Concrete Mixtures Made*
1569 *with Modern Cementitious Materials Using Thermodynamic Modeling*, in *Civil*
1570 *Engineering*. 2022, Oregon State University: Corvallis, OR. p. 327.
- 1571 49. Bharadwaj, K., et al., *Predicting Pore Volume, Compressive Strength, Pore Connectivity,*
1572 *and Formation Factor in Cementitious Pastes Containing Fly Ash*. Cement and Concrete
1573 Composites, 2021. **122**: p. 104113.
- 1574 50. Bharadwaj, K., et al., *Toward the Prediction of Pore Volumes and Freeze-Thaw*
1575 *Performance of Concrete Using Thermodynamic Modelling*. Cement and Concrete
1576 Research, 2019. **124**: p. 105820.
- 1577 51. Bharadwaj, K., B.O. Isgor, and J.W. Weiss, *Pozzolanic reactivity of SCMs from a*
1578 *thermodynamic perspective*. ACI Materials Journal, 2022. **In Review**.
- 1579 52. Bharadwaj, K., B.O. Isgor, and J.W. Weiss, *A Simplified Approach to determine the*
1580 *Pozzolanic Reactivity of Commercial Supplementary Cementitious Materials*. Concrete
1581 International, 2022. **44**(1): p. 27-32.
- 1582 53. Choudhary, A., et al., *Pozzolanic Reactivity Test of Supplementary Cementitious*
1583 *Materials*. ACI Mater J, 2022. **119**(2): p. 255-268.

- 1584 54. Glosser, D., et al., *Investigation of Reactivity of Fly Ash and Its Effect on Mixture*
1585 *Properties*. ACI Materials Journal, 2019. **116**(4): p. 193-200.
- 1586 55. Glosser, D., O.B. Isgor, and W.J. Weiss, *Non-Equilibrium Thermodynamic Modeling*
1587 *Framework for Ordinary Portland Cement/Supplementary Cementitious Material Systems*.
1588 ACI Materials Journal, 2020. **117**(6): p. 111-123.
- 1589 56. Lothenbach, B. and M. Zajac, *Application of thermodynamic modelling to hydrated*
1590 *cements*. Cement and Concrete Research, 2019. **123**.
- 1591 57. Kulik, D.A., et al., *GEM-Selektor geochemical modeling package: revised algorithm and*
1592 *GEMS3K numerical kernel for coupled simulation codes*. Computational Geosciences,
1593 2013. **17**(1): p. 1-24.
- 1594 58. Wagner, T., et al., *Gem-Selektor geochemical modeling package: TSolmod library and*
1595 *data interface for multicomponent phase models*. Canadian Mineralogist, 2012. **50**(5): p.
1596 1173-1195.
- 1597 59. Lothenbach, B., et al., *Cemdata 18: A chemical thermodynamic database for hydrated*
1598 *Portland cements and alkali-activated materials*. Cement and Concrete Research, 2019.
1599 **115**: p. 472-506.
- 1600 60. Lothenbach, B., et al., *Thermodynamic modelling of the effect of temperature on the*
1601 *hydration and porosity of Portland cement*. Cement and Concrete Research, 2008. **38**(1):
1602 p. 1-18.
- 1603 61. Lothenbach, B. and F. Winnefeld, *Thermodynamic modelling of the hydration of Portland*
1604 *cement*. Cement and Concrete Research, 2006. **36**(2): p. 209-226.
- 1605 62. Lothenbach, B., et al., *Effect of temperature on the pore solution, microstructure and*
1606 *hydration products of Portland cement pastes*. Cement and Concrete Research, 2007.
1607 **37**(4): p. 483-491.
- 1608 63. Myers, R.J., S.A. Bernal, and J.L. Provis, *A thermodynamic model for C-(N-) ASH gel:*
1609 *CNASH_{ss}. Derivation and validation*. Cement and Concrete Research, 2014. **66**: p. 27-
1610 47.
- 1611 64. Myers, R.J., et al., *Thermodynamic modelling of alkali-activated slag cements*. Applied
1612 Geochemistry, 2015. **61**: p. 233-247.
- 1613 65. Lothenbach, B., K. Scrivener, and R.D. Hooton, *Supplementary cementitious materials*.
1614 Cement and Concrete Research, 2011. **41**(12): p. 1244-1256.
- 1615 66. Zajac, M., et al., *Impact of microstructure on the performance of composite cements: Why*
1616 *higher total porosity can result in higher strength*. Cement and Concrete Composites, 2018.
1617 **90**: p. 178-192.
- 1618 67. Azad, V.J., et al., *Interpreting the pore structure of hydrating cement phases through a*
1619 *synergistic use of the Powers-Brownyard model, hydration kinetics, and thermodynamic*
1620 *calculations*. Advances in Civil Engineering Materials, 2017. **6**(1): p. 1-16.
- 1621 68. Glosser, D., et al., *An extension of the Powers-Brownyard model to pastes containing SCM*.
1622 ACI Materials Journal, 2019. **116**(5): p. 205-216.
- 1623 69. Bharadwaj, K., et al., *A New Mixture Proportioning Method for Performance-Based*
1624 *Concrete*. ACI Materials Journal, 2022. **119**(2): p. 207-220.
- 1625 70. Bharadwaj, K., et al., *CALTRANS: Impact of the Use of Portland-Limestone Cement on*
1626 *Concrete Performance as Plain or Reinforced Material - Final Report*. 2021, Oregon State
1627 University: Corvallis. p. 320.

- 1628 71. Isgor, B., et al., *Development of a performance-based mixture proportioning procedure for*
1629 *concrete incorporating off-spec fly ash*. 2020, Energy Power Research Institute (EPRI):
1630 Palo Alto, CA. p. 78.
- 1631 72. Ramanathan, S., et al., *Reducing GHG Emission Using Cellulose Nanocrystals, OPC, and*
1632 *Limestone*. ACI Materials Journal, 2023. **120**(1): p. 205-217.
- 1633 73. Han, D. and R.D. Ferron, *Effect of mixing method on microstructure and rheology of*
1634 *cement paste*. Construction and Building Materials, 2015. **93**: p. 278-288.
- 1635 74. Oguz, O., et al., *Poly (lactide)/cellulose nanocrystal nanocomposites by high-shear mixing*.
1636 *Polymer Engineering & Science*, 2021. **61**(4): p. 1028-1040.
- 1637 75. Barger, G.S., *A Fusion Method for the X-Ray Fluorescence Analysis of Portland Cements,*
1638 *Clinker and Raw Materials Utilizing Cerium (IV) Oxide in Lithium Borate Fluxes*.
1639 *Advances in X-ray Analysis*, 1985. **29**: p. 581-585.
- 1640 76. Tsui Chang, M., *The Evaluation of Cementitious Pore Solution Composition and Electrical*
1641 *Resistivity Using X-ray Fluorescence (XRF)*. 2017, Oregon State University.
- 1642 77. Castro, J., I.D.I. Varga, and J. Weiss, *Using isothermal calorimetry to assess the water*
1643 *absorbed by fine LWA during mixing*. Journal of materials in civil engineering, 2012. **24**(8):
1644 p. 996-1005.
- 1645 78. Zaw, M., *Automated Chemical Acidification Testing of Cementitious Materials*. 2021,
1646 Oregon State University.
- 1647 79. Fu, T. and W.J. Weiss, *The Ball-on-Three-Ball (B3B) Test—Application to Cement Paste*
1648 *and Mortar*. Advances in Civil Engineering Materials, 2020. **9**(1): p. 128-142.
- 1649 80. Börger, A., P. Supancic, and R. Danzer, *The ball on three balls test for strength testing of*
1650 *brittle discs: stress distribution in the disc*. Journal of the European Ceramic Society, 2002.
1651 **22**(9-10): p. 1425-1436.
- 1652 81. Kim, T. and J. Olek, *Effects of sample preparation and interpretation of thermogravimetric*
1653 *curves on calcium hydroxide in hydrated pastes and mortars*. Transportation research
1654 record, 2012. **2290**(1): p. 10-18.
- 1655 82. AASHTO, *AASHTO TP 119—Standard Method of Test for Electrical Resistivity of a*
1656 *Concrete Cylinder Tested in a Uniaxial Resistance Test*, in AASHTO, Washington, DC.
1657 2021.
- 1658 83. Spragg, R., et al., *Factors that influence electrical resistivity measurements in cementitious*
1659 *systems*. Transportation research record, 2013. **2342**(1): p. 90-98.
- 1660 84. Coyle, A.T., et al., *Activation energy of conduction for use in temperature corrections on*
1661 *electrical measurements of concrete*. Advances in Civil Engineering Materials, 2019. **8**(1):
1662 p. 158-170.
- 1663 85. AASHTO, *AASHTO TP 135—Standard Method of Test for Determining the Total Pore*
1664 *Volume in Hardened Concrete Using Vacuum Saturation*, in AASHTO, Washington, DC.
1665 2020.
- 1666 86. Barrett, E.P., L.G. Joyner, and P.P. Halenda, *The Determination of Pore Volume and Area*
1667 *Distributions in Porous Substances. I. Computations from Nitrogen Isotherms*. Journal of
1668 the American Chemical Society, 1951. **73**: p. 373-380.
- 1669 87. Rajabipour, F. and W.J. Weiss, *Electrical conductivity of drying cement paste*. Materials
1670 and Structures, 2007. **40**: p. 1143-1160.
- 1671 88. Leao, T.P. and M. Tuller, *Relating soil specific surface area, water film thickness, and*
1672 *water vapor adsorption*. Water Resources Research, 2014. **50**(7873-7885).

- 1673 89. Parrot, L.J. and D.C. Killoh, *Prediction of cement hydration*. British Ceramic Proceedings,
1674 1984. **35**: p. 41-53.
- 1675 90. Glosser, D., et al., *Estimating reaction kinetics of cementitious pastes containing fly ash*.
1676 Cement and Concrete Composites, 2020. **112**: p. 103655.
- 1677 91. Palacios, M., et al., *Effect of PCs superplasticizers on the rheological properties and*
1678 *hydration process of slag-blended cement pastes*. Journal of Materials Science, 2009.
1679 **44**(10): p. 2714-2723.
- 1680 92. Lerch, W., *The influence of gypsum on the hydration and properties of Portland cement*
1681 *pastes*. 2008.
- 1682 93. Niemuth, M.D., *Effect of fly ash on the optimum sulfate of Portland Cement*. 2012: Purdue
1683 University.
- 1684 94. Ramanathan, S., *Reactivity of Supplementary Cementitious Materials in Model Systems*
1685 *and Cementitious Pastes*. 2021, University of Miami.
- 1686 95. Valadez-Carranza, Y., et al., *Report - Working Group for Advancement of Cellulose Nano-*
1687 *Materials Use in Cement-Based Materials*. 2022, US Endowment.
- 1688 96. Haddad Kolour, H., W. Ashraf, and E.N. Landis, *Hydration and early age properties of*
1689 *cement pastes modified with cellulose nanofibrils*. Transportation Research Record, 2021.
1690 **2675**(9): p. 38-46.
- 1691 97. Matschei, T., B. Lothenbach, and F.P. Glasser, *The role of calcium carbonate in cement*
1692 *hydration*. Cement and concrete research, 2007. **37**(4): p. 551-558.
- 1693 98. Bharadwaj, K., O. Isgor, and W. Weiss, *Supplementary Cementitious Materials in Portland*
1694 *Limestone Cements*. ACI Materials Journal, 2022. **119**(2).
- 1695 99. Matschei, T., et al. *Relationships of Cement Paste Mineralogy to Porosity and Mechanical*
1696 *Properties*. in *International Conference on Modelling of Heterogeneous Materials with*
1697 *Applications in Construction and Biomedical Engineering*. 2007.
- 1698 100. Hisseine, O.A., et al., *Nanocellulose for improved concrete performance: A macro-to-*
1699 *micro investigation for disclosing the effects of cellulose filaments on strength of cement*
1700 *systems*. Construction and Building Materials, 2019. **206**: p. 84-96.
- 1701 101. Miller, S.A., et al., *Carbon dioxide reduction potential in the global cement industry by*
1702 *2050*. Cement and Concrete Research, 2018. **114**: p. 115-124.
- 1703 102. Bradford, K. and F. Lolli, *CONOMIC AND ENVIRONMENTAL IMPACT OF*
1704 *NANOCELLULOSE ADDITIVES IN PORTLAND CEMENT*, in *18th International*
1705 *Conference on Non-conventional Materials and Technologies (NOCMAT 2022)*. 2022.
- 1706 103. Nassiri, S., et al., *Comparison of unique effects of two contrasting types of cellulose*
1707 *nanomaterials on setting time, rheology, and compressive strength of cement paste*.
1708 Cement and Concrete Composites, 2021. **123**: p. 104201.
- 1709 104. Mateos, A., et al., *Structural Response of Concrete Pavement Slabs under Hygrothermal*
1710 *Actions*. Construction and Building Materials, 2020. **243**.

1711

1712 **8. Appendix**

1713 **8.1. CNC Amounts**

1714 Forest management helps reduce hazardous fuels and improves forest health. It is estimated that
1715 about 25 tons of biomass per thin-from-below prescription is obtained per acre from the forest
1716 management; this translates to about 12.5 bone dry tons per acre. CNC suspension yield from bone
1717 dry mass (without needles and bark) is estimated to be about 12.5% i.e., 1.5-ton CNC suspension
1718 per acre.

1719 Assuming that a freeway lane width is 12 feet and the cement content used in concrete pavements
1720 is 525 lb/yd³, Table 10 gives an estimated acres of forest management that will result in CNC
1721 suspension that can be used in constructing a lane mile of concrete pavement for different CNC
1722 dosages and pavement thicknesses.

1723 Table 10. Acres of forest management biomass that can be used in one lane mile construction of
1724 a freeway for different CNC dosages in concrete and different pavement thicknesses

Unit: acres/lane mile	CNC dosage (% CNC solids volume by volume of binder)		
Pavement thickness (in.)	0.2	0.5	1.0
8	2.5	6.4	12.7
10	3.2	7.9	15.9
12	3.8	9.5	19.1
15	4.8	11.9	23.8

1725

1726 To put the CNC amounts used in terms of cubic yard of concrete, for CNC dosages of 0.2, 0.5, and
1727 1.0% CNC solids volume per binder volume, it was calculated that 4.9, 12.2, and 24.4 lbs. of CNC
1728 suspension, respectively, is required for one cubic yard of concrete.

1729

1730

1731

1732

1733 8.2. Mill Certificates

1734 The following are the mill certificates of the OPC, PLC, and Slag used for the field trials.

		4200 E Jurupa St. Suite 312 Ontario, CA 91761 Telephone (909) 974-5469 FAX (909) 974-5525			CEMENT MILL TEST REPORT	
		Cement Identified as:				
Plant: Cemex Construction Materials Pacific LLC Location: Victorville, CA		Prod dates:		Beginning: 6/3/2022 Ending: 6/9/2022		
				Ref. No	44729	
STANDARD CHEMICAL REQUIREMENTS (ASTM C114)		ASTM C150 / AASHTO M 85 SPECIFICATIONS	TYPE I	TYPE II	TYPE V	TEST RESULTS
Silicon Dioxide (SiO ₂), %		Minimum	----	----	----	20.3
Aluminum Oxide (Al ₂ O ₃), %		Maximum	----	6.0	----	4.1
Ferric Oxide (Fe ₂ O ₃), %		Maximum	----	6.0	----	3.9
Calcium Oxide (CaO), %		Maximum	----	----	----	62.4
Magnesium Oxide (MgO), %		Maximum	6.0	6.0	6.0	4.9
Sulfur Trioxide (SO ₃), % **		Maximum	3.0	3.0	2.3	3.1
Loss on Ignition (LOI), %		Maximum	3.5	3.5	3.5	2.6
Insoluble Residue, %		Maximum	1.5	1.5	1.5	1.07
Sodium Oxide (Na ₂ O), %		Maximum	----	----	----	0.19
Potassium Oxide (K ₂ O), %		Maximum	----	----	----	0.41
Equivalent Alkalies (Na ₂ O+.658K ₂ O), % CO ₂ (%)		Maximum	0.60	0.60	0.60	0.46
Limestone (%)		Maximum	5.0	5.0	5.0	3.4
CaCO ₃ in limestone		Minimum	70.0	70.0	70.0	74.7
Inorganic addition		Maximum	5.0	5.0	5.0	2.1
Tricalcium Silicate (C ₃ S), %		Maximum	----	----	----	54
Dicalcium Silicate (C ₂ S), %		Maximum	----	----	----	16
Tricalcium Aluminate (C ₃ A), %		Maximum	----	8	5	4
Tetracalcium Aluminoferrite (C ₄ AF), %		Maximum	----	----	----	11
Heat Index (C ₃ S + 4.75C ₃ A)		Maximum	----	100	----	73
(C ₄ AF + 2C ₃ A) or (C ₄ AF + C ₂ F), %		Maximum	----	----	25	19
PHYSICAL REQUIREMENTS						
Heat of Hydration (ASTM C1702)		Informational data only				
7 days, kj/kg (cal/g)		Most recent value				301(72.4)
(ASTM C204) Blaine Fineness, cm ² /gm		Minimum	2600	2600	2600	4184
(ASTM C430) -325 Mesh, %		Minimum	----	----	----	98
(ASTM C191) Time of Setting (Vicat)						
Initial Set, minutes		Minimum / Maximum	45 / 375	45 / 375	45 / 375	108
Final Set, minutes		Minimum / Maximum	----	----	----	266
(ASTM C451) False Set, %		Minimum	50	50	50	89
(ASTM C185) Air Content, %		Maximum	12	12	12	6.1
(ASTM C151) Autoclave Expansion, %		Maximum	0.80	0.80	0.80	0.01
(ASTM C87) Normal Consistency, %		Maximum	----	----	----	26
(ASTM C1038) Expansion in Water %		Maximum	0.020	0.020	0.020	0.008
(ASTM C109) Compressive Strength, psi (MPa)						
1 Day		Minimum	----	----	----	2140(14.8)
3 Day		Minimum	1740(12.0)	1450(10.0)	1160(8.0)	3670(25.3)
7 Day		Minimum	2760(19.0)	2470(17.0)	2180(15.0)	4600(31.7)
28 Day (strength for Ref. No. 44701)		Minimum	----	----	3050(21.0)	5850(40.3)
<p>** The performance of CEMEX Type II, Type V has proven to be improved with sulfur trioxide levels in excess of the 2.3% limit for Type V. Note D in ASTM C150 allows for additional sulfate, provided expansion as measured by ASTM C1038 does not exceed 0.020%.</p> <p>CEMEX hereby certifies that this cement meets or exceeds the chemical and physical Specifications of:</p> <p>ASTM C150-21 Type I, Type II, and Type V Low Alkali portland cements ASTM C1157-20 Type GU Hydraulic Cement AASHTO M 85-20 Type I, Type II, and Type V Low Alkali portland cements CalTrans, Section 90-2.01 T II Modified and Type V (2006) CalTrans, Section 90-1.02B (2) (2010-2020) Arizona DOT Standard Specification 1006-2.01 Hydraulic Cement Nevada DOT Specification 701.03.01 C465 qualification data will be made available upon request</p>						
			By:  Quality Control Manager CEMEX - Victorville Cement Plant 16888 North "E" St., Victorville, CA 92394			

1735



4200 E Jurupa St
 Suit 312
 Ontario, Ca 91764
 Telephone (909) 974-5469
 Fax (909) 974-5525

**CEMENT
 MILL
 TEST
 REPORT**

Cement Identified as:

Plant: **CEMEX Construction Materials Pacific LLC** **TYPE IL (15)** Date: **10/30/2021**
 Location: Victorville, Ca
 Production Dates:
 Beginning: October 20, 2021
 Ending: October 25, 2021

STANDARD CHEMICAL REQUIREMENTS (ASTM C114)	TEST RESULTS		ASTM C595 Spec.	Type IL
Sulfur Trioxide (SO ₃), % **	3.6		Maximum	3.0
Loss on Ignition (LOI), %	5.6		Maximum	10
CO ₂ , %	5.0			
Limestone, %	14		Min. - Max.	5 - 15
CaCO ₃ in Limestone, %	85		Minimum	70
PHYSICAL REQUIREMENTS				
(ASTM C 204) Blaine Fineness, cm ² /gm	5470			----
(ASTM C 188) Density	3.06			----
(ASTM C 430) -325 Mesh, %	97.5			----
(ASTM C 191) Time of Setting (Vicat)				
Initial Set, minutes	135		Min. - Max.	45 - 420
Final Set, minutes	315			----
(ASTM C 185) Air Content, %	8		Maximum	12
(ASTM C 151) Autoclave Expansion, %	0.01		Contraction	0.2
			Expansion	0.8
(ASTM C 109) Compressive Strength, psi (MPa)	<u>psi</u>	<u>MPa</u>		
1 Day	2650	18.3		
3 Day	3970	27.4	Minimum	1890 (13.0)
7 Day	4790	33.0	Minimum	2900 (20.0)
28 Day	5820	40.1	Minimum	3620 (25.0)

CEMEX hereby certifies that this cement meets or exceeds the chemical and physical Specifications of:

ASTM C595 - 19 for Type IL Cement

James Martin
 Quality Control Manager
 CEMEX - Victorville Cement Plant

Slag Cement Test Report

CTC ID: 607 Slag Source: Rizhao Vessel: Monthly sample- Redwood City Sample Date: April 2022 Report Date: 5/27/2022 Sample Log CTC ID: 2022-227	Cemex Technical Center 6725 78th St, Riverview, FL, 33578 Phone: (813) 671-2266 Fax: (813) 677-7597
--	--

Specifications: ASTM C 989 Grades 100 & 120

Chemical and Physical Requirements	Test Result	Specifications	
Sulfur Trioxide (SO ₃) (ASTM C114), %	2.46	---	
Sulfide Sulfur (S) (ASTM C114), %	0.32	2.5 Max	
Chloride (Cl) (ASTM C114), %	0.013	---	
Aluminum Oxide (Al ₂ O ₃) (ASTM C114), %	17.5	---	
Blaine Fineness (ASTM C204), m ² /kg	478	---	
Fineness Retained - 45 Micron (ASTM C430), %	0.3	20 Max	
Specific Gravity (ASTM C188)	2.91	---	
Air Content (ASTM C185), %	3	12 Max	
Mortar Expansion (ASTM C1038) 14-day, %	0.018	0.020 Max	
Total Equivalent Alkalies (Na ₂ O+0.685 K ₂ O), (ASTM C114), %	0.45	---	
Slag Activity Index (ASTM C109)		Grade 100	Grade 120
7 Day - Individual, %	119	---	---
7 Day - Average of last 5, %	108	---	---
28 Day - Individual, %	133	90 Min	110 Min
28 Day - Average of last 5, %	123	95 Min	115 Min
Compressive Strength (ASTM C109)		Specifications	
7 Day - Reference Cement, psi	4126	---	
28 Day - Reference Cement, psi	5397	5,000 Min	
7 Day Slag and Cement Reference, psi	4906	---	
28 Day Slag and Cement Reference, psi	7164	---	
Reference Cement (ASTM C114 & C150)		Specifications	
Cement Type	Type I/II	Type I-Type II	
Total Equivalent Alkalies (Na ₂ O+0.685 K ₂ O), %	0.79	0.6 Min/ 0.9 Max	

This GGBFS meets requirements of ASTM C 989-18a and AASHTO M 302-19

- Grade 100 ASTM C989
- Grade 100 AASHTO M302
- Grade 120 ASTM C989
- Grade 120 AASHTO M302

Chemical testing completed by: YR

Physical testing completed by: YR



 Jose M. Dominguez
 Director at Cemex Technical Center USA